Characterizing Dam Augmented Flow in Downstream of a Hydropower Project to Assist Management Strategies

Submitted in partial fulfillment of the requirement for the degree of

Doctor of Philosophy

by

Dipsikha Devi
(Roll No.176104103)

Under the Supervision of

Prof. Arup Kumar Sarma

Department of Civil Engineering
Indian Institute of Technology Guwahati
November 2023

Dedicated

To my Parents and

Family

Declarations

I do hereby declare that the content embodied in this thesis entitled **"Characterizing Dam Augmented Flow in Downstream of a Hydropower Project to Assist Management Strategies"** is the result of investigation carried out by me at Department of Civil Engineering, Indian Institute of Technology Guwahati, Guwahati, India under the guidance of Prof. Arup Kumar Sarma.

Dipsikha Devi
Roll No. 176104103
Department of Civil Engineering
Indian Institute of Technology Guwahati
Guwahati, Assam, India

Certificate

This is to certify that the work described in this thesis entitled **"Characterizing Dam Augmented Flow in Downstream of a Hydropower Project to Assist Management Strategies,"** submitted by **Ms. Dipsikha Devi (Roll No. 176104103)** in partial fulfillment of the requirements for the award of the degree of Doctoral of Philosophy is an authentic record of the results obtained from the research work carried out under my supervision in the Department of Civil Engineering, Indian Institute of Technology Guwahati, India and this work has not been submitted elsewhere for a degree.

Dr. Arup Kumar Sarma
Professor
Department of Civil Engineering
Indian Institute of Technology Guwahati
Guwahati-781039

Acknowledgments

I sincerely thank my supervisor, Prof. Arup Kumar Sarma, from the Department of Civil Engineering at the Indian Institute of Technology Guwahati. His patience, valuable suggestions, motivation, and support throughout my research have been invaluable. I am earnestly thankful for his humble demeanor and for dedicating his valuable time and effort to instilling in me a scientific temperament and admirable work ethic. His guidance has been instrumental in shaping my research journey, and I am deeply grateful for his mentorship.

I want to express my sincere gratitude to all my doctoral committee members Prof. Rajib Kumar Bhattacharjya, Department of Civil Engineering, Indian Institute of Technology Guwahati, Prof. Ujjwal K. Saha, Department of Mechanical Engineering, Indian Institute of Technology Guwahati, Dr. Sreeja Pakket, Department of Civil Engineering, Indian Institute of Technology Guwahati, for their encouragement, valuable suggestions and advice during my seminars and progress reviews that have led to the successful completion of my thesis.

I am grateful for the support and assistance provided by the North Eastern Electric Power Corporation Limited, Government of India (NEEPCO), in sharing valuable data for my research. Additionally, I extend my heartfelt thanks to the NEEPCO officials, Mr. Kanchan Bhushan Paul, Mr. Debojit Das, and Mr. Dhiraj Das, whose help was instrumental in conducting this research.

I extend my heartfelt appreciation to the staff members of the Civil Engineering Department at IIT Guwahati for their kind and valuable cooperation during my research work. I would also like to express my profound gratitude to Prof. Chandan Mahanta for the unwavering support and encouragement throughout this journey.

I will forever cherish the firm support and camaraderie extended to me by my friends and colleagues at IIT Guwahati. I am deeply grateful to Dr. Gaurav Talukdar, Dr. Anupal Baruah, Dr. Ashutosh Sharma, Dr. Gilbert Hinge, Dr. Sagarika Patowary, Dr. Pulendra Dutta, Dr. Jayshree Hazarika, Dr. Santanu Pathak, Mr. P K Sarma, Ms. Dipima Sarma,

Tapas, Bhaswatee, Shakti Kalyani, Anurag, Sateesh, Shaivi, Arghya, Mamata, Prajna, Ved, Dhrubo, Jyotirmoy, Atanu, Sasanka, for their immense love and support.

I am deeply thankful to Amit, Bikul, and Debashish for their valuable assistance in carrying out my research work. Last, I would like to express my heartfelt gratitude to my dear friend Nayan, whose unwavering mental support and contributions to my research have been invaluable.

I am highly indebted to my parents, Mr. Bharat Nath Sarma (Deuta), Mrs. Dipanjali Devi (Ma), and my brother and aunt for all the sacrifice and the mental support provided during the entire journey. I also want to thank the rest of my family for their support. Moreover, I extend my heartfelt thanks to the Almighty for showering blessings upon me and granting me the patience and strength to carry out my research in good health.

Dipsikha Devi

Abstract

The recent surge in anthropogenic activities like damming across a river can attribute severe hydrologic alterations in downstream areas. Hydropower is a clean, renewable, and reliable electricity generation source. However, there are multifaceted adverse impacts of hydropower dams on riparian ecosystems, flow hydrology, and the socio-economic conditions of the downstream communities. A significant effect of dam construction is the disruption of natural flow patterns leading to erratic water levels, seasonal fluctuations, and sporadic sediment transport. An analysis of the characterization of downstream flow was performed on Lower Subansiri Hydropower Project (LSHP), Assam, India (proposed project) and Ranganadi Hydroelectric Project (RHEP), Arunachal Pradesh, India (in operation). LSHP is a non-inter-basin water transfer hydel project (NIBWT), as the powerhouse is located on the same river system. In the case of RHEP, the powerhouse is located on an adjacent watershed; thus, water is diverted for power generation. During the lean period, the impact of streamflow alteration is maximum in the case of an inter-basin water transfer (IBWT) hydel project. A scope of minimizing the degradation of biota exists by modifying the dam operation policy. This can be achieved by releasing a minimum Environmental Flow (EF) to meet the downstream Environmental Flow Requirement (EFR), estimated using Flow Duration Curve and Tennant's Method. The present study investigated the impact of an operational IBWT hydropower project on the downstream habitat of an endangered fish species, '*Tor Putitora*,' using an adaptive modelling framework consisting of a coupled reservoir operation and a hydrodynamic model. This study analyses the possible EFs from the hydropower dam to meet the EFR downstream with satisfactory power production efficiency. The analysis was conducted by incorporating a lean period inflow hydrograph into the coupled model with a series of alternate EFs. Two scenarios were explored, with 4 hours and 6 hours of peaking hours, along with the three cases of different initial reservoir storages. The total usable area over the river reach of the mentioned fish species was evaluated from the flow parameters simulated by the hydrodynamic component of the model. The power production efficiencies and area utilization rates of the target fish species were assessed in all the cases to prepare a decision support tool in a tabular form depicting the possible states of EF.

During the flood period, in the case of the NIBWT and IBWT hydropower projects, possible augmentation of the inflow hydrograph and its subsequent propagation to the downstream area was investigated using a reservoir simulation model and a hydrodynamic model. A comparative analysis of post and pre-dam flood scenarios for the same inflow hydrograph is carried out in the LSHP. Results indicate that although the frequency of flooding decreases with the dam's presence, the magnitude of maximum peak flow remains almost the same, with a significant increase in its flashy characteristics. The analysis has revealed that dam-induced flooding occupies second in the global hazard ranking considering various factors like the degree of severity, suddenness of onset, temporal and spatial extent, and socio-economic factors. Similarly, in the case of an IBWT hydropower project, the flood peak can be lowered, but the flashy characteristics of the release hydrograph increase, and the time to peak decreases. Again, to enhance the precision of flood modelling, it is imperative to incorporate the other flow contributions, like the lateral flow from the major tributaries downstream of a dam. The study also proposes a modelling framework that applies the coupled model to estimate flood downstream of a dam incorporating the flow contribution of ungauged tributaries located downstream using the Drainage Area Ratio (DAR) method.

Thus, dam-induced floods can initiate sudden flash floods that can cause severe cataclysm downstream of IBWT and NIBWT hydel projects. A viable flood management technique can include advanced strategic release from the dam before the arrival of the flood. Pre-releasing before the flood's arrival will modify the reservoir's existing operation policy. In this study, an inflow forecast-based adaptive flood management framework was developed by a coupled reservoir operation and a hydrodynamic model. The study harnesses a simulation-optimization model to quantify the advance release assuming perfect forecasts over diverse inflow forecast horizons (FH) before the arrival of the flood. The modelling framework consists of the coupled reservoir operation and hydrodynamic model to estimate the flood levels at downstream flood-prone areas. The novel methodology aims to determine the magnitude of advance release to minimize downstream flood levels with acceptable power production efficiency. An uncertainty analysis was also conducted by incorporating multiple inflow sequences developed based on Monte Carlo Simulation (MCS) into the coupled modelling framework. The model individually analyses each member of inflow sequences adopting a novel factor termed Flood Risk Factor (FRF) developed in the study. A reliability assessment of the system

performance was analyzed for different FH. The shortest FH with maximum reliability metric was considered the Effective Forecast Horizon (EFH), beyond which the system reliability performance did not improve. A decision-making EFH was then generated from the analysis based on inflow peak and volume. Another analysis was conducted to determine the EFH based on the catchment characteristics. Considering the fixed generated EFH, a sensitivity analysis was performed to check the impact of uncertainty on the system performance based on flood peak and peak flow arrival time (lag arrival time of peak and lead arrival time of peak). Results impart that with the increase of peak forecast error, the average FRF increases with lag time as well as lead time.

The coupled modelling approach developed in the study will help the decision-makers with effective reservoir system management depending on the downstream flow condition. The methodology adopted to integrate the EF will assist in maintaining a healthy downstream ecosystem. The study also aims to determine the EFH with the optimal advance release that can be utilized to moderate flood at downstream. A sensitivity analysis was conducted to test the impact of uncertainty associated with forecasts on the system performance.

Keywords: Hydropower Dams, Reservoir Operation, Hydrodynamic Model, Environmental Flow, Aquatic Habitat, Inflow Forecast Horizon

Contents

List of Figures

List of Tables

List of Symbols

Symbols	Description
ar	Advance Release
A	Flow Area
Ag	Area of the gauged catchment
Au	Area of the ungauged catchment,
Beff	Average Effective Usable Section
C_n	Courant Number
El_t	Reservoir elevation at time t
ε_t	Forecast Error at time t
g	Acceleration due to gravity
h	Power head
I_t	Inflow to the reservoir at time t
K	Reservoir Capacity
km	kilometer
m	meters
Nf	No. of times the downstream water level is greater than the flood level
Nf	Total no.of time periods
O_t	Total reservoir release
P_t	Power produced
Q	Discharge
Qg	Streamflow of the gauged catchment
Q_i	Initial discharge
q_l	Lateral Inflow
Q_l	Lateral flow contribution
Q_p	Peak discharge
Qs	Safe Discharge at Downstream
Qy	Streamflow of the ungauged catchment
R_t	Release at time t
S_0	Bed Slope
S_{as}	Active storage of the reservoir
S_{ds}	Dead storage of the reservoir
S_f	Energy Slope
S_{pt}	Spill from Reservoir at time t
St	Storage at time t
S_{t+1}	Storage at time t+1
t_i	Initial time

TWL	Tail water level
T_L	Lag Time
t_p	Time at peak discharge
z	Water Surface
α	Exponent factor
β	Distribution Factor
γ	unit weight of water
Δt	Temporal Grid Spacing
Δx	Spatial Grid Spacing
η	Turbine Efficiency
η_p	Power Production Efficiency
$\varphi(x)$	Flux Delimiter Fuction

List of Abbreviations

Terms	Abbreviations
1-D	One Dimension
2-D	Two Dimension
AOP	Adjusted Operating Policy
AUR	Area Utilization Rate
BA	Bat Algorithm
BRAHMA	Braided River aid Hydro Morphological Analyser
CEA	Central Electricity Authority
CRH model	Coupled Reservoir Operation and Hydrodynamic Model
CSI	Composite Suitability Index
CWC	Central Water Commission
DAR	Drainage Area Ratio
DC-FLWL	Dynamically Controlled Flood Limited Water Level
DE	Differential Evolution
DEM	Digital Elevation Model
DF	Downstream Flow
DH	Decision Horizon
DL	Danger Level
DP	Dynamic Programming
DE	Decision Efficiency
EF	Environmental Flow
EFH	Effective Forecast Horizon
EFR	Environmental Flow Requirement
ERE	Extreme Rainfall Events
ESP	Ensemble Streamflow Predictions
F.I.	Flashiness Index
F.R	Flood Protection Reliability
FDC	Flow Duration Curve
FDCA	Flow Duration Curve Analysis
FLWL	Flood Limited Water Level
FH	Forecast Horizon
FL	Flood Level
FRF	Flood Risk Factor
FRL	Full reservoir Level
FU	Forecast Uncertainty
GA	Genetic Algorithm
GRG	Generalized Reduced Gradient
HEC RAS	Hydrologic Engineering Centre River Analysis System
HSC	Habitat Suitability Curve
HSI	Habitat Suitability index
IBWT	Inter Basin Water Transfer
ICOLD	International Commission of Large Dams

IHA	International Hydropower Association
LFH	Long Forecast Horizon
LP	Linear Programming
LSHP	Lower Subansiri Hydropower Project
MAF	Mean Annual Flow
MCM	Million Cubic Meter
MCS	Monte Carlo Simulation
SDFI	Modified Flashiness Index
MW	Mega Watt
NA	Non-Attainment
NEEPCO	North Eastern Electric Power Corporation Limited
NHPC	National Hydroelectric Power Corporation
NIBWT	Non-Inter Basin Water Transfer
NLP	Non-Linear Programming
NSE	Nash Sutcliffe Efficiency
PERSIANN	Precipitation Estimation from Remotely Sensed Information using Artificial Neural Networks
PSO	Particle Swarm Optimization
RBI	Richard-Baker index
RHEP	Ranganadi Hydroelectric Project
RMSE	Root Mean Square Error
SOP	Standard Operating Policy
SRTM	Shuttle Radar Topographic Mission
SSE	Sum of Square Error
TGR	Three Gorges Reservoir
TUA	Total Usable Area
TVD	Total Variation Diminishing
TWh	Terawatt Hour
VI	Suitability Index corresponding to flow velocities
WI	Suitability Index corresponding to flow depth
WL	Warning Level

1

Introduction

1.1 Background

Hydropower is a clean, renewable, and reliable electricity generation source that constituted one-sixth of the global electricity production and reached 4418-Terawatt Hour (TWh) of power generation in 2020. According to the International Commission of Large Dams (ICOLD), there are 57875 large dams globally. Hydropower plants are not only used to generate electricity, but impounded reservoirs can provide several other benefits like recreation, flood protection, aquaculture, water allocation for irrigation, and potable water supply (Kaygusuz, 2004; Hogeboom et al., 2018). Hence, the expansion of hydropower is considered a potential solution to multiple challenges. Once in place, hydropower dams have produced affordable electricity for many decades, as experienced by numerous countries. Brazil has effectively utilized hydropower to maintain a power equilibrium amidst the fluctuating biofuel electricity production. In contrast, Norway's surplus power ensures an uninterrupted electricity supply to Germany and Denmark during periods of wind power shortage (Muller, 2009). In developing countries, hydropower production can increase by over 70% in the next few decades (Zarfl et al., 2015; IEA, 2016). Developing countries where millions of people are still not connected to the electricity grid (Moran et al., 2018) have been ramping up hydroelectric dam construction for decades. These often involve megaprojects, large dams that can adversely impact the environment.

The construction and operation of power plants have their shortcomings, in part with severe and long-term effects. Negative consequences include disruption of river ecology, causing substantial deforestation, generating a loss of aquatic and terrestrial biodiversity (Meile et al., 2011; Wang et al., 2019), changes in hydrology and sediment transport, fragmentation of fish migration pathways (Dugan et al., 2010; Baird et al.,

2020), severity of flood (Ghosh and Guchhait, 2016).

1.2 Impact of hydropower dams on downstream

The impact of hydropower dams in downstream regions may vary from place to place depending upon the purpose, size of the dam, and regional and meteorological conditions. A run-of-the-river scheme may not be able to alter much of the downstream streamflow. But, a hydropeaking dam upstream can affect the biodiversity of the downstream ecosystem through hydrologic alterations even if the project is a run-of-the-river scheme (Ray and Sarma, 2011). Again, the effect of Inter Basin Water Transfer (IBWT) and Non-Inter Basin Water Transfer (NIBWT) in downstream areas will also differ based on the flow conditions. Streamflow depletion can impede the biodiversity of downstream ecosystems and hinder the agricultural productivity of downstream communities. A mandatory minimum environmental flow release from the dam is thus necessary to mitigate the severe flow depletion. Environmental changes, socio-economic challenges, and ecological disruptions can arise from altered river flow, sediment accumulation, and water quality issues. Mitigation measures, such as comprehensive environmental impact assessments, integrated river basin management, and the incorporation of environmental flows, are necessary to minimize the negative consequences and promote sustainable hydropower development.

Hydropower dams can also boost the severity of floods in downstream regions. Large hydropower dams with buffer storage to absorb floods can minimize the frequency of floods downstream (Moreno et al., 2002). The analysis of China's Three Gorges Reservoir (TGR) has reduced the frequency of flooding (Xiong et al., 2022). But sudden release from the dam can create flash floods, which can be catastrophic. Extreme rainfall events can cause substantial damage within a region. During August 2018, Kerela experienced severe extreme rainfall events. The combination of the occurrence of extreme rainfall events along with the near full reservoir storage made the situation more challenging and compelled the dam authority to open the gates, resulting in severe flooding (Sudheer et al., 2019). Figure 1.1 shows a schematic illustration of downstream flooding due to a high rainfall event. Most downstream regions of hydropower dams are jacketed with embankments as river protection work. Thus, flooding occurs only when the embankment fails. Therefore, sudden water level fluctuation can cause the river bank's failure, and

progressive bank failure can eventually cause the embankment to fail. Thus, a comprehensive understanding of the downstream impact of hydropower dams is essential for sustainable development. By considering the downstream impacts, a balanced approach can be generated to harness the benefits of hydropower while safeguarding the well-being of downstream communities and ecosystems.

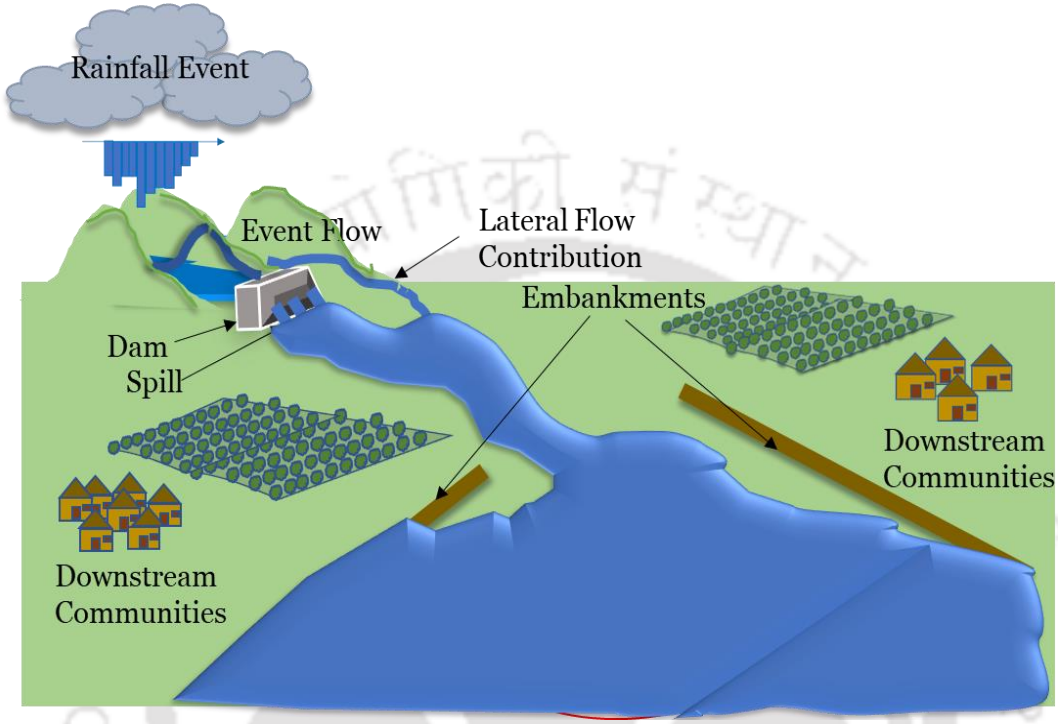

Figure 1.1: Schematic Illustration of flooding at downstream due to sudden release from the dam

1.3 Motivation for the Study

Hydropower dams are well-recognized as a clean, renewable energy source of electricity generation and significantly support the economic development of a nation. While hydropower is often portrayed as a sustainable and versatile source of economic growth in a specific region, it is vital to acknowledge the numerous detrimental effects of hydropower dams on the riverine ecosystem and the socio-economic conditions of communities located downstream. A hydropeaking dam upstream, especially during the lean period, can affect the biodiversity of the downstream ecosystem through hydrologic alterations. The artificial fluctuations in water flow due to hydropeaking can hinder the sustenance rate of aquatic organisms. During the monsoon period, the sudden release of excess water from the dam is a serious concern, as it can lead to a disastrous situation in the downstream region. Further, a pondage hydropower dam cannot mitigate a flash

flood event caused by short-duration, high-intensity rainfall. Thus, the risk associated with the sudden release from the dam amplifies, making breaching embankments in the downstream areas a highly probable scenario. The impact of IBWT and NIBWT hydropower dams in downstream regions will differ depending on the catchment and meteorological characteristics. Therefore, a comprehensive analysis of the downstream effect of a hydropower dam is necessary to reduce the sudden water release.

This study analyzes the downstream impact and addresses the challenges and consequences associated with hydropower projects. The adverse effects of IBWT hydropower dams can severely impact the downstream habitat due to flow alteration during the lean period. A modelling framework consisting of a coupled reservoir operation and hydrodynamic model is developed to check the downstream flow condition due to dam release. During the lean period, the scope of releasing a minimum flow from the dam to meet the downstream environmental flow requirement is investigated, considering the effect of power production. To understand the impact of the dam release on the spawning biology of the species, a habitat suitability analysis of an endangered fish species is conducted. During the flood period, the sudden release of water from the dam can create flash floods, leading to embankment failure. Compared to the existing studies and to understand the severity of dam impact in downstream areas, this study proposes that coupling reservoir operation and a routing model is essential to fully understand the reservoir system's effect in downstream. Thus, an adaptive modelling framework using the coupled modelling approach is developed to moderate the severity of the downstream flood by optimally releasing flow before the occurrence of the flood.

1.4 Organization of the Thesis

The work of the thesis has been divided into several phases and is described in the following chapters.

Chapter 1 briefly overviews hydropower dams, their benefits to society, and their adverse impact on the system environment.

Chapter 2 focuses on understanding the relevant literature on the implementation of mathematical modelling on reservoir operation and flood modelling, the impact of hydropower dams on downstream ecology, and flood moderation operating policy. The

critical assessment of the literature review stating the necessity of the present study has been discussed.

Chapter 3 describes the detailed description of the study area used in the analysis. The basin characteristics, along with the reservoir characteristics, are depicted in detail. The data used in the analysis are described in detail. In this chapter the detail charateristics of both the NIBWT and IBWT hydropower dams are described.

Chapter 4 discusses the development of the mathematical model implemented in the analysis. The development of the reservoir operation and hydrodynamic models is described in detail, along with all the necessary equations. The models are validated using the actual field data. The modelling approach is utilized for different objectives in the subsequent chapters. These models are coupled to assist the management strategies that are discussed in the subsequent chapters.

Chapter 5 summarizes the characterization of the flow hydrograph in the presence of the dam in the case of NIBWT and IBWT hydropower projects. The streamflow alteration of the downstream flow of an operational hydropower dam considering pre-dam and post-dam conditions is also analyzed. A Flashiness Index (F.I.) is developed and applied to the NIBWT hydropower dam to check the severity of the flood. To make a more generalized index to map the severity, a Standard Flashiness Index (SDFI) is developed. An analysis was conducted to rank the dam-induced flood among the global hazard list based on the factors provided by Bryant in 2005.

Chapter 6 proposes a modelling framework that applies the developed reservoir operation and hydrodynamic model described in Chapter 4 to estimate flood downstream, incorporating the flow contribution of ungauged tributaries downstream of a hydropower dam using the Drainage Area Ratio (DAR) method. The model is then validated with actual stage and discharge data.

Chapter 7 depicts the development of an adaptive flood management framework by coupling the two models along with the tributary contribution described in Chapter 6 to control downstream floods. The work uses a simulation-optimization model to quantify advance release, assuming perfect forecasts over different inflow forecast horizons (FH) before the arrival of the flood. The methodology aimed to determine the optimal advance

release. Multiple inflow sequences using Monte Carlo Simulation are integrated into the coupled model to determine the effective forecast horizon.

Chapter 8 analyses the scope of releasing different environmental flows from the reservoir using the coupled modelling framework along with the tributary contribution to meet the sustainable downstream flow requirement for the aquatic ecosystem with an acceptable power production efficiency.This chapter assesses the impact of an inter-basin transfer hydroelectric project on the Environmental Flow Requirement (EFR) at downstream. The EFR at downstream was analyzed by Tennant's Method and Flow Duration Curve Analysis (FDCA). The impact of environmental flow released from the dam on the downstream habitat of a fish species, 'Tor Putitora', is investigated using a coupled reservoir operation and a 1-D hydrodynamic model

Chapter 9 summarizes the major findings from the present investigation and highlights some of the recommendations for future studies.

2

Literature Review

2.1 Introduction

Hydropower dams play a crucial role in meeting the growing demand for energy worldwide. They harness the power of flowing or falling water to generate electricity, making them an essential source of renewable energy. Hydropower reservoirs have a large number of potential cross-sectoral impacts, including changes in downstream flows and water quality, dam safety, in-stream and reservoir fisheries, resettlement, ecological impacts, and flood control. One of the critical impacts of hydropower dams on downstream ecosystems is the alteration of flow regimes (Chen et al., 2015; Borgohain. 2019). These dams can interrupt the natural flow of rivers and streams, which disrupts the ecological processes that depend on steady or fluctuating water levels. This alteration of flow regimes can have significant consequences for downstream ecosystems, including changes in water quality and the loss of essential fish habitats (World Commission on Dams 2000, IHA 2004). Hydropower dams obstruct the natural flow of nutrients downstream, affecting fisheries production by reducing water flow, particularly in winter. This chapter reviews the significant research and work in reservoir system planning and management.

2.2 Impact of hydroelectric project on downstream.

2.2.1 Flow characteristics downstream of a hydroelectric project

The construction of hydropower dams can lead to changes in downstream flow patterns, which can adversely affect the ecosystems that rely on these flows. For example, dams can cause a reduction in downstream flow during specific periods, resulting in decreased water availability for ecosystems and potentially leading to the drying up of

wetlands and the disruption of riparian habitats. Additionally, sudden water releases from the dam can cause abrupt and unpredictable changes in downstream flow, which can be detrimental to aquatic organisms and terrestrial ecosystems that depend on a consistent flow regime for their survival and functioning. Moreover, the alteration of flow regimes can also affect water quality downstream. For example, the reduced flow caused by dams can lead to increased water temperatures, decreased oxygen levels, and changes in sediment transport (Branquinho & Brito, 2016). These changes in water quality can have cascading effects on downstream ecosystems, impacting the health and abundance of aquatic organisms, as well as the availability of food resources for downstream communities and wildlife.

Furthermore, the alteration of downstream flow can directly impact fisheries and aquatic ecosystems. Studies have shown that the obstruction of flow caused by hydropower dams can hinder fish migration, obstruct fish passage, and eliminate critical spawning and rearing habitats for migratory species (World Commission on Dams 2000, IHA 2004). William (1984) examined the impacts of 21 alluvial river dams on various factors downstream, including channel factors, bed materials, vegetation, etc. Flood peaks generally decreased due to the dams, but other water-discharge characteristics varied across different rivers. The study found that sediment concentrations and loads decreased significantly for long distances downstream of the dam. The study found that bed degradation ranged from negligible to 7.5 meters in the studied cross sections.

Pokhrel (2018) implemented hydrodynamic model simulations to see the impacts of flow regulation on downstream river-floodplain dynamics in the Mekong region, which is predictable along the mainstream. The study found that flow regulations are expected to significantly affect areas experiencing less than five months or over six months of flooding. In comparison, areas flooded for 5-6 months may experience the most negligible impact. Annys et al. (2020) studied the effects of the Tekeze hydropower dam on downstream hydrology and river morphology were studied. Their results showed that high flows (Q5) were reduced by a factor 5 and low flows increased by a factor of 27 with local aggradation near the tributary confluence. Petts (2021) developed a typical channel response model immediately below a dam. The response models showed complex variations in bed degradation and channel narrowing within and between rivers. Tomczyk et al. (2021) assessed the impact of hydropower plants on river hydro morphological conditions considering 42 indicators, including physical, coastal habitats,

morphology, etc. They summarized that a moderate hydro morphological state upstream and poor conditions downstream were observed. Anthropogenic pressures, obstacles in the riverbed, river regulation, and changes in the hydrological regime are significant influences. Chaudhari and Pokhrel (2022) quantitatively analyzed the historical and potential impacts of existing and planned dams in the Amazon region. They remarked that existing dams have significantly altered downstream river flow and flooding patterns, with some subbasins experiencing a three-orders-of-magnitude change in flow amplitude. The collective operation of existing and planned dams could further modify river flow downstream. These findings highlight the hydrological impacts of large hydropower dams and their implications for sustainable operation and development in the Amazon and globally.

Sudden release from the dam can also cause severe flooding downstream.(Sudheer et al., 2019) This study presents the findings and analysis of a modeling exercise utilizing HEC-HMS to simulate and examine the impact of dams and reservoir operations on the August 2018 Kerela flood. The occurrence of extreme rainfall events along with near full reservoir level made the situation challenging. It coerced the dam authorities to open the gates, leading to disastrous flooding.

2.2.2 Impact of hydropower projects on downstream aquatic habitat

Several studies worldwide have reported the detrimental impact of hydropower dams on aquatic fauna. This section reviews some studies of the effects of hydropower dams on downstream aquatic habitats.

Anderson et al., 2006 compared fish assemblage composition and aquatic habitat upstream and downstream of diversion dams along the dewatered reach of the Puerto Viejo River. The results indicated that fish assemblages directly upstream and downstream of the dam on the third-order Puerto Viejo River were dissimilar, suggesting that the small dam hindered fish movement. The results indicated that the effects of stream dewatering may be most pronounced for a subset of species with more complex reproductive requirements. Agostinho et al., 2008 described the patterns in the alterations and the decline of fish diversity in the Parana River basin, the most affected by dams in Brazil. In addition to flow regulation, other vital alterations inevitably follow dam construction, such as blockage of migration routes for some fish species. Lobera et al., 2017 studied the flow regulation's impact on bed disturbance, invertebrate assemblages,

and traits in the Siurana River (NE Iberian Peninsula) within the broader Ebro River catchment. The Siurana Reservoir alters the flow regime, reducing flood magnitude and disrupting natural patterns. They concluded that the upstream region experiences frequent bed disturbance due to torrential floods, while downstream areas show minimal geomorphological activity.

Abdo et al. (2018) assessed the impact of the Irape reservoir on the reproductive behavior of the migratory species *Prochilodus Hartii*. The results showed a negative effect on the reproduction of *P. hartii* immediately downstream of the Irapé dam, while there were favorable conditions for reproduction upstream of the reservoir. They suggested a mitigation measure is the appropriate regulation of water release from the dam during the breeding season to reduce the effect on reproduction. Zarfl et al., 2019 classified planned dam locations according to their potential impact on freshwater megafauna species at different spatial scales, with attention to potential conflicts between climate mitigation and biodiversity conservation. Fráguas and Pompeu (2021) examined the impact of a dam on the trophic structure of fish assemblages in lotic areas located upstream and downstream of the Irape Hydroelectric Power Plant. Before the dam construction, the trophic structure and species composition were similar upstream and downstream. However, after the dam was built, changes in the assemblages occurred in both sections. Upstream saw an increase in detritivore biomass and a decrease in piscivores and omnivores, while downstream experienced the opposite trend. These changes resulted in a differentiation between the two assemblages. Qiu et al. (2022) studied the effect of dam operation on the spawning habitat suitability of four major Chinese carp in the middle reach of the Yangtze River below TGR. The results showed that the spawning habitat suitability of the carps decreased due to TGR operation, primarily due to reduced water temperature suitability and a narrower window of suitable temperatures. They suggested dam outflow conditions of discharge volume ranging from 10,000 to 22,500 m^3/s and a discharge temperature of 22 to 23.5°C to optimize spawning habitat suitability.

2.3 Modelling Frameworks to evaluate the downstream impact

Managing the downstream impact of hydroelectric projects requires a robust modeling framework that can assess environmental and social consequences. Several key components of such modelling framework include reservoir operation modelling,

hydraulic modelling, ecological assessment, and risk and uncertainty analysis. The significant research on the modelling frameworks is discussed below.

2.3.1 Reservoir Operation Models

The chronological order of reservoir operation optimization innovation and techniques starts with the traditional models: linear programming (LP), non-linear programming (NLP), and dynamic programming (DP). There are many release policies that can be implemented in different situations. A Standard Operating Policy (SOP) is one of the simplest policies considered in planning a reservoir system. The SOP aims to release a quantity of water that is equal to the water demand. The SOP does not preserve water for future use (Neelakantan and Sasireka., 2013; Ashrafi and Dariane. 2017). There are many other rules, like hedging rules, pack rules, and linear decisions. In a water deficit system, a hedging rule is often implemented as this rule attempts to preserve water for future use (Fang et al., 2014 ; You and Yu. 2013; Neelakantan and Sasireka. 2015).

The reservoir operation policies can be derived from several optimization algorithms. Yeh (1985) reviewed the state-of-the-art mathematical models developed for reservoir operations. He surveyed the algorithms and methods, including LP, DP, NLP, and simulation. The historical development of each key model was critically reviewed. The evolutionary algorithms include genetic algorithms (GA) and differential evolution (DE), which have gained popularity in recent decades. Oliveira and Loucks (1997) explained the use of GA to derive multi-reservoir operating policies for water supply and hydropower reservoir systems. The algorithms employed elitism, crossover, mutation, and replacement to generate operating policies. Labadie (2004) reviewed the current state and future directions of reservoir system optimization. He examined methods to handle the complexity of reservoir systems, including high-dimensionality, dynamics, nonlinearity, and stochasticity. The study also explored multiobjective optimization and the use of heuristic programming, neural networks, and fuzzy rule-based systems for deriving operating rules. The time order for reservoir modelling is now turned to evolutionary (GA), bio-inspired algorithms like Particle Swarm Optimization (PSO), physics-based (Simulated Annealing), human-based (teaching-learning)(Ghimire and Reddy, 2013; Fang et al., 2014b). Jamshidi and Shourian (2019) developed an optimal operation of a reservoir by incorporating a hedging policy and Bat Algorithm (BA).

Results showed that BA is a suitable, easy algorithm and can be applied for optimal reservoir operation planning and management. Azad et al., (2020) discussed the recent research and development activities in hydropower optimization using a metaheuristic approach. They also discussed the efforts to optimize hydropower systems and provided a comprehensive analysis of extending operating policies of hydraulic structures using metaheuristic algorithms. Lai et al., 2022 discussed reservoir optimization models and the challenges associated with optimal reservoir operations. They highlighted the importance of hybrid approaches that address individual algorithms' limitations and consider variables' suitability in solving reservoir optimization objectives. Nguyen et al., 2022 investigated the independent and global optimization operation strategies for cascaded hydropower plants to maximize total power energy. The first strategy involves optimizing upstream plants first and then using the results to operate downstream plants. Several bio-inspired search algorithms were implemented for the second strategy. They summarized that the first strategy benefits upstream plants more, while the second strategy is more suitable for downstream hydroelectric plants and is more effective in maximizing total energy.

2.3.1.1 Inflow Forecast Horizon for reservoir operation

Reliable inflow forecasting can be vital in effectively managing reservoirs with sufficient lead time during floods and droughts (Collischonn et al., 2007; Zhao et al., 2011; Lee et al., 2019; Maddu et al., 2022). The inflow forecast horizon, which refers to the duration of predicted inflow data, plays a significant role in optimizing reservoir operations (Gragne et al., 2015; Amnatsan et al., 2018). It provides reservoir operators with valuable information for timely decision-making, efficient water allocation, flood control, hydropower generation, and adaptation to changing climatic conditions. Accurate inflow forecasts over an extended horizon enable effective planning and optimize the utilization of water resources, ensuring sustainable development and resilience in the face of future challenges (Zhao et al., 2011; Zhao et al., 2012). Simonovic and Burn (1989) introduced an improved methodology that treats the operating horizon as a dynamic decision variable. Their study determined the optimal operating horizon by balancing the reliability of shorter forecast horizons and the improved reservoir operation achievable with longer horizons. You and Cai (2008) tried to determine the forecast horizon (FH) for dynamic reservoir operation models considering a decision horizon

(DH). Factors like water stress, reservoir size, inflow uncertainty, rate of evaporation, and discount rate are analyzed. They also remarked that inflow characteristics and reservoir capacity impact the FH, with economic factors significant under high water stress. Zhao et al., 2012 introduced the concept of Effective Forecast Horizon (EFH), which balances FH and Forecast Uncertainty (FU) for optimal decision-making. Results showed that when FH is short, it dominates decision-making, leading to quick performance improvement as FH increases. With a long FH, uncertain inflow information becomes dominant. At a medium FH, reservoir performance depends on the combined effects of FU and FH, and EFH represents a balanced level. Denaro et al., 2017 employed the Information Selection Assessment framework, a machine learning approach, to compare forecasts with various lead times against the perfect forecast (actual observed inflow). By iteratively testing different projections, the study identified the forecast that yielded the closest value to the perfect forecast. Q. Zhao et al., 2019 derived the properties of long forecast horizon (LFH) and EFH from a multistage, deterministic optimization model for the operation of single water supply reservoir. The case study results showed that the LFH and EFH are affected by multiple factors such as reservoir capacity, inflow variability, decision reliability, etc.

2.3.2 Hydrodynamic Models

Hydrodynamic models are mathematical representations of fluid flow and are widely used for simulating and analyzing flow patterns in rivers, estuaries, coastal areas, and other water bodies. Hydrodynamic models can be implemented to route the reservoir releases to check the downstream impact. Several vital components and data inputs are required to perform flow simulations using hydrodynamic models. These include the geometric representation of the study area, such as the river network, bathymetry, topography, and land use characteristics. Boundary conditions, such as inflows, outflows, and initial conditions, are also essential for accurate simulations (Viero et al., 2013; Bürgler et al., 2022). Numerical methods, such as finite difference, finite volume, or finite element methods, are employed to discretize the governing equations of fluid flow, resulting in a system of algebraic equations that can be solved iteratively. Over the last few decades, hydrodynamic software packages such as HEC RAS, MIKE, and TUFLOW have gained significant popularity. These software tools are widely used in various water flow and hydraulic modeling applications due to their advanced capabilities and efficient

simulations (Morsy et al., 2018; Garcia et al., 2020; Talukdar et al., 2022). Pramanik et al., 2010 implemented the MIKE 11 hydrodynamic model with the cross-section values extracted from SRTM DEM. The model parameter Manning's n was adjusted to achieve consistent stage discharge. The model accurately simulated stage hydrographs, validating its performance.

SRTM DEM-extracted cross-sections are valuable when measured data is scarce. Patowary and Sarma (2017) introduced a modified hydrodynamic model capable of accurately predicting flow scenarios, especially in a piedmont zone. This model combines unsteady free surface flow equations with the Green-Ampt infiltration equation as the governing equation. They employed the Beam and Warming implicit finite difference scheme to solve these governing equations. The model's validity was established by comparing its predictions with field data from Trout Creek River, exhibiting excellent agreement. Furthermore, the validated model was then applied to a hypothetical river reach resembling the major tributaries of the Brahmaputra Basin in India. Kalita (2020) developed a new morphodynamic model for flow simulation in open channels proposed in this study. Using a coupled approach, it solved the one-dimensional shallow water equations and the Exner sediment continuity equation. A Total Variation Diminishing (TVD) based MacCormack predictor-corrector method was employed to solve the equations. The model was validated against various test cases, including sediment overloading, sediment shut-off, dam break flow, and movable bumps. Results showed excellent agreement with experimental and approximate solutions, with no oscillations near sharp gradients. Baruah and Sarma (2021) proposed a modified 2D shallow water model coupled with emergent vegetation. The TVD MacCormack method was used to solve the equations with boundary-fitted coordinates for complex geometry. The model incorporates vegetation effects by calculating Manning's roughness parameter 'n.' The model was calibrated and validated against experimental data for different vegetation densities. The model was also applied to various channel types and compared with published results and field data. Baruah and Sarma (2021b) extended their work and integrated a hydrologic and hydrodynamic model to estimate the ecological flow requirement in the Bhogdoi River. Kalita (2022) extended his work to introduce a hybrid numerical model for morpho-dynamic flow simulation in open channels. The deviatoric version of Saint Venant's equations was solved using the Beam and Warming implicit

finite difference scheme, while the Exner sediment continuity equation was solved using a simple finite difference scheme. The hydrodynamic and sediment transport models were coupled using a semi-coupled approach. Due to its implicit nature, the model efficiently handled undulated river beds and allowed for larger time steps. It was tested in various scenarios and produced satisfactory results compared to existing models, even with high time steps.

2.3.3 Coupled Reservoir Operation and Hydrodynamic Model

Coupling reservoir operation and hydrodynamic models is paramount in water resources management and decision-making. This integration allows for a more comprehensive understanding and effective management of water systems. Coupling reservoir operation and hydrodynamic models enables a more accurate representation of the complex interactions between reservoir dynamics and the downstream flow regime. By considering the dynamic behavior of the reservoir and the downstream river system, the models can capture the intricate relationships between water release strategies, reservoir storage levels, and downstream water flow patterns. Mateo et al., 2014 combined the hydrological and hydrodynamic models to assess the impact of reservoir operation on flooding in the Chao Phraya River Basin, Thailand. By integrating the hydrologic and routing model, they accurately simulated the 2011 flood and evaluated different reservoir operation rules. The results showed that reservoir operation reduced the flood volume substantially. Simple modifications in reservoir operation further reduced the flood volume. This study highlights the importance of coupling reservoir operation with hydrodynamic modeling to understand and manage floods effectively. Zhu et al., 2022 introduced an approach for calculating reservoir capacity and inflow using hydrodynamic and water balance calculation models, focusing on the TGR. The proposed model demonstrated an improved accuracy compared to the traditional methods. The application highlighted the potential of this approach in supporting five reservoir operations. Zeng et al., 2023 developed a large-scale coupled hydrological-hydrodynamic-dam operation model that was used to evaluate the TGR's hydrological effects. The model demonstrated effective hydrological, hydrodynamic regimes simulations, and hydropower generation. Results showed that the maximum daily flood peak had reduced due to dam operation and provided significant hydropower generation.

However, dam operation could cause higher water levels at Cuntan in the flood season, while low flow velocities near the dam need attention during the dry season.

2.4 Flood Moderation Strategy with Optimal Operating Policy

Yun and Singh (2008) introduced two approaches, multiple duration limited water level and dynamic limited water level, to increase water storage in reservoirs while ensuring flood control safety. Multiple duration limited water level uses a design storm with various durations, taking into account the likelihood of consecutive large storms. The dynamic limited water level is based on conditional probabilities of large storms obtained through a multivariate autoregressive model. The methods were applied to the Menlou drainage area in China, and their benefits for water supply were examined. Li et al., 2010 proposed a dynamic control operation model for reservoirs that considered inflow uncertainty consisting of three modules: pre-release estimation, refill operation, and risk analysis. The model was applied to the TGR in China using a systematic linear model for inflow forecasting. Results showed that dynamic control of the reservoir's flood-limited water level effectively increases hydropower generation and floodwater utilization without raising flood control risk. Ding (2015) presented a two-stage model for dynamically controlling reservoirs' flood-limited water level (DC-FLWL), considering forecast uncertainty and acceptable flood risk. The study demonstrated that DC-FLWL applies to certain inflow levels but is influenced by forecast uncertainty and downstream risk. The derived hedging rules guide balancing water conservation and flood control objectives under different uncertainty and risk levels. Lu et al., 2020 proposed a method to determine the upper limit of flood-limited water level (FLWL), considering water supply and flood control. An improved truncated Gaussian distribution and a normal distribution were implemented; the excess storage can be derived based on forecast-based pre-release. The method is applied to the Xianghongdian Reservoir, demonstrating its effectiveness in determining allowable excess storage under acceptable risk levels. The study also revealed that excess storage decreases as the safety margin for downstream increases at the same risk level. Nguyen and Gourbesville (2022) proposed a flood control operating strategy using spillway gates in multi-reservoir systems to reduce downstream flood damage. An optimization algorithm, coupled with a simulation model, was employed to determine the optimal levels of spillway gate stages. The Shuffled Complex Evolution algorithm and Mike 11 from the DHI simulation model

were used for optimization. The results demonstrated that the proposed method effectively balances flood control and hydropower generation objectives.

2.5 Conclusions from the literature review

From the literature survey, it can be assessed that significant scientific evidence supports the role of hydropower dams in disrupting the natural flow hydrology of a river. These alterations can disturb the downstream ecosystem's natural balance, affecting the habitat and organisms that rely on them. The hydropower dams can initiate environmental, socio-economic, and ecological consequences on downstream regions.

The literature survey also concluded that the impact of hydropower dams on downstream streamflow is significant and needs to be studied thoroughly before any release decision. Implementing environmental flow management is essential to maintain the natural flow patterns of rivers downstream of the dam. These flows should be based on scientific assessments of the ecological requirements of downstream ecosystems and can be integrated into the dam's operation and release schedules. In the case of large reservoirs with flood control benefits, the Flood Limited Water level (FLWL) is generally fixed, which has its own benefit of flood control. However, it also comes with several disadvantages. A fixed FLWL can limit the reservoir's capacity to store water during severe floods and lack the flexibility to adjust to changing weather patterns and seasonal variations. The pre-release technique in conjunction with the FLWL, allows for enhanced flood control efficiency. It involves gradually discharging water from the reservoir before the occurrence of flood events. In the case of the reservoir with high storage capacity with buffer storage for flood control, the integrated application of advance release with predefined FLWL can effectively manage the downstream flood. The pre-release method can also be a practical management technique for low reservoir storage capacity. The pre-release method can be consistent for flood moderation if the inflow forecast is reliable. The estimation of optimal pre-release is of utmost importance for altering the existing operating policy for flood moderation downstream. This will be more effective if a simulation-optimization model constituting a reservoir operation and a hydrodynamic model exists. However, limited studies were conducted to determine the optimal pre-release within a forecast horizon based on the downstream flow information.

2.6 Research Objectives

The primary objective of this study is to analyze the impact of hydropower dams on downstream flow in both the lean period and flood period to suggest management measures to mitigate the adverse effects, if any. The objectives are defined as follows.

1. Development of an adaptive modelling framework consisting of a reservoir operation and hydrodynamic model.

2. To characterize reservoir outflow from hydropower dam and its downstream propagation using the developed model considering lateral tributary contributions.

3. To develop a coupled reservoir operation and hydrodynamic (CRH) model to explore the scope of mitigating downstream floods through advance release within an effective forecast horizon.

4. Coupling the habitat suitability model with the CRH model for deciding environmental flows to sustain a specified endangered species at downstream during the lean period.

Figure 2.1 shows the entire methodology adopted in this thesis work.

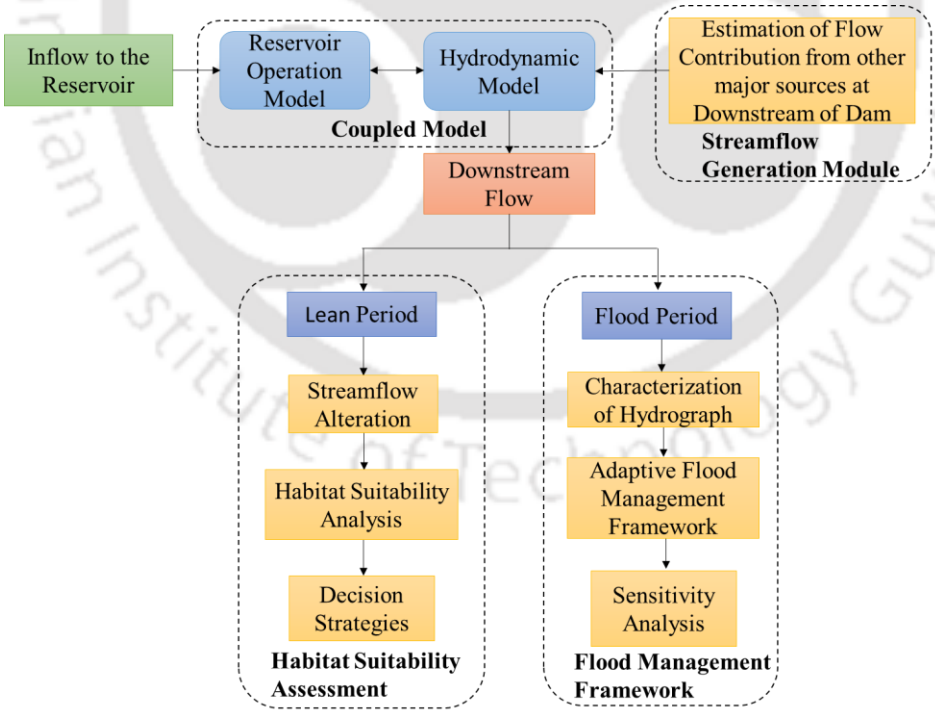

Figure 2.1 :Methodology adopted in the Analysis

3

Study Area

3.1 Introduction

The Subansiri Basin is the largest river basin of the Brahmaputra Valley. The river originates from the Himalayan foothills of Tibet and finally joins the Brahmaputra at Majuli. The total catchment area upto the confluence of Brahmaputra is around 35000 km^2, out of which 40 % lies in Tibet and the rest 60% in India. The major tributaries of Subansiri include Laro, Nye, Yume, Tsari, Kamla, Jiyadhol, Ranganadi, and Dikrong. In 2001, the Central Electricity Authority (CEA), India, identified 22 projects with 15,191 MW in the Subansiri River. Ranganadi and Dikrong are the major tributaries joining Subansiri before the Majuli confluence. Subansiri basin consists of two hydroelectric projects, namely the Lower Subansiri Hydroelectric Project (LSHP), a proposed hydropower project. The second project is the Ranganadi Hydroelectric Power Project (RHEP), an operational hydel project.

3.2 Hydropower Projects

Two significant hydropower projects are located in the Subanisri Basin of the North Eastern part of India. The first one is the Lower Subansiri Hydroelectric Project (LSHP), a proposed NIBWT hydropower project with an installed capacity of 2000 MW. Situated at Gerukamukh, Assam, India, LSHP aims to harness the region's hydroelectric potential. On the other hand, the second project, the Ranganadi Hydroelectric Project (RHEP), has been operational since 2003. RHEP is categorized as an IBWT hydroelectric project involving the diversion of water to an adjacent watershed for power generation. To gain insights, a comprehensive analysis of the characterization of dam release was conducted for both the hydel projects. However, as LSHP is not yet operational, any potential

downstream impact remains unobservable at this point. Being fully functional, RHEP's downstream impact is apparent. Consequently, the study also put forth managerial strategies to effectively address the downstream effects of RHEP, minimizing the negative consequences of the downstream implications of sustainable power generation. The detailed characteristics of the two hydel projects are mentioned in the subsequent sections.

3.2.1 Lower Subansiri Hydropower Project (LSHP)

The Subansiri is the largest transboundary tributary of the Brahmaputra River. The river's total length is 468 km up to the confluence with Brahmaputra (Gogoi and Goswami 2014). On entering the plains of Assam, fanning out of the river flow was observed, forming several braiding channels due to the sudden drop in the terrain height starting from the Arunachal hills to the Assam plains (CWC 2019). The Lower Subansiri Hydropower Project (LSHP) is a proposed hydropower project located at Gerukamukh, at the Assam-Arunachal Pradesh Border. The flood-prone area called Chouldhowaghat is located 13 km downstream of the dam site. The LSHP is a run-of-the-river hydropower project with a 2000 Mega Watt (MW) installed capacity. Eight power units are available, each consisting of 250 MW. The gross capacity of the reservoir is 1365 million cubic meters (MCM). Stream flow near the dam site varies significantly between monsoon and non-monsoon periods. The average lean period flow is in the range of 500 m^3/s, and the monsoon period flow is in the range of 2500 m^3/s. From Gerukamukh to Chouldhowaghat, the river bed is mainly composed of sand, gravel, and silt.

The powerhouse is located in the same river. The total reservoir releases constitute the spill from the reservoir and discharge required for power generation. The total reservoir releases contribute to the flow of the Subansiri River.

3.2.2 Ranganadi Hydroelectric Power Project (RHEP)

The Ranganadi River is the major tributary of the Subansiri River. The Ranganadi River originates from the Himalayan foothill of Arunachal Pradesh, enters Assam, and joins the Subansiri River in the Lakhimpur district of Assam. The Ranganadi Hydro Electric Power Project (RHEP) is a run-of-the-river scheme with a small pondage to harness the hydropower of the Ranganadi River with the powerhouse located in the adjacent watershed of Dikrong River at Hoz, Papum Pare District. There are three units of turbines, each having a capacity of 135 MW with a gross capacity of 7.71 MCM. The

total plant capacity of RHEP is 405 MW. A maximum flow of 160 m^3/s is diverted from Ranganadi to Dikrong Basin to meet the power demand. The power generation hour of RHEP can go as high as 24 hours a day during the monsoon period, whereas during the lean period, the peaking operation ranges from 4 to 6 hours a day. The salient features of LSHP and RHEP are shown in Table 3.1. In this analysis, the downstream gauged section at NT Road Crossing, Lakhimpur, is considered, which is around 46 km from the dam site. From the Ranganadi Basin's stream network, two major tributaries join the main channel downstream of the dam. One tributary is located 12 km from the dam site, and the other joins 31 km from the dam site. No other significant contributions are observed upto the main reach of the downstream section. The detailed information of the two tributaries is discussed in Chapter 6. The subbasins are located within the Ranganadi Basin. Figure 3.1 shows Subansiri Basin, Ranganadi, and Dikrong Basin along the dam site location, powerhouse, and downstream sections considered.

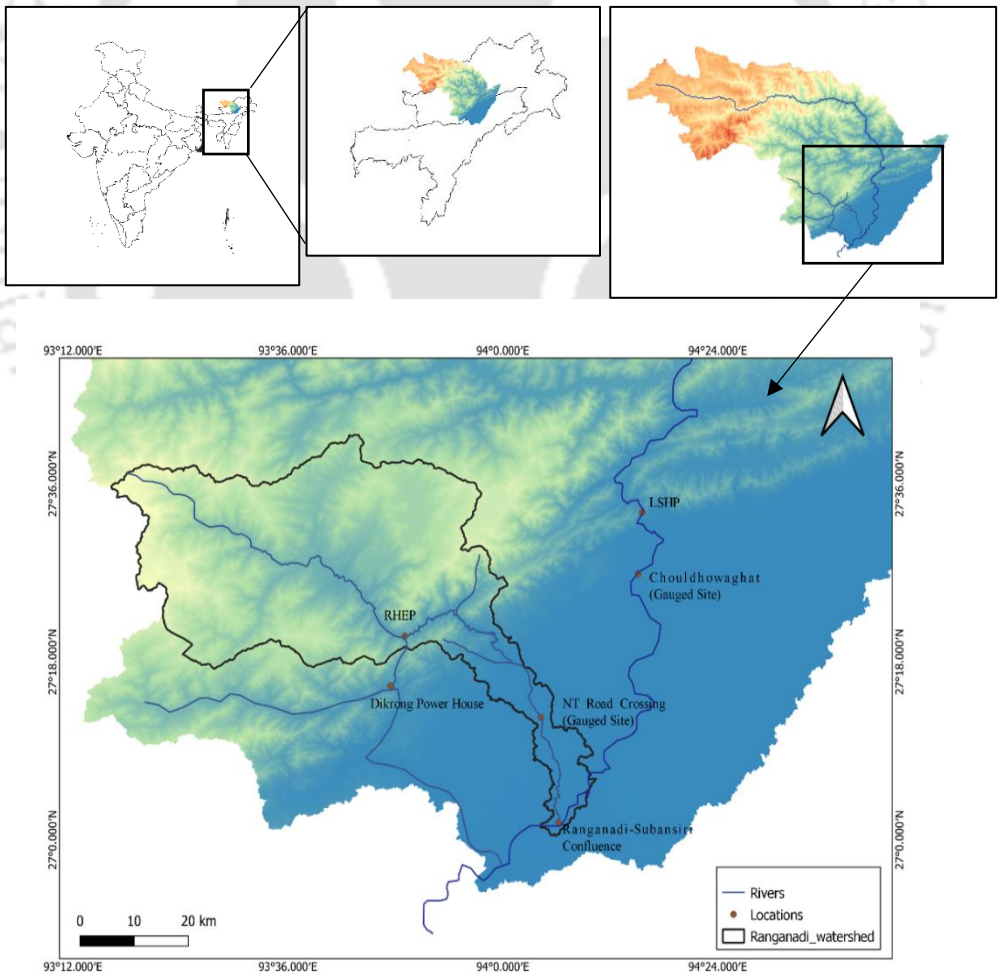

Figure 3.1 :Case Study Area

Table 3.1 :Characteristics of the reservoirs considered in the study

Reservoirs	Dead Storage (MCM)	Gross Storage (MCM)	Effective Storage (MCM)	Tail Water Level (m)	Max Water Level (m)
LSHP	720	1365	645	109	208
RHEP	3.28	7.71	4.43	246.45	567

3.3 Data Used

3.3.1 LSHP

The capacity-area-elevation curves of LSHP are obtained from National Hydroelectric Power Corporation (NHPC) Limited, and the downstream stage-discharge data (1983-2015) of Chouldhowaghat are collected from Central Water Commission (CWC), Govt. of India. Cross-sectional data are available for the downstream portion and used along with the SRTM DEM of 30 m resolution to generate the terrain data for the hydrodynamic model. Figure 3.2 shows the stage-discharge data of Chouldhowaghat. The river has an embankment, and flooding occurs only when the embankment fails. Therefore, the elevation of the natural ground level on the river bank, which was observed to be 97 m at the downstream flood-prone location (27° 26' 54.1" N, 94° 15' 33.2" E), has been considered as critical for flooding for this comparative study. As historical ten daily streamflow data is available, a hypothetical flow hydrograph of 48 hours with two flood events has been considered in this analysis.

The maximum water level of LSHP is proposed at 208 m elevation. From Figure 3.3, the area capacity elevation curves, the maximum height of the dam is 210 m. The corresponding area and capacity at 210 m are 3700 Ha and 1532 MCM, respectively.

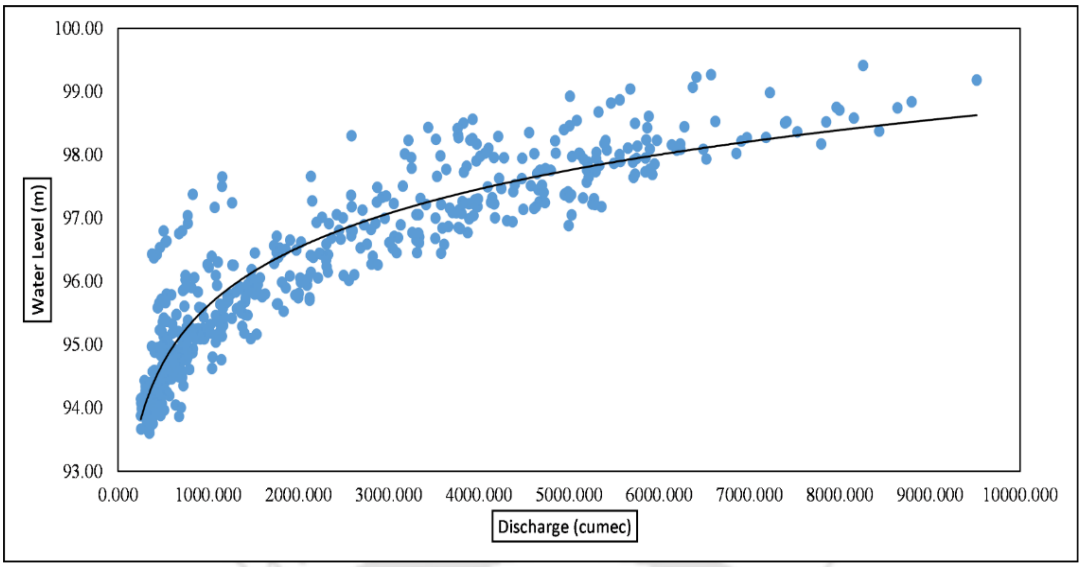

Figure 3.2: Downstream Stage- Discharge Data of Chouldhowaghat

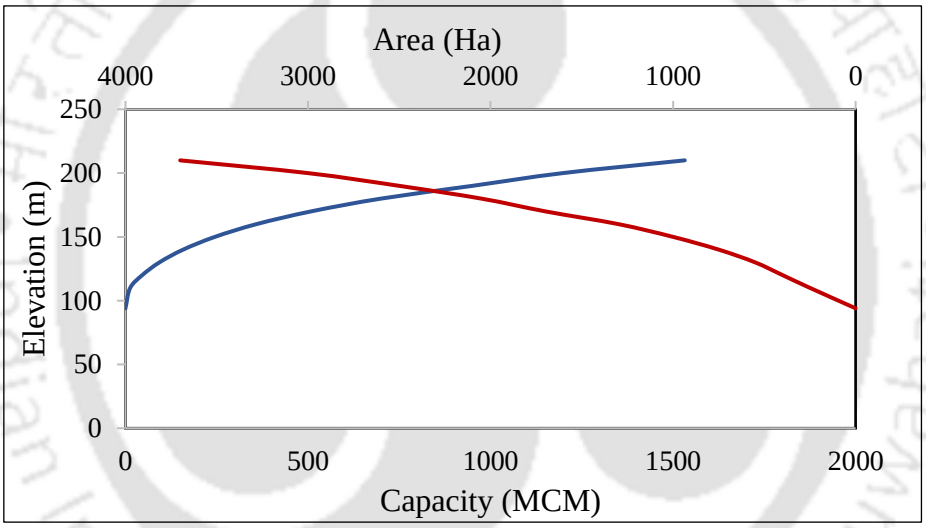

Figure 3.3: Capacity-Area-Elevation Curve of LSHP (Source: NHPC)

The relationship among area-elevation-capacity is derived using polynomial regression analysis and is incorporated into the reservoir operation model. The relationships are shown in Equations 3.1 and 3.2.

Elevation-Capacity Relationship

$$-5\times10^{-5}S^2+0.130S+112.3 \quad (3.1)$$

Area-Capacity Relationship

$$-7\times10^{-6}S^2+0.055S+98.53 \quad (3.2)$$

Where S is the reservoir capacity in MCM.

3.3.2 RHEP

The daily inflow to the reservoir data available from 2011-2021 and inflow events were collected from North Eastern Electric Power Corporation Limited, Government of India (NEEPCO). The daily downstream streamflow data of NT Road Crossing, Lakhimpur (2000-2012), along with capacity area-elevation curves of RHEP, were also collected from NEEPCO. Figure 3.4 shows the reservoir capacity area elevation graphs of RHEP. Thus, two years of common inflow and downstream data were available.

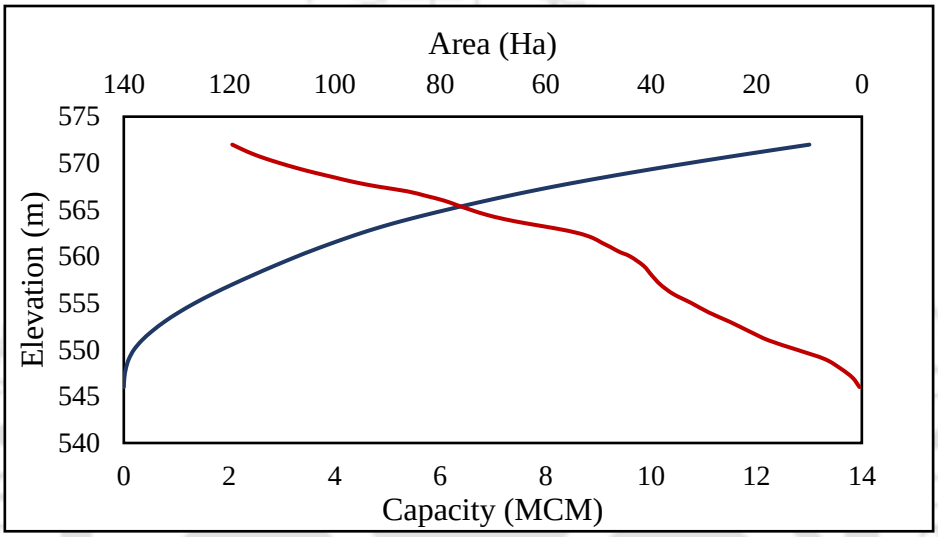

Figure 3.4: Capacity-Area-Elevation Curve of RHEP (Source: NEEPCO)

The capacity-area-elevation relationships of RHEP are shown in Equations 3.3 and 3.4.

Elevation-Capacity Relationship

$$0.0049S^3 - 0.2129S^2 + 3.318S + 549.54 \quad (3.3)$$

Area-Capacity Relationship

$$6\times10^{-5}S^3 - 0.0035S^2 + 0.0949S + 0.1237 \quad (3.4)$$

Figure 3.5 shows the daily inflow to the reservoir data. From the historical inflow data, it can be seen that the average peak flow ranges from 500-700 m^3/s.Figure 3.6 shows the daily downstream stage dscharge data.

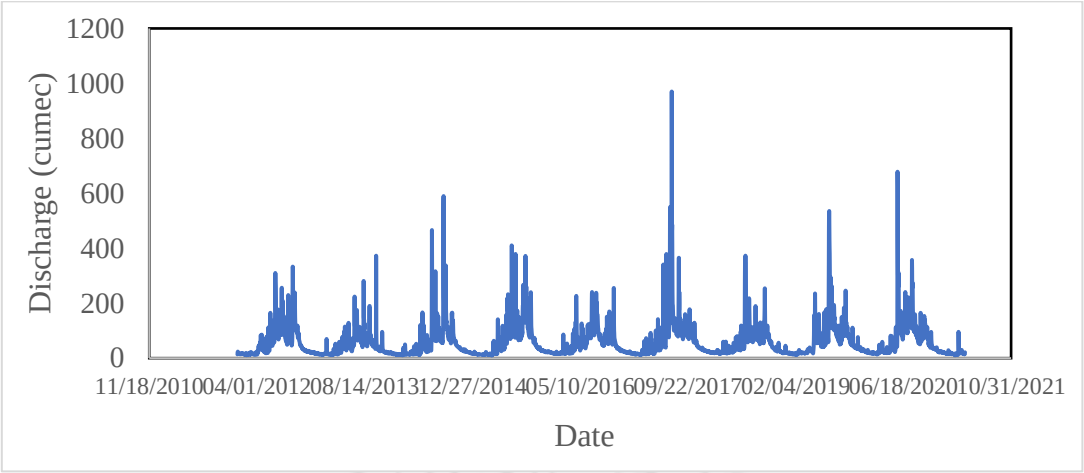

Figure 3.5: Daily Inflow Data

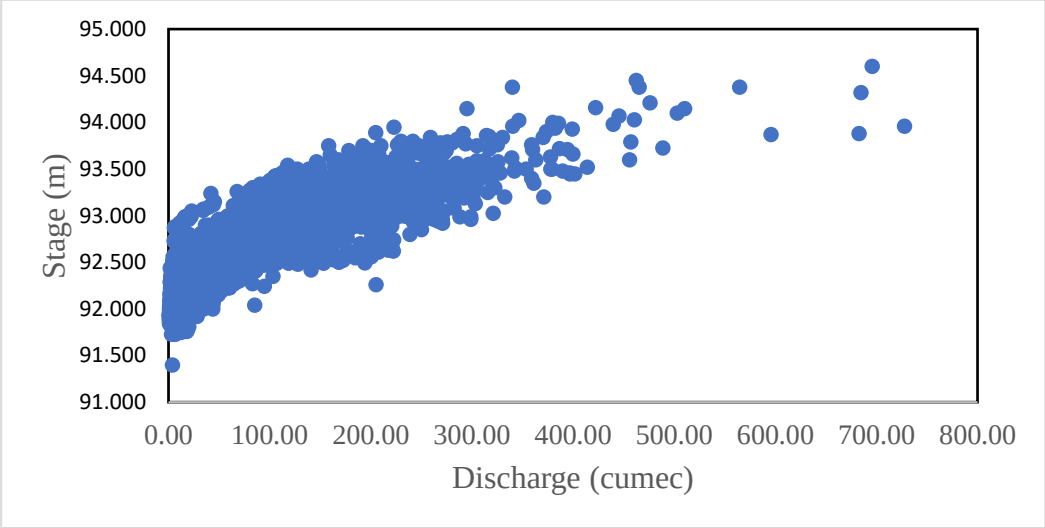

Figure 3.6: Daily Stage Discharge at NT Road Crossing, Lakhimpur

A bathymetric survey was conducted from the dam site upto the confluence with the Subansiri river. The cross-sectional data extracted from the bathymetric survey were then incorporated into the 1-D hydrodynamic model.

3.4 Conclusions

The LSHP and RHEP are the two major hydroelectric projects located in the Subansiri Basin. The LSHP is the proposed hydropower dam which is under construction and yet to be in operation. For power generation, the powerhouse is located on Subansiri; thus, total release from the reservoir consists of power release and reservoir spill. The project is a run-off-the-river scheme, so the seasonal flow will not influence much.

However, hydropeaking can initiate some adverse impacts on downstream areas through diurnal variation. The RHEP is located on the Ranganadi River, a major tributary of Subansiri. This has been operating since 2003 and has successfully generated the desired target power amount. The downstream impact of RHEP is clearly evident. This project is also a run-off-the-river scheme with a low capacity. However, the powerhouse is located in the Dikrong basin, a neighboring watershed of Ranganadi. Thus, water is diverted to the Dikrong basin for power generation. Due to water diversion, downstream streamflow alteration can be observed and is a prime problem of the basin. The Ranganadi and Subansiri river flows through the district of Lakhimpur and joins the Brahmaputra at Majuli. The district of Lakhimpur suffers significantly during the monsoon period due to the flooding caused by the two rivers annually. A clear understanding of the impact of hydropower dams downstream is necessary for any release decision or an optimal operating policy. Chapter 4 depicts the mathematical model development to investigate the downstream flow impact of hydropower dams. This developed mathematical framework is the basis for various applications described in the following chapters.

4

Development of Mathematical Model

4.1 Introduction

Mathematical modelling involves generating a set of numerical equations that can capture the essential aspects of a real-world phenomenon. Advanced mathematical modeling techniques can solve complex water resource systems with reliable computational methods (Viero et al., 2013). Mathematical modelling can be a powerful approach for ensuring efficient water management strategies that balance competing demands in deriving optimal reservoir operating policy. The development of a reservoir operation model can simulate the behavior and performance of the reservoir system (Ahmed and Sarma, 2005; Gragne et al., 2015; Feng et al., 2019). The simulation process can explore different operational scenarios and their impact on the system environment. In the case of hydropower dams, reservoir operation models can determine the optimal release pattern to maximize power generation while maintaining adequate storage levels. A reservoir operation model can also incorporate environmental considerations to ensure sustainable water management. The optimal reservoir releases can be routed downstream using hydrodynamic models. These models are the mathematical representations of the fluid flow phenomenon. The continuity and momentum equations are widely used in the hydrodynamic simulations of rivers, lakes, estuaries, etc. Depending on the type of problem, these equations can be expressed in one-dimensional, two-dimensional, and three-dimensional forms. Numerous open-source and license-based models like HEC RAS and MIKE are available and are widely implemented by the research communities (Song et al., 2019).

The reservoir operation model and a hydrodynamic model can be utilized to assess the ecological impacts of reservoir operation on downstream ecosystems, including aquatic biota. In the case of flooding, the release decision can be made based on the downstream flow. Thus, by incorporating environmental and downstream flow constraints and objectives into the models, decision-makers can devise operational strategies that can minimize ecological disturbances and the severity of flooding.

The modelling exercise in the study involves reservoir operation and hydrodynamic models. A reservoir operation model following a Standard Operating Policy was developed. The reservoir releases obtained from the operating policy were incorporated into the hydrodynamic model to determine the downstream flood levels. The source code of Braided River-Aid Hydro Morphological Analyzer (BRAHMA), a MATLAB-based indigenous model developed by IIT Guwahati was utilized for the hydrodynamic analysis. The source code underwent further revisions, incorporating several modifications before applying the model. The 1-D hydrodynamic model was then utilized to couple with the reservoir operation model to devise managerial implementation.

4.2 Development of the Model

To assess the effects of the hydropower dam on the immediate downstream area, employing a reservoir operation model proves advantageous. Similarly, the hydrodynamic model facilitates the simulation of reservoir releases downstream to understand its influence on the far downstream region. The comprehensive detail of the two models is discussed in the following sub-sections.

4.2.1 Reservoir Operation Model

The primary function of the reservoir system is to regulate the natural streamflow for various purposes and utilization of water from the dam. The state of the system characterizes the reservoir's storage at the beginning of the time period and the inflow to the reservoir (Vedula and Mujumdar 1992). The operation policy adopted in the work is the Standard Operating Policy (SOP). SOP is the widely implemented reservoir operation policy in which the release is made in each time period based on the water availability. The principle of the SOP for hydropower generation is that if the water availability is more than the power demand, the power release will be made to meet the demand else the available water will be released (Ashrafi and Dariane 2017; Jamshidi and Shourian

2019). After power release, water remaining more than the storage capacity, if any, will be spilled.

The rate of evaporation is considered negligible in this analysis. The model is developed in a MATLAB environment.

The continuity equation in reservoir operation is

$$S_{t+1} = I_t + S_t - S_{pt} - R_t \tag{4.1}$$

I_t is the inflow to the reservoir at time t; R_t is the release at time t; S_{pt} is the spill from the reservoir at time t; S_t is the initial storage at time t; S_{t+1} is the final storage at the end of the time period t. In the case of LSHP, the reservoir release consists of spill and power release, whereas in the case of RHEP, the reservoir release constitutes the spill that will contribute to the flow of Ranganadi.

The power head is determined using Equation 4.2

$$h = El_t - TL \tag{4.2}$$

where h is the power head in m, and El_t is the reservoir elevation at time t. TL is the tailwater level.

The power produced at a particular time period is estimated using Equation 4.3

$$P_t = \gamma h R_t \eta$$

(4.3)

where P_t is the power produced at time t in MW, γ is the unit weight of water, h is the power head in m, R_t is the discharge in m^3/s, η is the efficiency considered 0.8.

Active storage or live storage is defined as the reservoir storage utilized for various purposes and is determined in Equation 4.4. The active storage and the dead storage comprise the total reservoir capacity.

$$S_a = I_t + S_t - S_d \tag{4.4}$$

where S_a is the active storage, I_t is the inflow at time t, S_d is the dead storage of the reservoir.

The final storage at the end of the time period is determined using Equation 4.5 and Equation 4.6.

$$S_{t+1} = K \text{ ; if } (S_a + S_d - R_t) > K \tag{4.5}$$

$$S_{t+1} = (S_a - R_t + S_d) \text{ ; if } (S_a + S_d - R_t) < K \tag{4.6}$$

where K is the reservoir capacity

The spill from the reservoir occurs when the storage at a time period exceeds the total reservoir capacity, which is estimated using Equation 4.7 and Equation 4.8.

$$S_{pt} = S_t - K \text{ ; if } S_t > K \tag{4.7}$$

$$S_{pt} = 0 \text{ ; if } S_t < K \tag{4.8}$$

$$O_t = S_{pt} + R_t \tag{4.9}$$

O_t is the total reservoir release. For LSHP, the total release from the reservoir constitutes spill and power release.

$$O_t = S_{pt} \tag{4.10}$$

In RHEP, the spill from the reservoir is the total flow from the dam as power release is diverted to the Dikrong Basin. The sudden spilling from the reservoir constitutes flooding in downstream. The reservoir spill hydrographs were then incorporated into the hydrodynamic model.

4.2.2 1-D Hydrodynamic Model

The reservoir releases generated from the reservoir operation model can be routed to check the flow, flood levels, and velocities at downstream flood-prone sections. This can be achieved by a hydrodynamic model.

In this analysis, the modified source code of the BRAHMA model considering lateral flow contribution has been employed to estimate the flood levels and discharge at the downstream section. The model was developed by solving the 1D governing equations in conservation form. The equations in matrix form can be written as

$$U_t + F_x + S = 0 \tag{4.11}$$

$$U = \begin{bmatrix} A \\ Q \end{bmatrix} \quad F = \begin{bmatrix} Q \\ \frac{Q^2}{A} + gA\bar{y} \end{bmatrix} \quad S = \begin{bmatrix} 0 \\ -gA(S_0 - S_f) \end{bmatrix}$$

(4.12)

Q is the streamflow (m^3/s), A is the flow area (m^2), x and t are the spatial and temporal variables, g is the acceleration due to gravity, S_0 is the bed slope, and S_f is the energy slope.

1. Initial and Boundary Conditions

In unsteady flow, the initial conditions are defined at the starting time. This analysis specified the initial steady-state flow depths and velocities as the initial conditions. Considering a uniform discharge, the initial depths and velocities at all the sectional grids were analysed using Manning's flow equation.

The outflow hydrograph from the reservoir was allocated as the upstream boundary condition in the analysis. The normal depth of the far downstream section at the Ranganadi-Subansiri confluence point was assigned as the downstream boundary condition. For the incorporation of lateral flow contribution, intermediate boundary conditions were defined at the confluence point of the tributary with the main channel. The comprehensive analysis of the ungauged tributary contribution is described in Chapter 6.

2. Stability

The Courant-Friedrichs-Lewy condition needs to be satisfied for the stability of the numerical scheme. According to this condition, the Courant Number (C_n) should be less than 1.

$$C_n = \frac{\text{Actual Wave Velocity}}{\text{Numerical Wave Velocity}} = \frac{|V| \pm c}{\Delta x / \Delta t} \tag{4.13}$$

3. Numerical Scheme

The MacCormak Scheme, an explicit two-step predictor-corrector scheme capable of capturing shocks, was employed as the numerical scheme in the model. The numerical scheme used in this analysis incorporated a backward finite difference scheme in the

predictor part, followed by a forward difference scheme in the corrector part (Kalita 2020; Baruah and Sarma 2021). The parameters estimated using the predictor step were incorporated into the corrector step. A Total Variation Diminishing (TVD) scheme was integrated, which suppresses the oscillations in the steep regions. The TVD variables were calculated from the computed hydrodynamic parameters in each iteration and are added in the steep gradients (Patowary and Sarma 2017). The following equations give the MacCormak Predictor Corrector scheme.

Predictor Scheme –

$$\frac{\partial U}{\partial t} = \frac{U_i^p - U_i^k}{\Delta t} \tag{4.14}$$

$$\frac{\partial F}{\partial x} = \frac{F_i^k - F_{i-1}^k}{\Delta x} \tag{4.15}$$

$$U_i^P = U_i^k - \frac{\Delta t}{\Delta x}\left(F_i^k - F_{i-1}^k\right) - S_i^k \Delta t \tag{4.16}$$

Corrector Scheme –

$$\frac{\partial U}{\partial t} = \frac{U_i^c - U_i^p}{\Delta t} \tag{4.17}$$

$$\frac{\partial F}{\partial x} = \frac{F_{i+1}^p - F_i^p}{\Delta x} \tag{4.18}$$

$$U_i^c = U_i^k - \frac{\Delta t}{\Delta x}\left(F_{i+1}^p - F_i^p\right) - S_i^p \Delta t \tag{4.19}$$

The value of U_i at the unknown time level k+1 is given by

$$U_i^{k+1} = \frac{1}{2}\left(U_i^p + U_i^c\right) \tag{4.20}$$

where Δt and Δx represent the temporal and spatial grid spacing in secs and m, superscript 'k' and subscript 'i' denotes the temporal and spatial axes, and the superscripts c and p represent corrector and predictor values, respectively.

4. Total Variation Diminishing (TVD)

The MacCormack Predictor Corrector Scheme can capture river flow's shock and strong discontinuities. However, dispersion error may result due to the second-order accuracy of the numerical scheme. This error can propagate erroneous oscillations, leading to an unstable solution. A Total Variation Diminishing (TVD) scheme is thus added to the Predictor Corrector scheme's final step to overcome this error. Thus, Equation 4.20 can be written as

$$U_i^{k+1} = \frac{1}{2}\left(U_i^p + U_i^c\right) + TVD \tag{4.21}$$

$$TVD = [G(r_i^+) + G(r_{i+1}^-)]\Delta U^k_{1+\frac{1}{2}} - [G(r_{i-1}^+) + G(r_i^-)]\Delta U^k_{i-\frac{1}{2}} \tag{4.22}$$

$$r_i^+ = \frac{\Delta A^k_{i-\frac{1}{2}}.\Delta A^k_{i+\frac{1}{2}} + \Delta Q^k_{i-\frac{1}{2}}.\Delta Q^k_{i+\frac{1}{2}}}{\Delta A^k_{i+\frac{1}{2}}.\Delta A^k_{i+\frac{1}{2}} + \Delta Q^k_{i+\frac{1}{2}}.\Delta Q^k_{i+\frac{1}{2}}} \tag{4.23}$$

$$r_i^- = \frac{\Delta A^k_{i-\frac{1}{2}}.\Delta A^k_{i+\frac{1}{2}} + \Delta Q^k_{i-\frac{1}{2}}.\Delta Q^k_{i+\frac{1}{2}}}{\Delta A^k_{i-\frac{1}{2}}.\Delta A^k_{i-\frac{1}{2}} + \Delta Q^k_{i-\frac{1}{2}}.\Delta Q^k_{i-\frac{1}{2}}} \tag{4.24}$$

The function G() in the Equation 4.22 can be expressed as –

$$G(x) = 0.5C[1 - \phi(x)] \tag{4.25}$$

$$\phi(x) = \max\{0, \min(2x, 1)\} \tag{4.26}$$

where φ(x) is the flux delimiter function

$$C = C_n(1\text{-}C_n) \text{ if } C_n \leq 0.5 \tag{4.27}$$

$$= 0.25 \quad \text{if } C_n > 0.5 \tag{4.28}$$

where Cn is the local Courant Number

$$C_n = \frac{(u + \sqrt{gh})\Delta t}{\Delta x} \tag{4.29}$$

where u is the velocity in m/s.

This section states the detailed analysis of the two independent models necessary to understand the characteristics of the reservoir outflow and its impact on downstream region. The reservoir operation and the hydrodynamic model were developed to check the alteration of the output hydrograph of the reservoir along with the estimation of the

flood levels at the downstream flood-prone section. However, to manage the reservoir operation based on the downstream flow situation, the two models need to be coupled for an integrated adaptive modelling system. The integrated modeling framework can be employed to devise management strategies for mitigating the downstream consequences of hydropower projects. During the lean period, the modelling framework can be utilized to generate multiple scenarios for determining the minimum EF. During the flood period, the integrated modelling approach with a pre-release strategy can be viable. The downstream flood level will modify the reservoir operating policy by releasing an additional pre-flood release within a forecast horizon without compromising the power generation. The modelling framework developed has other potential advantages of acquiring information like power production, spill volume, and the flood scenario downstream for different release decisions. The proposed model can also be utilized for sensor-based inflow in real-time and triggering flood warnings in the event of a flood. The development and application of the coupled model deciding management strategies for flood moderation is discussed in Chapter 7. The scope of applying this coupled model for evaluating the habitat suitability of an endangered aquatic species is presented in Chapter 8.

4.3 Validation of the Independent Models

In this section, the validation of both the reservoir operation model and the 1-D hydrodynamic model was conducted using the available observed data for RHEP. The RHEP being in operation made it was possible to obtain relevant downstream data for validating the models effectively.

4.3.1 Reservoir Operation Model

The reservoir operation model was first developed as per the methodology depicted in Section 4.2. A daily inflow sequence for the temporal window 2012-2020 was incorporated into the mathematical formulation of SOP. The model was validated with the available spill data using the following performance metrics.

1. Coefficient of Determination (R^2) :

$$R^2 = \left[\frac{N\left(\sum_{i=1}^{N} Q_o * Q_p\right) - \left(\sum_{i=1}^{N} Q_o\right)\left(\sum_{i=1}^{N} Q_p\right)}{\sqrt{\left[N\sum_{i=1}^{N} Q_o^2 - \left(\sum_{i=1}^{N} Q_o\right)^2\right]\left[N\sum_{i=1}^{N} Q_p^2 - \left(\sum_{i=1}^{N} Q_p\right)^2\right]}} \right]^2 \quad (4.30)$$

2. Nash Sutcliff Efficiency (NSE):

$$NSE = 1 - \frac{\sum_{i}^{N}\left(Q_{o,i} - Q_{p,i}\right)^2}{\sum_{i=1}^{N}\left(Q_{o,i} - \overline{Q_{o,i}}\right)^2} \quad (4.31)$$

3. Percent Bias (PBIAS):

$$PBIAS = \frac{\sum_{i=1}^{N}\left(Q_{o,i} - Q_{p,i}\right)}{\sum_{i=1}^{N}\left(Q_{o,i}\right)} \quad (4.32)$$

Q_o is the observed reservoir releases, $\overline{Q_o}$ is the mean of the observed reservoir releases, Q_p is the model simulated reservoir releases, and N is the sequence length.

Table 4.1: Performance Metrics of the observed and the simulated dataset.

R^2	NSE	PBIAS (%)
0.93	0.94	15

Model simulation is generally satisfactory if NSE >0.5, R^2>0.7, and PBIAS is ±25% (Moriasi et al., 2007). Table 4.1 shows the performance metrics of the observed and simulated reservoir releases. The values are within the satisfactory range. Figure 4.1 shows the comparative analysis of the observed and model-simulated reservoir releases.

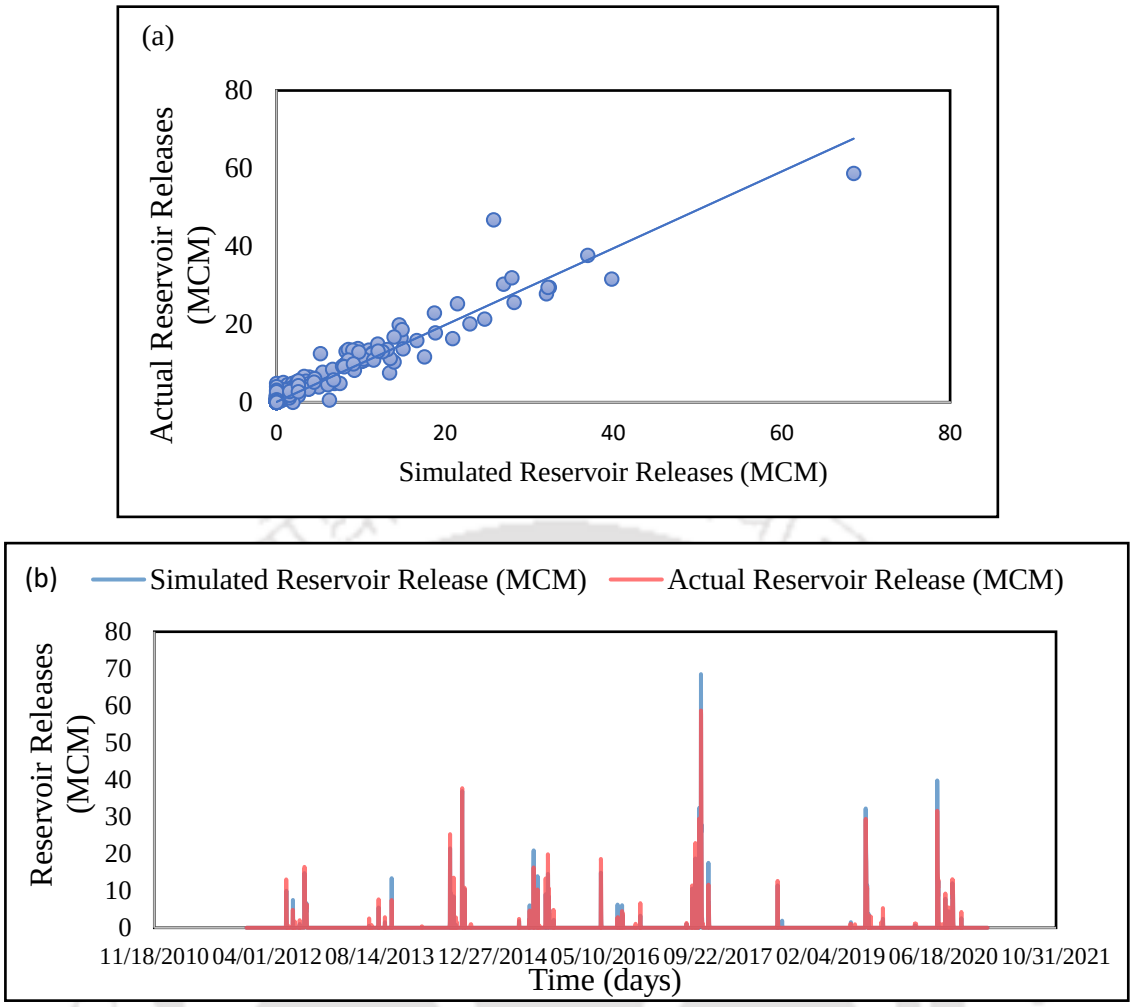

Figure 4.1:(a) Scatter Plot of actual and simulated reservoir releases in MCM (b) Time series plot of actual and model simulated reservoir releases

4.3.2 1-D Hydrodynamic Model

The 1-D hydrodynamic model explained in Section 4.2.2 was utilized to route the reservoir releases to estimate the downstream stage and discharge at NT Road Crossing. The model was validated for RHEP, as it is in operation. The computational time step of 2 secs and grid spacing of 500 m were considered in this analysis. The Manning's Roughness parameter *'n'* was taken as 0.03 based on a calibration with the observed downstream stage discharge. The stability of the model was checked by the CFL condition mentioned in Section 4.2.2, and the values were found satisfactory. Several trial hydrographs were incorporated into the model. The model was validated based on the observed stage discharge. However, as the corresponding hydrographs are not available, direct validation was not possible. The model-generated discharge values were compared with observed stage values and vice-versa. Figure 4.2 shows the simulated and observed

water surface elevations at 150 m^3/s, 354 m^3/s, 510 m^3/s. Figure 4.3 depicts the simulated and observed stage.

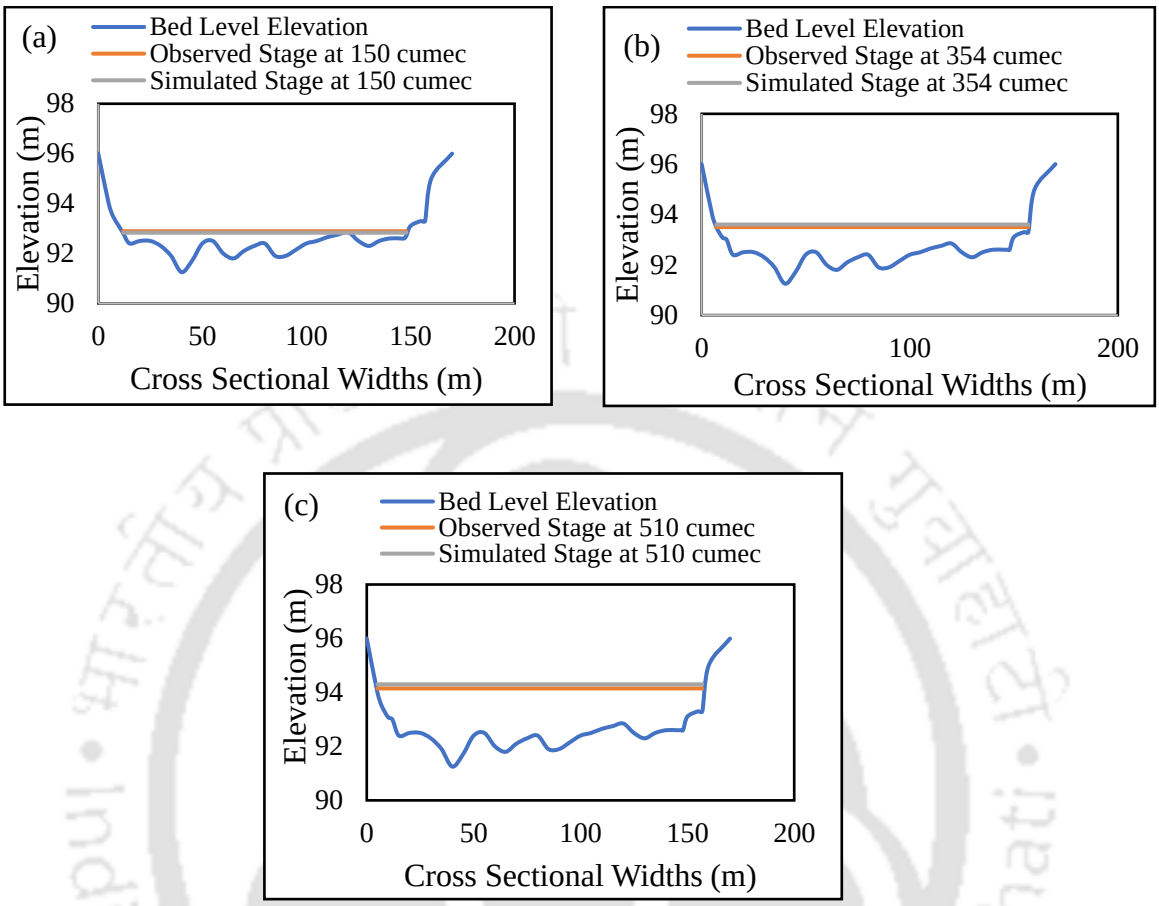

Figure 4.2: Water Surface Elevation at (a) 150 cumec (b) 354 cumec (c) 510 cumec

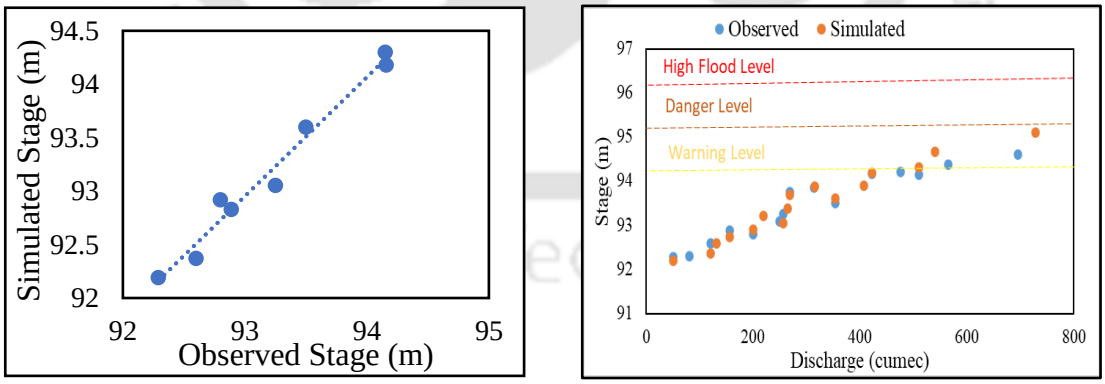

Figure 4.3: (a) Simulated and Observed Stage (b) Observed -Simulated Stage Discharge

4.4 Field Survey

A field survey was conducted on the downstream flood-prone section of NT Road Crossing, Lakhimpur, Assam. This survey aimed to assess the accuracy and reliability of a numerical model used to simulate flood events in the area.

The flood-prone reach is approximately 46 km downstream of the dam. In this region, areas are susceptible to flooding, and to protect against floodwaters, embankments have been constructed on both sides of the river. To ensure the finer accuracy of the bathymetry, a total station survey was carried out in this reach. Using the total station, elevation measurements were taken at various points along the river and the floodplain area. Figure 4.4 shows the photographs of the field survey conducted.

Figure 4.4: Photographs captured during the field survey.

4.5 Conclusions

This chapter has described the reservoir operation model and the hydrodynamic model developed for the simulation of the reservoir and its impact on downstream flow scenarios. The governing equations of the models, along with all the essential parameters, are described in this chapter. The source code of BRAHMA was utilized for the hydrodynamic analysis in the study, with several modifications performed. The model was validated for RHEP, as it is in operation. The reservoir operation model was first analyzed for daily operation and was validated with the actual data available. A field survey was conducted to obtain cross-sectional detail and was also focused on assessing the channel characteristics so that the logical value of the roughness parameter could be used. For the 1-D hydrodynamic model, several trial hydrographs were incorporated into the model. The model-generated discharge values were compared with observed stage values and vice-versa. The correlation coefficient of observed and simulated stages for the discharges was obtained as 0.96. The two models can be employed in any river system with a dam upstream. Chapter 5 depicts the application of the models on both LSHP and RHEP to characterize the reservoir outflow and its impact on the downstream section. Coupling the two models can effectively develop strategic management policies that can help the decision-maker. Details of this coupled model and its application are mentioned in Chapter 7 and Chapter 8.

5

Characterization of Downstream Flow of a Hydropower Dam

5.1 Introduction

Flooding due to sudden release from the dam is a grave concern, leading to disastrous situations downstream, particularly during high-intensity precipitation. Depending upon the needs and purpose, dams are classified into different categories, out of which hydropower, a source of renewable energy in electricity generation, is of utmost importance (Chernet et al. 2014). According to the International Hydropower Association (IHA), the total installed capacity was more than 1308 GW globally in 2019 (IHA 2020). Due to climate change and anthropogenic activities, floods and extreme precipitation are projected to increase in the future over different climatic regions (Tabari, 2020; Kim and Bae, 2020). Under climate change scenarios, in most global catchments, dams can reduce the frequency of floods and the extent of flooded areas (Boulange et al., 2021). Although the frequency of flooding decreases with a dam's presence, Extreme Rainfall Events (ERE) can cause substantial damage in downstream areas, leading to catastrophic events, and it is expected to increase in the near future due to climate and anthropogenic impacts (Guhathakurta et al., 2011; Banerjee and Dimri, 2019; Myhre et al., 2019; Chen et al., 2020). In August 2018, Kerala in India experienced a severe flood due to two major EREs. Before the rainfall events, the reservoir levels were almost near the Full Reservoir Level (FRL). The EREs and the reservoir level position worsened the situation and compelled the authorities to open the gates (Sudheer et al., 2019).

Dam operation methods are another important aspect that may change the hydrologic regime downstream (Kern et al., 2012; Kim et al., 2012; Cui et al., 2020). From the viewpoint of the disaster potential, there is still a lack of scientific analysis to get insight

into the extent of alteration a flood hydrograph can undergo due to dam operation. This often leads to contradictory claims from the downstream community, dam authority, and disaster manager. Sudden dam release often leads to flooding akin to flash floods. Flash floods are generally characterized by heavy rains, suddenness, and unpredictability, leading to rapid inundation of low-lying areas downstream in a short period (Georgakakos and Hudlow 1984; Ali et al., 2017; He et al., 2018; Mishra and Nagaraju 2021). The execution of strategic management plans and decision-making is challenging as massive flash flood events vary significantly in spatiotemporal characteristics (Stefanescu 2013; Silvestro et al., 2016; Zhai et al., 2021). Flash floods are typically differentiated from regional floods by the degree of flashiness and can be defined as the sudden rate of flow change from one magnitude to another (Poff et al. 1997; Caporali 2001). Baker et al., 2004 developed an index termed the Richard- Baker Index (RBI). This index is calculated for each water year as the sum of the absolute value of the difference between the first day and the previous day's flow divided by the sum of daily discharges. Flash floods are generally associated with a suddenness characteristic. The word ‘suddenness’ is closely related to the word ‘disaster.’ A natural event is composed of three major features: the magnitude of energy release, the frequency of occurrence, and the time factor i,e., the suddenness of the event (Kates, 1971). Recent advancements in science and technology have made the possibility of mapping the regions prone to natural disasters; however, a comprehensive response is lacking. Bryant (2005) ranked some of the world’s natural hazards based on temporal, spatial, socio-economic, and suddenness of onset. The ranking mapped the catastrophic events based on the mentioned factors. The suddenness of calamities often results in delayed, unplanned, and unscientific rescue operations, resulting in even greater loss (Guo, 2010). The sudden flooding, its degree of severity, and the frequency have a vast impact on people's mental health. In the aftermath of a severe flood event, individuals may experience symptoms of post-traumatic stress disorder (PTSD), depression, and anxiety. Secondary stressors like vacating a home following the flood, previous experience with flooding, and poor health are some factors associated with greater psychological distress (Mason et al. 2010).

This chapter explores the characterization of downstream floods considering pre-dam and post-dam scenarios. The analysis was first carried out for LSHP with a hypothetical flood hydrograph. With the presence of a dam, the reservoir was operated to achieve maximum

power production with the given inflow hydrograph. SOP was utilized as the reservoir operation policy in this analysis. The releases, consisting of power releases and spills, were checked with different initial storages within the active storage zone. The upstream hydrograph was then compared with the different reservoir outflow hydrographs to check the flashy characteristics. Hydrographs thus generated using the reservoir simulation model were routed using a 1D hydrodynamic model to study the downstream flood levels. The models were also employed in RHEP as well to check changes in the flashiness characteristic in the presence of the dam. Based on the degree of severity and suddenness, temporal and spatial extent, and the socio-economic impact, the ranking was assigned to the dam-induced flood, regional and flash floods among the global hazards. With the available downstream streamflow data of RHEP, the streamflow alteration was analyzed considering pre-dam and post-dam conditions.

5.2 Methodology

The outflow hydrographs from the reservoir were analyzed to check the flashy characteristics of the hydrographs at the immediate downstream and far downstream sections from the two dam sites selected. The first dam site considered was the LSHP. The downstream flood was checked for two scenarios-first without dam (natural flow condition) and second with dam condition. Considering without dam scenario, the upstream hydrograph was directly routed to the downstream flood-prone region with a 1-D hydrodynamic model. The hourly time series of the reservoir releases were mainly the spill and power release. The outflow from the reservoir was assigned as the inflow boundary condition into the 1-D hydrodynamic model to route the flow to the downstream flood-prone area. The releases from the reservoir were checked with different initial storages within the active storage. The overall impact of the reservoir on the downstream flooding was quantified using the reliability factors. Reliability, in general, is the probability that the system is in a satisfactory state (Hashimoto et al. 1982). The Flooding Protection Reliability (F.R) is the probability that the water levels at the downstream section are below the flood levels. The F.Rs were checked for all the initial storages considered in this study. The flashy characteristics of the outflow hydrographs were checked using a Flashiness Index (F.I.). To make a more generalized index to map the degree of severity, SDFI was developed and applied to both LSHP and RHEP. Figure 5.1 shows the flowchart of the methodology adopted for the analysis of F.I.

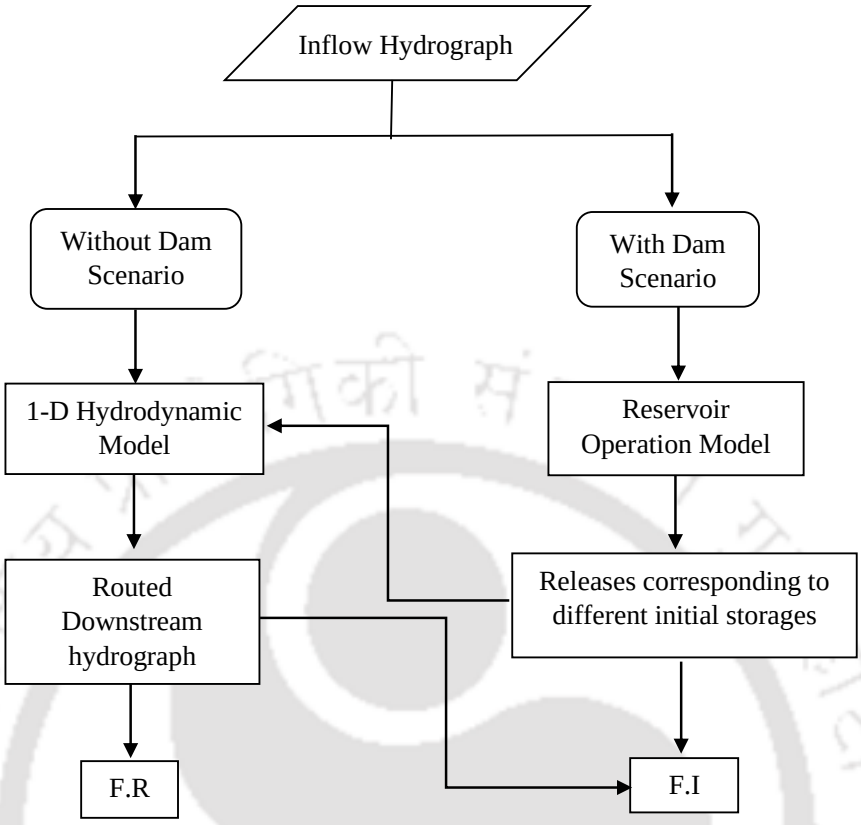

Figure 5.1: Methodology Adopted in the Study

5.2.1 Flood Protection Reliability (F.R)

The concept of system reliability is widely used in the field of water resources systems and is implemented in the decision-making process. Reliability, in general, is the probability that the system is in a satisfactory state (Hashimoto et al. 1982). The F.R. reflects the ability of the system that the water levels at downstream flood-prone areas are below the flood level. The F.R. for this hourly analysis is checked by Equation 5.1.

$$F.R. = 1 - \frac{N_f}{N} \tag{5.1}$$

where N_f = No. of times the downstream water level is greater than the flood level and N = Total no. of time periods.

5.2.2 Flashiness Index (F.I.)

In this analysis, an event-based hourly reservoir operation was conducted. The flashiness here is mapped by analyzing the slope of the rising limb. Flash flood hydrographs are characterized by steep rising limbs and a small-time lag. The F.I. is

calculated for reservoir releases at the immediate downstream section and at far downstream section. The average slope of the rising limb is given by Equation 5.2.

$$\frac{dQ}{dt} = \frac{Q_p - Q_i}{t_p - t_i} \tag{5.2}$$

(F.I.) is then calculated by

$$F.I. = \frac{\frac{Q_p - Q_i}{Q_i}}{\frac{t_p - t_i}{\Delta t}} \tag{5.3}$$

Q_p is the peak discharge, Q_i is the initial discharge, t_i is the initial time, t_p is the time at peak discharge, $\triangle t$ is 1 hr. Figure 5.2 shows the characteristic parameters of a flood hydrograph.

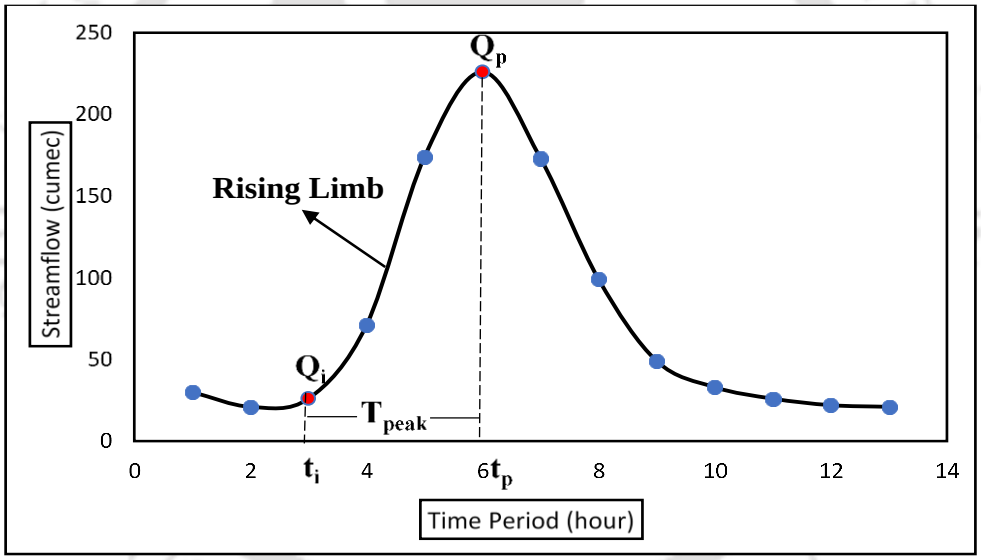

Figure 5.2: Various parameters of a hydrograph

As per Equation 5.3, the Flashiness Index is a more case-specific index. This index is very sensitive to the initial flow. If the initial flow is considerably less than the peak flow, then the numerical value of this index can be more than unity and very high. Thus, this index will provide a higher numerical value of flashiness in an IBWT hydropower project as the flow is diverted to a different river, and the initial flow of the river under consideration can become very low. Although this numerical value indicates the severity of flashiness characteristics, prov ing becomes difficult. Thus, the Index is more suitable to compare flashiness characteristics of the same river in different time periods or to

analyze a dam's impact on its downstream because of reservoir operation. Therefore, a more generalized index SDFI was developed to determine the flashiness of different flood events as shown in Equation 5.4.

$$SDFI = \frac{Q_p - Q_i}{Q_p} * \frac{t_i}{t_p} \tag{5.4}$$

While applying this equation in the case of multiple peaks, the events should be isolated and analyzed as a single flood event. The flashy characteristics of the LSHP and RHEP flood hydrographs were quantified using the SDFI.

5.2.3 Ranking of Dam-Induced Floods among Global Hazards

Bryant (2005) ranked some of the global natural hazards based on the various factors in Annexure I. A total of 31 hazards were rated using a Likert scale of 1-5, where 1 and 5 represent the most significant and the least important factors, respectively. The factors include the degree of severity, period of the event, spatial extent, total death toll, economic consequences, social disruption, long-term impact, lack of prior warning or suddenness of onset, and the number of associated hazards. The overall socio-economic physiological effect of the hazard was ranked using these criteria.

Hazards were ranked based on the summation of the Likert scale scores assigned to the mentioned factors of each hazard. The ranking of the global natural hazards was then obtained, with the least additive score occupying the highest rank. The hazards were assessed subjectively and listed in order based on the scale assigned. As the ranking of the hazards was prepared for world hazards, it will differ for individual countries and latitudes. For instance, based on the degree of severity, death toll, and socioeconomic loss, the most common hazards in the United States are tornadoes and hurricanes. Similarly, China is highly susceptible to flooding at a large scale based on the mentioned factors. The Additive Likert Scale Scores are equivalent to some of the natural hazards. In such cases, prioritization was emphasized on the factors while collecting the global hazard statistics.

5.2.4 Streamflow Alterations due to the presence of the dam

The presence of a hydroelectric dam can alter the streamflow downstream. A streamflow downstream of RHEP was analyzed based on the available data considering

the pre-dam and post-dam conditions. The whole data series was fractionated into two parts. The first part consists of the streamflow dataset before the dam's operation. The second part represents the dataset posterior to the dam operation. The dam operation was initiated in the year 2003. Hence, 2000-2002 was considered the pre-dam condition, and 2003-2012 was the post-dam condition. Regarding flow magnitude, the annual mean, the daily minimum, and the daily maximum flow values were differentiated considering the two conditions. The flashy characteristics of daily streamflow were also evaluated using the Richard-Baker Flashiness Index (R-B Index)(Baker et al., 2004). The R-B Index scaled the flashiness of the streamflow by assessing the daily streamflow rate of change summed up over a water year as per Equation 5.5. The high value of the R-B Index indicates high flashy characteristics.

$$\text{R-B Index} = \frac{\sum_{i=1}^{n} |q_i - q_{i-1}|}{\sum_{i=1}^{n} q_i} \tag{5.5}$$

where q_i is the streamflow on an i^{th} day, and q_{i-1} is the streamflow on the i-1 day.

The seasonal variation was checked for both conditions. The variation was analyzed for monsoon, pre-monsoon, post-monsoon, and winter periods. The monsoon period was considered for July-September, the post-monsoon from October-December, the lean period from January-March, and the pre-monsoon period from April-June. The FDC of the pre-dam and post-dam conditions were developed, corresponding to the various seasons.

5.3 Results and Discussion

5.3.1 Analysis of flow characteristics without dam scenario

Hydropower reservoir systems are generally operated monthly, ten daily, or, at best, daily. In conventional analysis, a short-duration flood event goes unnoticed. To foresee how upstream flash flood occurring during the regional flood gets amplified through a hydropower dam, the reservoir needs to be simulated hourly. The lack of short-duration flow data in interior project areas, particularly in developing countries, hinders such analysis. The inflow hydrograph of a 48-hour flood event was routed downstream to check the flooding situation and its characteristics using a 1-D hydrodynamic model.

Cross-sectional data were available for the downstream portion and were used along with the SRTM DEM of 30 m resolution to generate the terrain data for the hydrodynamic model. The d50 value was taken from the study of particle size distribution and found to be 0.2 mm (DHI Report, 2019). The corresponding Manning's n value is calculated using Strickler's equation and used in the analysis. The inflow hydrograph was assigned at the upstream boundary, and the friction slope was assigned at the downstream section. The downstream water levels were calculated from the routed hydrograph considering the available stage-discharge relationship. The flood levels were then checked from the generated water levels. Figure 5.3 shows the upstream hydrograph and the routed hydrograph in natural flow conditions, i.e., without dam conditions. The flood peak attenuation (Q_a) of 188.00 m^3/s and 270.59 m^3/s was observed for the first and the second flood peak, respectively.

The water levels at downstream sections were assessed from the stage-discharge relationship considering the routed downstream flow hydrograph. If the downstream level exceeds the level of 97 m, then it is counted as a flood event. Considering hourly observation of flood possibility status, it was observed that the water level exceeds the flood level of 97.00 m 16 times in 48 hours of continuous observation.

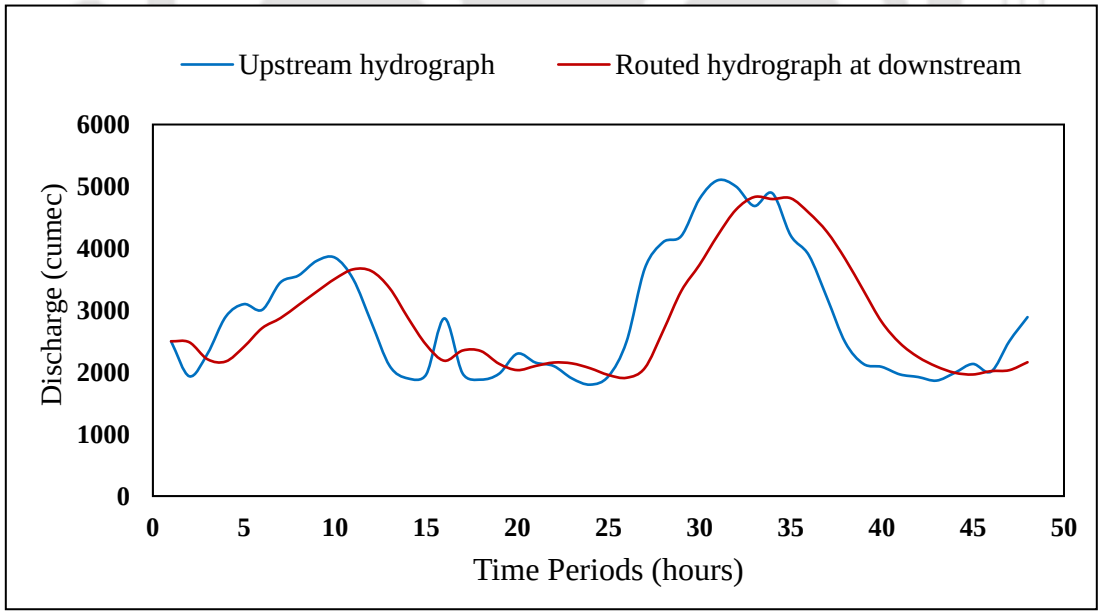

Figure 5.3:Routed hydrograph downstream without considering the dam

The F.R was thus found to be 0.6. It is worth mentioning that this index was used to compare reliability with and without dam conditions, and it does not represent absolute

reliability, as flood protection provided by the embankment was not considered in this study.

5.3.2 Analysis of flow characteristics with dam scenario

The power generation hour of LSHP can go as high as 24 hours during the flood period (Ray and Sarma, 2011). In this analysis, subject to water availability, the turbines were allowed to be operated for 24 hours daily. The dam release consists of spill and power release. The initial storages were selected within the active storage of the reservoir, i.e., from dead storage (720 Mm^3) to the gross storage (1365 Mm^3). The model simulation showed that the reservoir begins to spill when the initial storage reaches 1305 MCM, below which the reservoir release is only power. Thus, the spill increases with the increase of the initial storage. Figure 5.4 (a) shows the total reservoir outflow corresponding to different initial storages. The releases from the reservoir were routed to the flood-prone area 13 km downstream of the dam site, corresponding to different initial storages. The flood levels were observed when the water level at the downstream section was above the specified flood level. The flood protection reliability at the downstream area was assessed using Equation 5.1 and was checked for different initial storages. The downstream water levels calculated from the 1-D hydrodynamic model indicate that the levels exceed the flood level when the spilling starts. Considering the scenarios mentioned, Figure 5.4 (b) shows the different routed hydrographs downstream. At FRL, i.e., at gross storage 1365 Mm^3, the first peak rises with an attenuation of 245.00 m^3/s compared to the downstream inflow hydrograph peak.

(a)

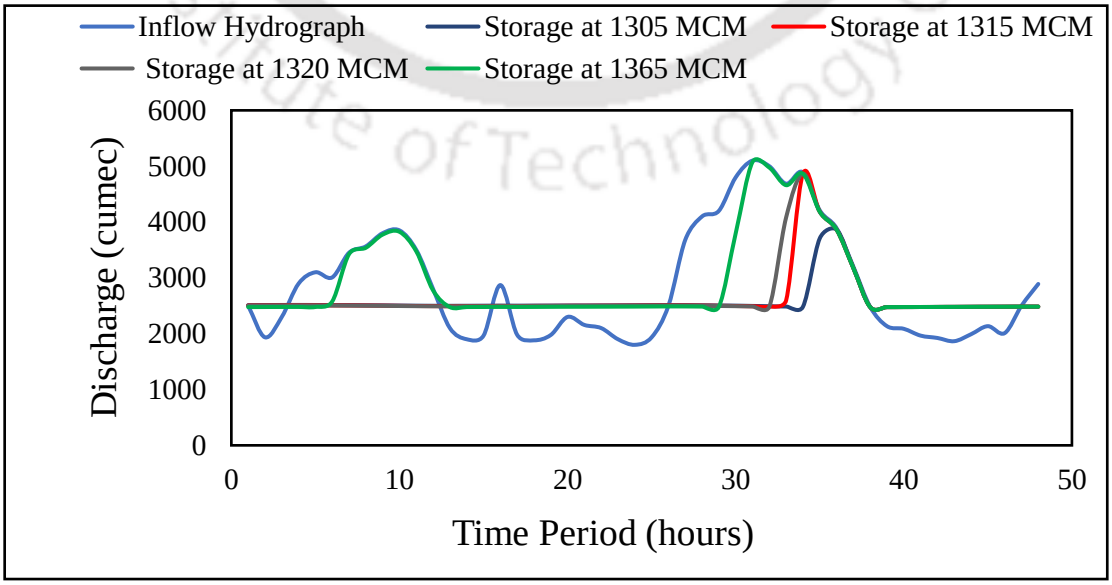

(b)

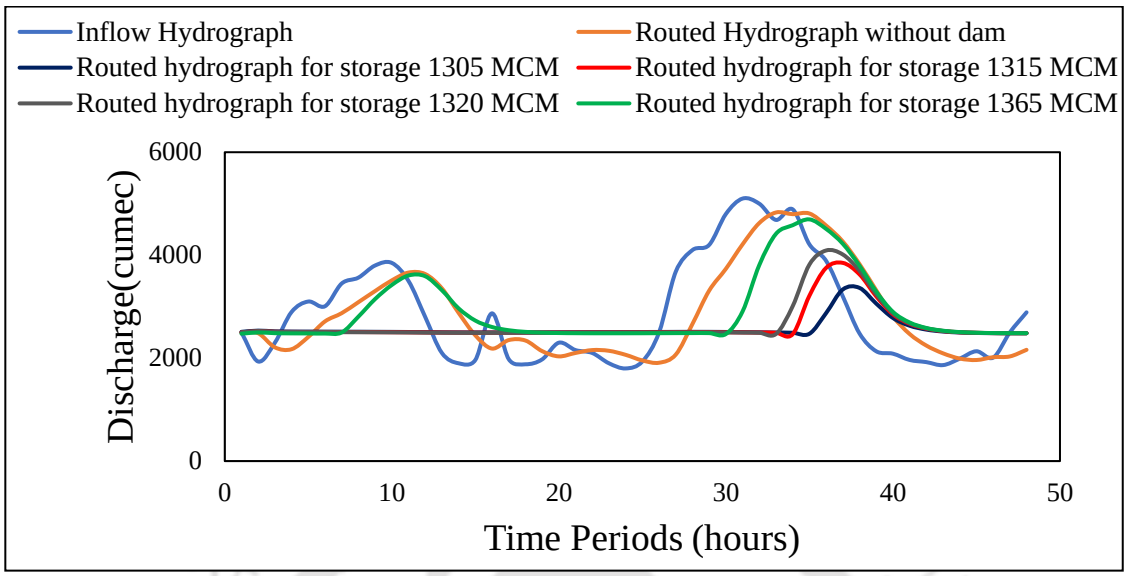

Figure 5.4: (a) Total reservoir outflow with different initial storages. (b) Routed hydrographs in downstream considering with-dam and without-dam scenarios

The flood peak attenuation Q_a and the percentage peak attenuation of the second flood event compared to the peak of the inflow hydrograph are shown in Annexure II. Annexure II shows that the percentage of flood peak attenuation is lowered with the increase in the reservoir's initial storage. The second flood peak in natural flow condition was 5100 m^3/s, and the peak of the reservoir outflow when it is at its gross storage was 5074.70 m^3/s. At FRL, the percentage of peak attenuation at 13.00 km downstream concerning the inflow hydrograph is 7.9%, and without the dam, the percentage peak attenuation was observed as 5.3%. This shows that when the reservoir level is at FRL, although the peak reduces marginally as compared to the no dam condition, the magnitude remains almost the same as that of the natural flood condition.A decreasing trend of F.R can be observed with the increasing initial storages shown in Table 5.2.

Table 5.1:F.R corresponding to different initial storages

Initial Storages (Mm^3)	No. of Flood Count	F.R
720	0	1
880	0	1
970	0	1
1050	0	1
1270	0	1
1305	2	0.95
1315	3	0.93
1320	4	0.91
1365	12	0.75

5.3.3 Analysis of the flashy characteristics

1. Flashiness Index (F.I.)

The index was calculated using Equation 5.3 for both scenarios, considering the two flood peaks at the upstream and downstream sections. For natural conditions, the inflow hydrograph is the flow hydrograph at the upstream section, routed directly to the downstream section using the hydrodynamic model mentioned in Section 2.3. Thus, F.I. for no dam condition at the upstream section was calculated from the inflow hydrograph. For with dam scenario at the upstream section, F.I. was calculated from the reservoir outflow hydrographs corresponding to the various initial storages. These outflow hydrographs from the reservoir were then routed to the downstream section to check the corresponding F.I. Table 5.2 shows the F.I. and T_p for the first flood peak for the immediate downstram section. The F.I. for with-dam and without-dam scenarios was estimated as 0.1.

The T_p for the natural condition was observed as 8 hours, whereas it changed to 5 hours for with dam scenario. From this, it can be assessed that although the F.I. is the same for both scenarios, an abrupt change in the T_p is observed.

Table 5.2: F.I. and Tp for the first flood peak at the immediate downstream section

	F.I.	T_p (hours)
Without Dam Scenario		
Natural Flow Condition	0.1	8
With Dam Scenario		
Initial Storage at 1365 Mm^3	0.1	5

Table 5.3: F.I. and Tp for the second flood peak at the immediate downstream section

	F.I.	T_p (hours)
Without Dam Scenario		
Natural Flow Condition	0.26	7
With Dam Scenario		
Initial Storage at 1305 Mm^3	0.27	2
Initial Storage at 1315 Mm^3	0.47	2
Initial Storage at 1320 Mm^3	0.48	2
Initial Storage at 1365 Mm^3	0.52	2

In natural conditions, i.e., without the dam, the F.I. was estimated as 0.26 in the upstream section, as shown in Table 5.3, and a value of 0.21 was obtained in the downstream section. The value of T_p was calculated as 7 hours in both sections. With the presence of the dam for the second flood peak at the immediate downstream section F.I. ranges from 0.27 when the reservoir starts spilling to a significant value of 0.52 when it reaches its total capacity shown in Table 5.3.

For the downstream section, F.I. and T_p were calculated from the routed hydrographs. The F.I. was calculated as 0.098 and 0.1 in natural flow conditions and with dam scenario, respectively.These values shows that F.I. and Tp for the first flood peak at the downstream flood-prone section. The T_p changes from 7 hours in natural flow conditions to 4 hours with the presence of the dam (vide Table 5.4).

Table 5.4: F.I. and Tp for the first flood peak at the downstream flood-prone section

	F.I.	T_p (hours)
Without Dam Scenario		
Natural Flow Condition	0.098	7
With Dam Scenario		
Initial Storage at 1365 Mm^3	0.1	4

Table 5.5: F.I. and Tp for the second flood peak at the downstream flood-prone section

	F.I.	T_p (hours)
Without Dam Scenario		
Natural Flow Condition	0.21	7
With Dam Scenario		
Initial Storage at 1305 Mm^3	0.11	3
Initial Storage at 1315 Mm^3	0.18	3
Initial Storage at 1320 Mm^3	0.21	3
Initial Storage at 1365 Mm^3	0.22	3

Table 5.5 shows for the second peak at the downstream flood-prone section, the values of F.I. range from 0.11 to a value of 0.22, corresponding to the routed hydrographs when the initial storages are at 1305 Mm^3 and the gross capacity, respectively.

This indicated that at the downstream section, owing to the presence of a dam, a substantial hydrologic alteration of the streamflow can be observed from the values of F.I. The F.I.s increases with the increment of the initial reservoir levels. At the downstream flood prone section, as the flow moves downward, although the flashy characteristic seems to be attenuated, an increasing trend is observed with the F.I. when the reservoir levels increase. The value of F.I. will magnify if there is a catchment contribution with high-intensity precipitation occurring downstream.

On the other hand, a meager reduction of the flood peak at FRL can be observed, maintaining the same magnitude as that of the natural or regional flood. Thus, without much attenuation of magnitude cataclysmic capability of the regional flood is sustained.

It is observed that the with-dam scenario exaggerates the flashy characteristic significantly as compared to without dam scenario, which is gradual. This flashiness of the hydrograph increases with the rise in the initial storage levels and hence depends on the regional flood situation. Thus, from the viewpoint of disaster characterization, an associated auxiliary factor, 'suddenness,' gets associated with the natural flood with the presence of a dam.

2. Standard Flasiness Index (SDFI)

As discussed in Equation 5.4, the F.I. is modified to make it more generalized. The SDFI has been applied in LSHP and RHEP, considering the initial storage at FRL. The index has been checked for the inflow hydrograph at the immediate downstream and far downstream sections. For LSHP, the far downstream is located 13 km from the dam site with no tributary contribution. In the case of RHEP, there are two major tributary contributions at the far downstream section.

Figure 5.5 shows the SDFIs of the hydrograph at different locations of the LSHP. The inflow hydrograph was routed to the downstream section using a 1-D hydrodynamic model. It can be assessed that the magnitude of SDFI is higher at the immediate downstream section and at the far downstream section than in the natural condition.

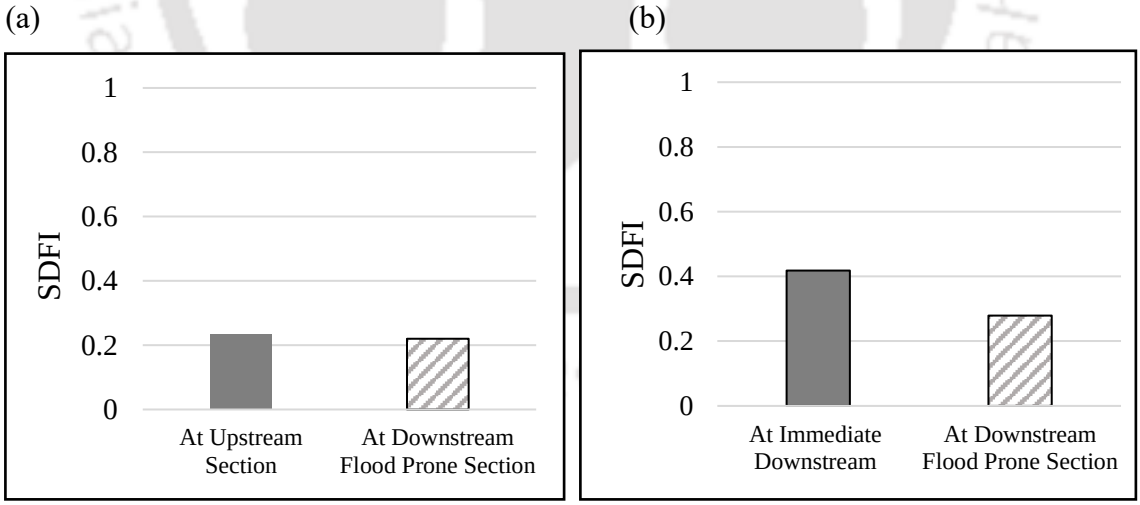

Figure 5.5: SDFI for the second flood event at different locations of LSHP (at FRL) (a) Without Dam Condition (b) With Dam Condition

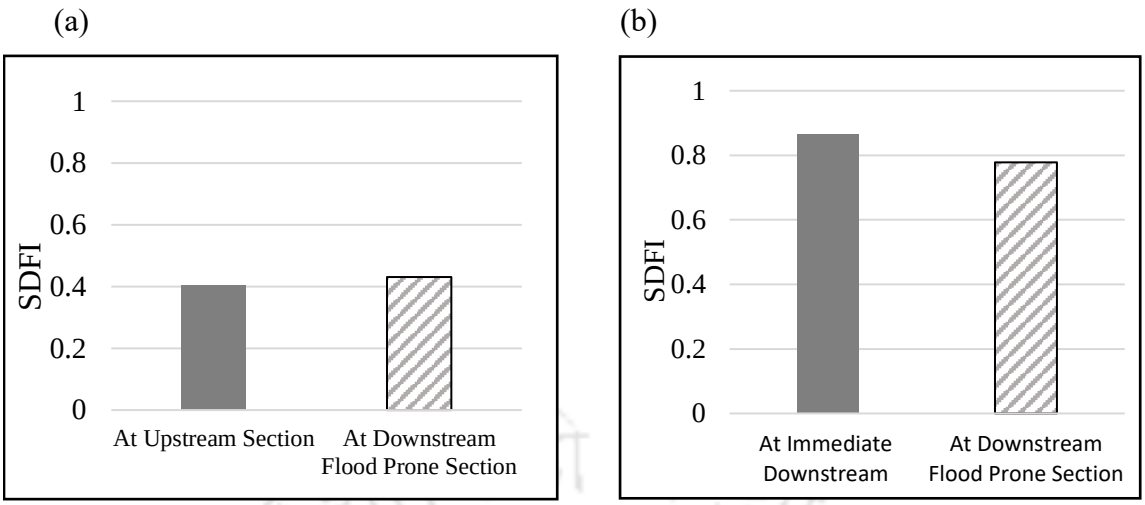

Figure 5.6: SDFI for a flood event at different locations of RHEP (at FRL) (a) Without Dam Condition (b) With Dam Condition

A similar observation can be seen in the case of the IBWT hydroelectric project (RHEP). Figure 5.6 shows the SDFIs of the flood hydrograph at different locations of RHEP. In RHEP, the rate of change of streamflow is substantial. The reservoir releases sharply increased from a minimum flow of 6 m^3/s to 375.3 m^3/s within 3 hours. As a result, the severity of the flood increases. Thus, in the case of both hydel projects, the dam's presence alters the inflow hydrographs, thereby increasing the hazardous potential of the flood.

5.4 Ranking of Dam-Induced Flood

As per the prioritization, regional flood and flash flood occupy the 3rd and 20th positions, respectively, as shown in Annexure I. The hazards associated with anthropogenic factors are not included in the list. With the increasing demand for power, hydropower production is now becoming unavoidable. Unlike dam break disasters, flooding downstream during dam release is now almost a regular phenomenon. It is also associated with the natural phenomenon of regional floods and upstream torrential rain. Therefore, dam-induced flood, though related to anthropogenic activity, is a combination of regional and flash floods.

In other words, a hydropower dam induces the suddenness factor in a regional flood event. Therefore, considering the suddenness and other factors of the regional flood is essential to evaluate the hazard potential of flood downstream of a dam. Following the ranking mentioned in Section 5.2.3 and allotting the same significant scores of regional

flood and flash flood as Bryant gave, prioritization of Dam Induced Flood is established among the global natural hazards. The rank of dam-induced flood needs to be considered to occupy the second-highest position in the global natural hazard list, as shown in Table 5.6, with an additive Likert Scale score of 15.

Although the rank of the flash flood has attained 21st among the hazards, the most significant factor dominating flash floods is suddenness. For this reason, flash floods can potentially induce severe damage to life and property. The sudden release from the dam has the same impact as the flash floods and the effect of the regional flood; as such, dam-induced flood occurs during high monsoon having the condition of the regional flood**.** Sudden water level fluctuation can also cause river bank failure, and progressive bank failure can eventually cause the embankment to fail. The lack of prior warning can lead to devastating damage downstream, leading to fear psychosis among the dwellers.

Table 5.6: Ranking of Dam-Induced Flood considering Bryant's factors

Rank	Event	Additive Likert Scale Score
2	Dam Induced flood	15
4	Regional flood	18
21	Flash flood	35

5.5 Streamflow alterations on an existing operational hydroelectric project

The preceding analysis states that for a proposed hydropower dam, it was concluded that the presence of a hydropower dam enhances the flashy characteristics of the reservoir release, increasing the intensity of flash floods downstream. This finding is significant as it suggests that the dam's operation has adversely affected downstream hydrology and flood conditions.

In the case of the operational hydropower project RHEP, an IBWT hydropower project, the dam's downstream impact is evident. Streamflow alteration caused by the dam's

presence was investigated by comparing pre-dam and post-dam conditions using available streamflow data. This comparison allows a clearer understanding of the dam's influence on downstream water flow patterns.

5.5.1 Streamflow alterations due to the presence of the dam

A significant decrease in the annual mean flows can be observed in the post-dam scenario compared to the pre-dam scenario, as shown in Figure 5.7. In 2000, the annual mean flow was around 118 m^3/s, reduced to 69 m^3/s in 2012. A similar trend can be observed in the minimum flow of the river. The minimum daily flow decreased from 28 m^3/s observed in 2001 to 0.84 m^3/s observed in 2011 shown in Figure 5.8. This shows that a severe streamflow alteration was observed downstream in the post-dam scenario. In the daily peak flow case, uneven streamflow fluctuation was marked. In the post-dam condition, a peak flow of 728 m^3/s and 179 m^3/s were observed in 2005 and 2006, respectively, as shown in Figure 5.8.

Figure 5.9 shows the pre-dam streamflow observed in 2000 and two post-dam streamflows in 2008 and 2012. In the post-dam, sudden spikes in the peak flow can be observed compared to the pre-dam. This test indicates that the sudden release from the dam leads to flash floods at downstream of the dam.

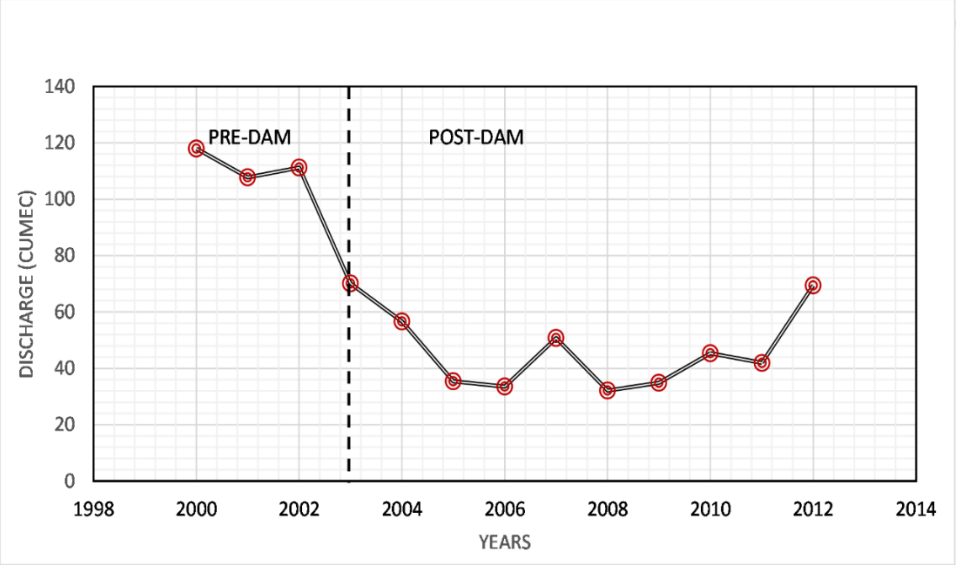

Figure 5.7:Annual Mean Flow observed in pre-dam and post-dam condition

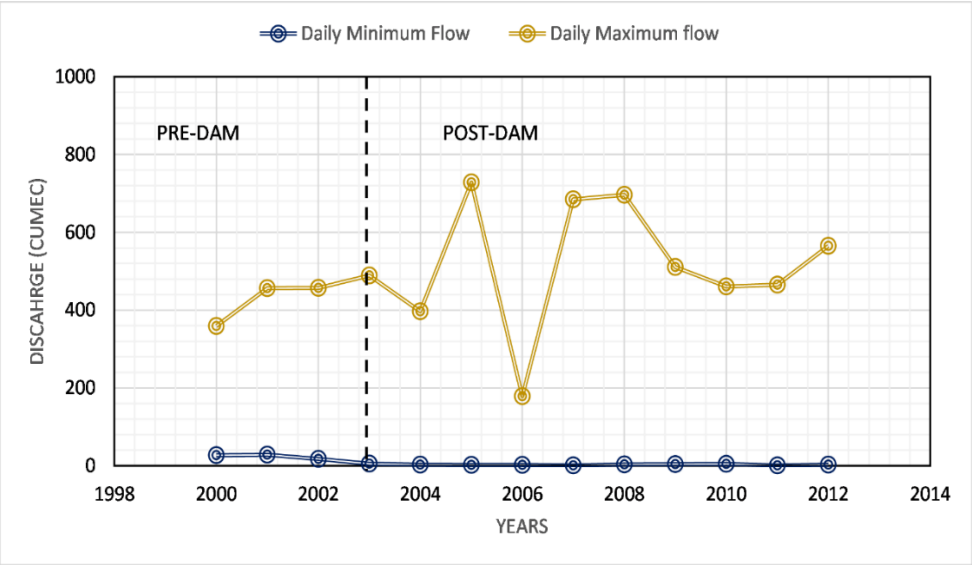

Figure 5.8: Daily Minimum and maximum daily flow observed in pre-dam and post-dam conditions

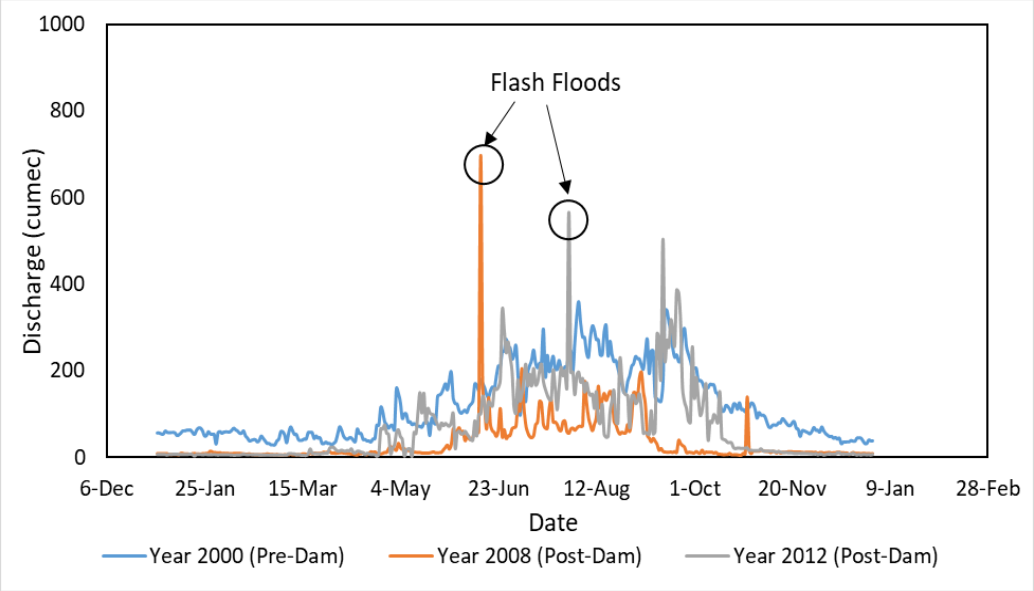

Figure 5.9: Pre-dam and Post-Dam Streamflow

Figure 5.10 shows the R-B Index calculated over a year to check the degree of flashiness. It can be seen that the R-B Index increased from 0.12 in 2000 to a maximum of 0.4 in 2005. Thus, a substantial increment of the flashy characteristic of the streamflow can be observed.

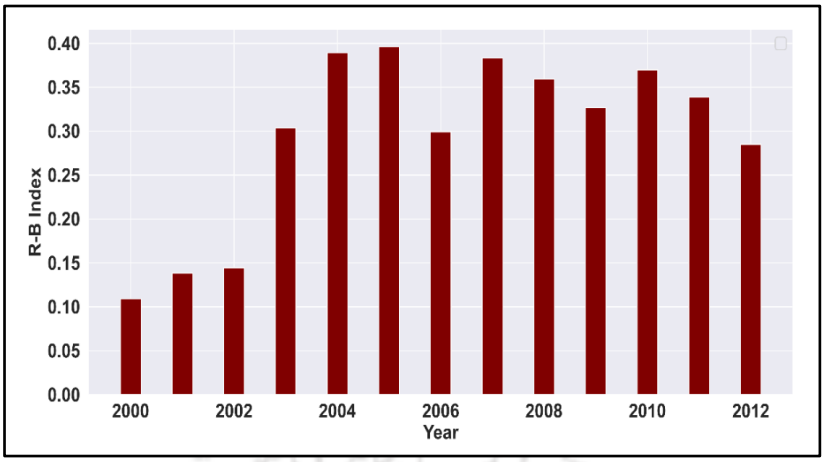

Figure 5.10: R-B Index observed in pre-dam and post-dam condition

5.5.2 Seasonal Variation of Streamflow

A significant variation can be observed from the FDCs in all the seasons of both conditions. From Figure 5.11, it can be assessed from the FDCs that the flow has depleted substantially in all the seasons in the post-dam state compared to the pre-dam state. Significant flow depletion can be observed in the Winter and Pre-Monsoon periods. This flow depletion has exacerbated the negative impacts on the riparian ecosystem and the downstream communities. Thus, minimum flow downstream is needed to nourish the downstream ecosystem. This can be achieved by releasing environmental flow from the dam.

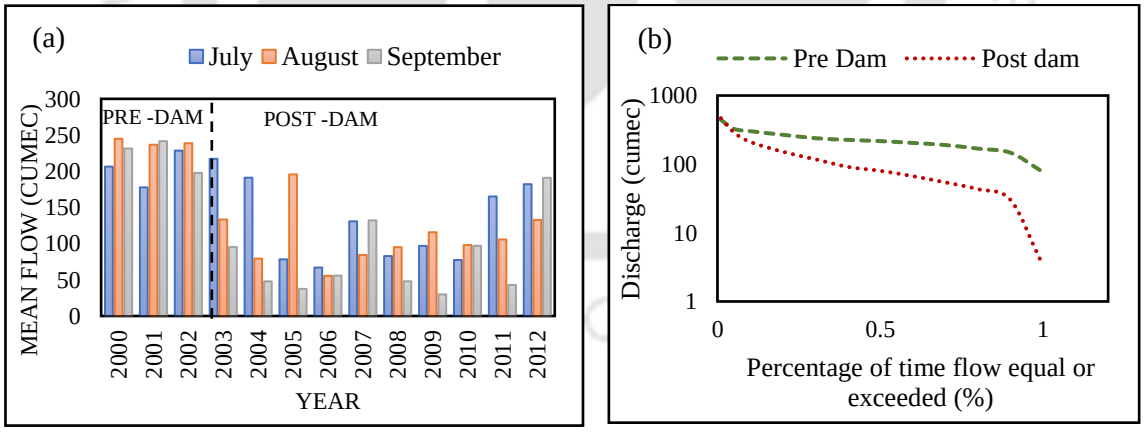

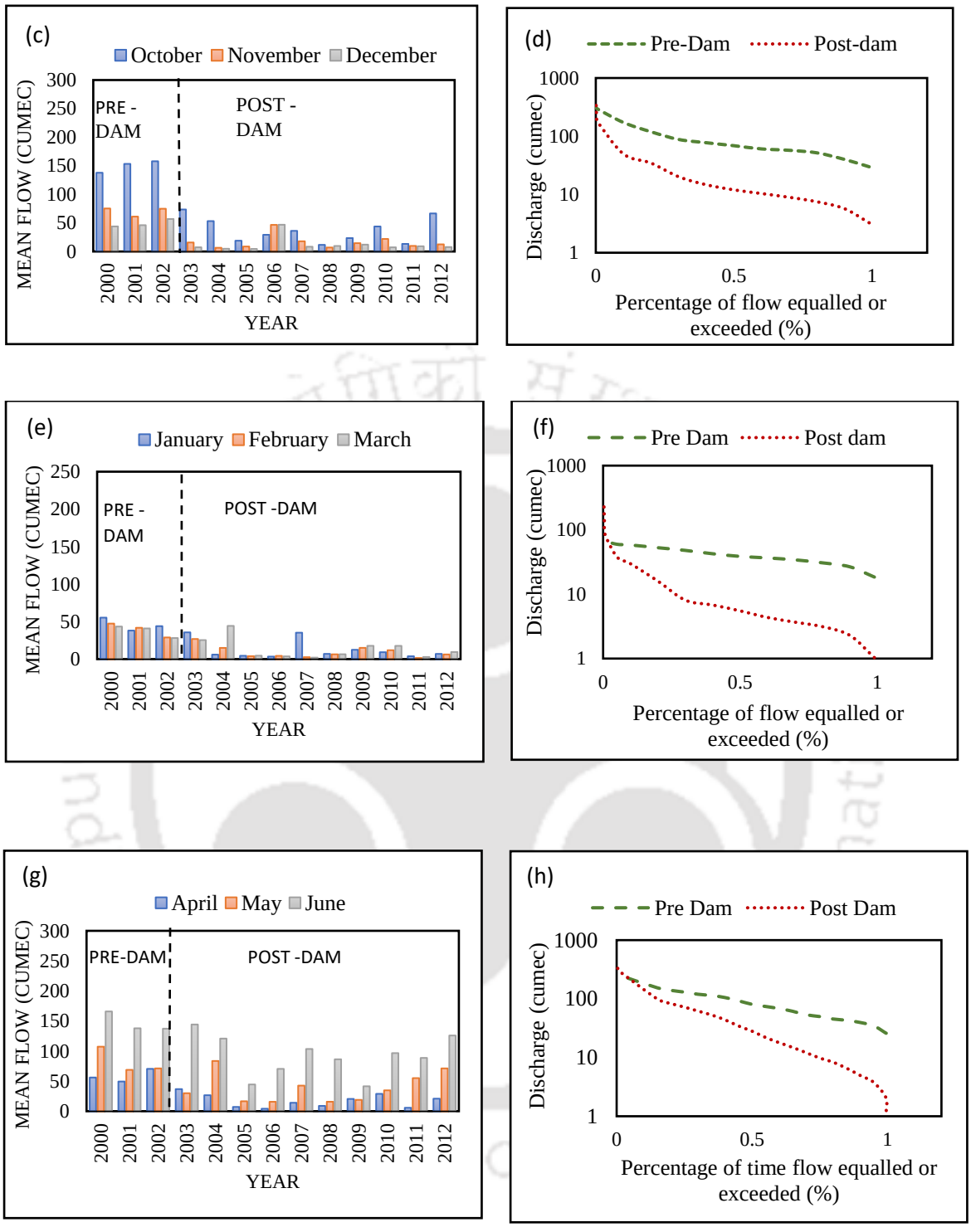

Figure 5.11 : (a) Mean Flow in the Monsoon Period (b) Flow Duration Curve of Monsoon Period (c) Mean Flow in the Post Monsoon Period (d) Flow Duration Curve of Post Monsoon Period (e) Mean Flow in the Winter Period (f) Flow Duration Curve of Winter Period (g) Mean Flow in the Pre-Monsoon Period (h) Flow Duration Curve of Pre-Monsoon Period

5.6. Conclusions

In this chapter, a comparative analysis of downstream flood scenarios for both with and without the presence of a dam is presented, considering a proposed hydroelectric project. Different initial storages were considered while analyzing the downstream flood in the presence of a dam. The study inferred that although the frequency of flooding with the presence of a dam gets reduced. The magnitude of the peak remains almost the same as that of the regional flood, and the flashy characteristics of the outflow hydrograph increase alarmingly. The F.I.s increases from a meagre value of 0.26 for the natural condition to a high value of 0.52 with the existence of the dam filled up to its full reservoir level at the dam site. At the downstream flood-prone section, although the values of F.I. decrease, an increasing trend of the magnitude can be observed with the increase of initial storage of the reservoir. The analysis also shows an abrupt decrease in the peak time. The time to peak decreases from 7 hours to 2 hours with the insertion and operation of the dam, thus reducing the rescue time for disaster managers or the disaster response time by 5 hours. The study introduced the F.I. which is a case-specific metric and exhibits a high sensitivity to the initial flow conditions. The numerical value can be very high if the initial flow is considerably lower than the peak flow. Therefore, this index is better suited for comparing the flashiness of the same river at various time periods. Consequently, a more generalized metric, SDFI, was developed to assess the flashiness of diverse flood events. The SDFI has been implemented in both the NIBWT and IBWT hydropower dams. Results showed that the magnitude of SDFI increases in the with-dam condition as compared to the without-dam condition in the case of both NIBWT and IBWT hydropower dams.

As dam-induced flood is a combination of regional and flash floods, a comparative analysis was performed to rank the dam-induced flood considering Bryant's factors. The study concludes that dam-induced floods will take the second highest rank in the global hazard ranking list based on the factors. Agreement to this logical ranking will go a long way in redesigning flood disaster management policy downstream of a hydropower dam.

With this inference, an analysis of streamflow variation downstream of the dam was conducted on an operational IBWT hydroelectric project. The streamflow alteration was analyzed considering the pre-dam (natural state) and the post-dam (present) states. The results indicate that the flow during the dry period has decreased alarmingly with the

dam's presence. The minimum discharge was lowered to 0.84 m^3/s in the present state from 28 m^3/s in the pre-dam condition. The R-B Index rose from 0.12 in the pre-dam condition to a maximum of 0.4 in the post-dam condition, indicating the increment of flashy characteristics during the wet period. This depicts the severity of streamflow alterations, which implies the necessity of EF from the dam to sustain the aquatic biodiversity. The detail has been discussed in Chapter 8.

The analysis was conducted for two distinct hydropower projects: LSHP, which is a proposed NIBWT hydropower project, and RHEP, an operational IBWT hydropower project. The primary focus of LSHP involved the characterization of dam releases and the evaluation of their downstream effects in flood-prone regions. However, the downstream consequences are not observable, given the project's current proposed status. For RHEP, being an operational project, the analysis aimed to assess the evident downstream impact resulting from the presence of the dam using the models. The practical significance of analyzing RHEP lies in the opportunity to apply management strategies directly in the field. In subsequent chapters of the thesis, all analyses were centered around RHEP.

6

Flow Assessment at Downstream of a Hydropower Dam in Ungauged Areas

6.1 Introduction

Hydroelectric power serves as a dependable, renewable, and environmentally-friendly means of generating electricity. Although it is designated as the clean, flexible source of economic development in a region (Berga 2016), there are myriad negative impacts of dams on the riverine ecosystem (de Carvalho Barreto et al. 2020; Marak et al. 2020; Zolfagharpour et al. 2022) and socio-economic aspects of the downstream communities. The sites of the hydropower dams are primarily located on hilly terrain for higher head generation. The immediate downstream areas, in most cases, are located in the deep gorge and remote areas. The far downstream areas are mostly valley regions composed of habitation and settlements susceptible to flooding. The gauge stations of streamflow measurement are primarily available in downstream locations.

Flash floods in hilly areas due to short-duration high-intensity precipitation are among the most catastrophic natural disasters (Azmeri et al., 2016 ; Kansal and Singh. 2022). In case of a flash flood due to a short-duration high-intensity rainfall event, a pondage hydropower dam cannot attenuate such flood events. Thus, the risk associated with the sudden release from the dam amplifies, which may lead to the breaching of embankments in the downstream areas. Dam-induced flood combines regional and flash floods occupying the second position among the global hazards as depicted in Chapter 5. Thus, dam operation methodology requires more scientific investigation to satisfy the reservoir rule curves (You and Cai. 2008; Wang et al., 2021; Xu et al., 2021). Flood modelling on

a catchment scale does not rely solely on the release hydrograph from the reservoir. Several other contributions, including the lateral flow from major tributaries and rainfall at downstream areas, add to the total flow contribution at the downstream flood-prone areas. It is imperative to know how the flow is progressively increasing towards the downstream areas by adding flow contribution at the confluence point with the release hydrograph from the dam. Thus, determining optimum model parameters employing optimization algorithms is vital in water resources planning and management (Maier et al., 2014; Yildiz and Vrugt. 2019).

The major challenge in quantifying lateral flow contribution is that most tributaries are ungauged. Getting a conventional gauging station of lateral flow contribution in remote areas is difficult. Researchers have adopted several methodologies in the last few decades to estimate streamflow in the ungauged catchment, including hydrologic models (Tsegaw et al., 2019; Althoff et al., 2022), regionalization method (Gibbs et al., 2012), flow duration method (Nruthya and Srinivas 2015). However, implementing the mentioned models requires meteorological data and various catchment-based parameters. Nagesh Kumar et al. (2010) calculated the downstream flow contribution by subtracting the routed reservoir release from the downstream flow data. The lateral flow was incorporated into the hydrologic routing model using the Muskingum method. O'Donnell (1985) proposed a Muskingum Model that can include lateral flow contribution into its governing equations of storage and continuity. Further researchers incorporated lateral flow in the Nonlinear Muskingum Model (Karahan et al., 2015; Spiliotis et al., 2021). Spada et al., 2017 implemented the reverse routing technique using the MAST 1D hydraulic model to estimate the hydrograph and the lateral flow hydrographs in the main channel, assuming the lateral inflow to be concentrated in small confluences. Hydrodynamic software like HEC RAS and MIKE 11 can incorporate lateral flow as an additional boundary condition of flow hydrograph where the lateral flow contribution is significant (Andrei et al., 2017). The quantification of the flow contribution of the tributary to the mainstream is necessary to incorporate into the models. The Drainage Area Ratio (DAR) method is the commonly used hydrological methodology that does not require additional information other than the streamflow of the donor catchment. In several regional studies, the DAR method has accurately predicted the streamflow of the ungauged catchments (Gianfagna et al., 2015; Asquith et al., 2006).

This chapter describes a modelling framework that applies a reservoir operation and a hydrodynamic model to estimate flood downstream of a dam incorporating the flow contribution of ungauged tributaries located downstream using the DAR method. Generally, inflow to the reservoir is gauged, and geospatial analysis can determine the catchment area contributing to the reservoir inflow. In the practical field, an improved flood forecasting model incorporating other ungauged significant contributions will help in more effective communication between disaster management authority downstream and dam authority to make an optimal decision. Thus, improving the precision of the flood forecasting model for an efficient and reliable flood warning system is essential. The basic assumption adopted in this framework is that the precipitation characteristics in hilly terrain at the dam's upstream and downstream sites are similar. Therefore, the flow contribution of a tributary located in the inaccessible hilly area downstream of the dam can be estimated by applying the DAR method based on their catchment areas. The discharge of the ungauged tributaries was thus calculated using the DAR method. The model parameters were estimated using various optimization algorithms. The best model parameters were then obtained using the error metrics. The modelling framework described in Chapter 4 was then employed with hourly reservoir inflow hydrographs to examine the flood levels at the downstream section. The lateral flow hydrographs were incorporated as the intermediate boundary conditions at the main channel's sections where the tributaries join. Two scenarios were checked, considering the model a) without lateral flow contribution and b) with lateral flow contribution, and compared.

6.2. Materials and Methods

6.2.1 Methodology

This analysis proposes a modeling framework that involves the reservoir operation model and a hydrodynamic model with significant contributions from ungauged tributaries using the DAR method. The optimal model parameters were estimated using optimization algorithms. The model calibration and validation was done using the available daily downstream data. Two inflow events of 2012 that occurred on 25/6/2012 (moderate) and 14/9/2012 (high), labeled as Event 1 and 2, respectively, were utilized in the study. A comparative analysis was performed to check the increase in the peak flow considering a) lateral flow contribution and b) without lateral flow contribution. The

simulated stage-discharge was then compared with the observed downstream stage discharge data. Figure 6.1. shows the flowchart of the methodology adopted.

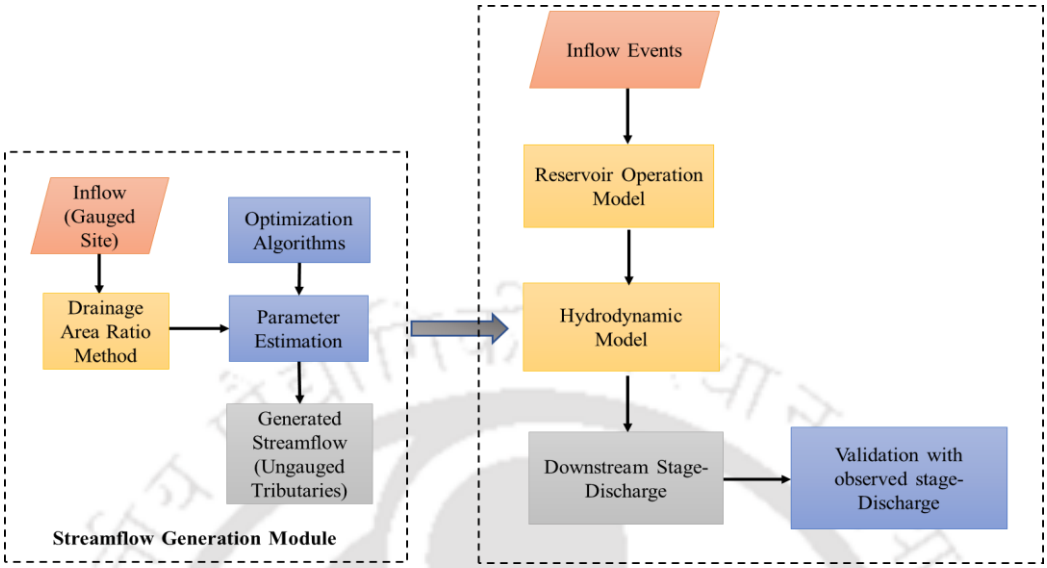

Figure 6.1 : Flowchart of the methodology adopted

6.2.2 Total Downstream Flow

The total flow downstream of a Hydroelectric Power Project constitutes the discharge release for power generation, reservoir spill, and contribution from lateral flow if tributaries exist between the dam site and the downstream section. Equation 6.1 gives the expression of the total downstream flow.

$$DF = R + S_p + Q_l \tag{6.1}$$

DF is the total downstream flow, R is the discharge release for power generation, S_p is the spill from the reservoir, and Q_l is the lateral flow contribution.

The total downstream flow of the RHEP comprises of spill from the reservoir and lateral flow contribution as power release is diverted to Dikrong Basin. Hence, Equation 6.1 can be written as

$$DF = S_p + Q_l \tag{6.2}$$

6.2.3 Assessment of Lateral Flow Contribution

6.2.3.1 Drainage Area-Ratio Method

The DAR is the widely used method of estimating flow in an ungauged catchment when a hydrologically similar gauged catchment is present. The underlying principle of this methodology states that the streamflow from the gauged watershed can be transferred to the ungauged watershed, considering the drainage area ratio of the gauge to the ungauged watershed.

The mathematical expression of DAR is as per Equation 6.3.

$$Q_y = \left(\frac{A_u}{A_g}\right)^{\alpha} Q_g \tag{6.3}$$

Q_y is the streamflow of the ungauged catchment, Q_g is the streamflow of the gauged catchment, A_u is the area of the ungauged catchment, A_g is the area of the gauged catchment, α is the exponent factor of the model for systematic adjustment in the drainage area ratio to the flow ratio. The exponent factor ' α ' ranges from 0-1, where the 0 value depicts the drainage area ratio will not affect the streamflow of the catchment, the value 1 describes the streamflow ratio, and the area ratio of the catchments is directly proportional to each other.

The method depicts that the flow is directly proportional to the catchment area. The choice of the reference gauge can be ascertained by the geographic proximity of the catchments or by clustering the catchments possessing the same hydrologic responses.

The central hypothesis in this analysis is that the DAR will more accurately predict the daily streamflow of the ungauged catchment when the rainfall is uniformly distributed in the catchments.

Ranganadi Basin consists of two gauged sites, one at the upstream site of the dam used for inflow monitoring. The other site is 46 km downstream of the dam at NT Road Crossing, Lakhimpur. The downstream gauged site cannot be utilized to transfer streamflow to the ungauged catchment as it constitutes regulated flow released from the dam. Thus, in this analysis, the upstream gauged site is used to transfer flow to other ungauged sites. Two lateral flows join the main channel of Ranganadi, as shown in Figure

6.2. The first tributary joins the main channel at around 12 km from the dam site, and the second tributary meets the main channel at 31 km from the dam site. Thus, the expanded form of the downstream flow with two major lateral flow contributions adopted in the analysis is shown in Equation 6.4.

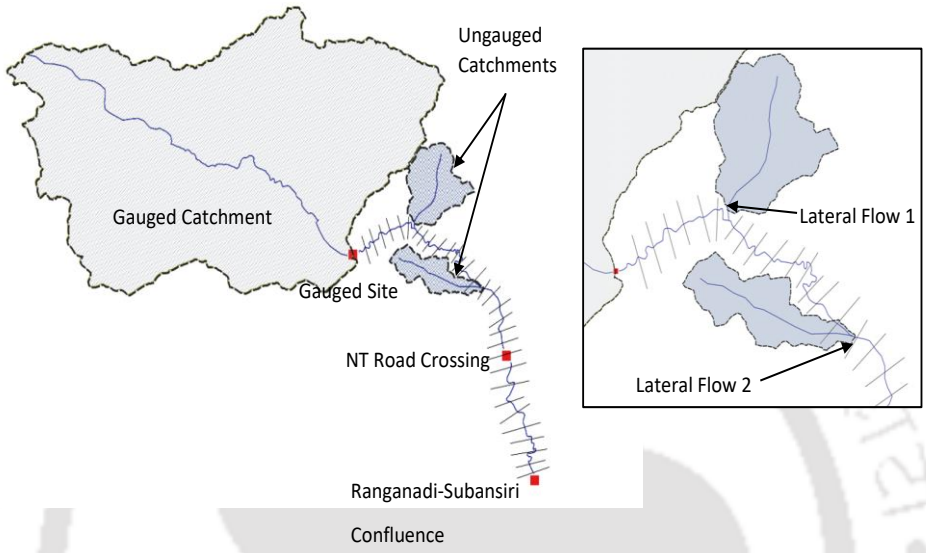

Figure 6.2: Lateral Flow Contributions to the main channel of the case study area

$$DF = S_p + Q_{y_1} + Q_{y_2} \tag{6.4}$$

$$DF = S_p + \left(\frac{Au_1}{A_g}\right)^{\alpha_1} Q_g + \left(\frac{Au_2}{A_g}\right)^{\alpha_2} Q_g \tag{6.5}$$

Q_{y1} and A_{u1} are the flow contribution of the first tributary and Q_{y2} and A_{u2} are the flow contribution of the second tributary, α_1 and α_2 are the model parameters.

The Shuttle Radar Topography Mission (SRTM) of the 30 m spatial resolution Digital Elevation Model (DEM) was analyzed to delineate the watersheds.

6.2.3.2 Parameter Estimation

The magnitude of the model exponent factor ' α ' can be determined by regression analysis from the reference gauged site depending on the hydrological responses of the

catchments. The parameters 'α_1' and 'α_2' were approximated by minimizing the sum of square errors between the observed and predicted downstream flow values.

The objective function is defined as –

$$\text{Minimize } Z = \sum_{i=1}^{N} (DF_{o,i} - DF_{p,i})^2 \tag{6.6}$$

Subject to:

$$0 \leq \alpha_1 \leq 1$$
$$0 \leq \alpha_2 \leq 1$$

where Z is the objective function, DF_o is the observed streamflow downstream, DF_p is the predicted downstream flow, and N is the sample size.

Multiple algorithms have been employed for the optimum parameter in MATLAB and Excel environments. For the MATLAB environment, the algorithms implemented are- fmincon, Genetic Algorithm (GA), and Particle Swarm Optimization (PSO). For the Excel environment, GRG Nonlinear was implemented. A comparative analysis was then conducted to identify the best values using the Performance Indices (RMSE, SSE, NSE).

1. Nonlinear Optimization

A solver based nonlinear optimization MATLAB function *fmincon* can optimize constrained nonlinear objective function. *fmincon* is a reliable and efficient function with high computational efficiency (Chuan et al., 2014). It is capable of finding the minimum of a function with linear and non-linear inequality, equality constraints, and bound constraints. *fmincon* can also incorporate user-defined Hessian information (Ji and Shao, 2021). The iterative process initiates with an initial guess and terminates when all the conditions are met. It offers various algorithms, including interior- -point, trust-region method, active-set, etc. Although *fmincon* is a robust optimization algorithm, the function has certain limitations. The main limitation is its sensitivity to the initial guess. If the initial point considered is far from the optimal minimum, it may converge to a local minimum instead of a global minimum. Thus, the initial point should be carefully considered for a reliable solution.

2. Genetic Algorithm (GA)

Genetic Algorithm (GA) is a heuristic search method formulated by Holland in 1975 based on biological evolution. The GA process includes selection, crossover, and mutation to obtain the population with the best generation chromosomes. The optimal solution is arrived at with the population evolving over successive generations (Katoch et al. 2021). Unlike the gradient method, they have no requirement for differentiability, convexity, continuity of the objective, and constraints. However, the execution time required by GA is more than the other evolutionary algorithms. GA is directly applicable to unconstrained problems. However, during the past few decades, several methodologies were proposed for handling constraints by GA (Yeniay, 2005)

3. Particle Swarm Optimization (PSO)

PSO is a more recent bio-inspired heuristic search approach for an optimal solution in the solution space. Recently, the algorithm has been widely implemented in the field of water resources and hydrology (Zhang and Zhang 2021). The algorithm solves an objective function considering the population of candidate solutions termed particles. The particles move in the search space influenced by their position and velocities. The motion of a particle will give the best local position. The solution set is updated with better solutions with other particles moving in different directions and velocities. PSO and GA are similar algorithms in the sense that the two algorithms are population-based search methods. PSO is faster and more reliable in handling continuous problems than GA (Hassan et al. 2005).

4. Generalized Reduced Gradient (GRG)

GRG technique is a nonlinear form of the simplex method of linear programming (LP) developed by Ladson et al. 1978. It is suitable for problems with equality and inequality constraints. The algorithm performs a line search that can solve a system of nonlinear equations at each step (Bhattacharjya 2011; Zakwan 2018). The algorithm explores the entire search space by updating the decision variables to improve the objective function by satisfying all the constraints. Two techniques are used to determine the GRG solve search direction, including quasi-Newton and the conjugate gradient method. The variables are separated as basic variables and non-basic variables. The computational efficiency of the GRG nonlinear algorithm is very fast compared to evolutionary

algorithms (Barati 2013; Zakwan et al. 2017). One limitation of the algorithm is the sensitivity to the initial guess. So, the initial guess should be considered with a thorough knowledge of the search space.

6.2.3.3 Performance Metrics

Performance Metrics were utilized in this analysis to evaluate the best parameters from the mentioned algorithms. Based on the evaluation of the metrics, rankings were assigned to the algorithms. Following are the details of the performance metrics used in the analysis.

1. Root Mean Square Error (RMSE)

$$RMSE = \sqrt{\frac{\sum_{i=1}^{N}\left(DF_{o,i} - DF_{p,i}\right)^2}{N}} \tag{6.7}$$

2. Sum of the Square Error (SSE)

$$SSE = \sum_{i=1}^{N}\left(DF_{o,i} - DF_{p,i}\right)^2 \tag{6.8}$$

3. Nash Sutcliffe Efficiency (NSE)

$$NSE = 1 - \frac{\sum_{i}^{N}\left(DF_{o,i} - DF_{p,i}\right)^2}{\sum_{i=1}^{N}\left(DF_{o,i} - \overline{DF_{o,i}}\right)^2} \tag{6.9}$$

6.3 Results and Discussion

6.3.1 Assessment of lateral flow contribution

The geospatial analysis of the study area enunciated that the drainage areas of Tributary 1, Tributary 2, and the Gauged Site were 82.46 km^2, 49.09 km^2, and 2449.9 km^2, respectively. As stated in Chapter 3, Section 3.3.2 shows two years of common inflow and downstream data. Hence, the model was calibrated and validated for 2011 and 2012, respectively. The optimal parameters obtained from the calibration phase were then used for the model validation phase. Table 6.1 shows the optimal model parameters obtained using the mentioned algorithms in Section 6.2.3.2. The prioritization of the

algorithm was done based on the magnitude of the Performance Metrics. Among the algorithms utilized in the analysis, the lowest RMSE value was observed with GRG Nonlinear both in the calibration and validation phase, whereas the highest value was observed with GA in the calibration and validation phase. A similar observation can be detected in the case of SSE. In the case of PSO, an RMSE value of 47.13 with an NSE of 0.51 was observed in the calibration phase, whereas 46.91 was observed in the validation phase with an NSE value of 0.71. Thus, PSO showed a good agreement in the validation phase compared to the calibration phase. In terms of computational efficiency, the execution time taken by GRG nonlinear was found to be 0.8 secs, whereas the execution time taken by GA was 733.7 secs, which depicts the requirement for more computational efficiency and time. This analysis prioritizes the algorithms based on the error metrics used. The ranking of the algorithms showed that GRG Nonlinear occupies the highest rank based on the Performance Metrics in both calibration and validation periods. Hence, the optimal parameters obtained from the GRG Nonlinear algorithm were used as the model parameters. Thus, the GRG technique has been found to be a reliable and efficient tool among all the algorithms implemented in the study. Again, the GRG nonlinear algorithm is easy to implement without complex mathematical formulation. From the analysis, the computational efficiency of the GRG nonlinear algorithm is very fast compared to the other algorithms.

The α_1 and α_2 values obtained are 0.24 and 0.26, respectively. Hence, the lateral flow contribution as per Equation 6.3 for Tributary 1 is $0.44Q_g$, and for Tributary 2 is $0.36Q_g$. This implies that the total flow contribution by Tributary 1 is 44% of the gauged streamflow, and the contribution by Tributary 2 is 36% of the gauged streamflow. Thus, the tributaries contribute a substantial amount of flow to the main channel. This relationship was adopted in the hourly analysis while routing the flood hydrograph downstream. The lateral flow hydrographs determined were then incorporated into the 1D hydrodynamic model as the intermediate boundary conditions. Figure 6.3 shows the observed and simulated discharge at the downstream section.

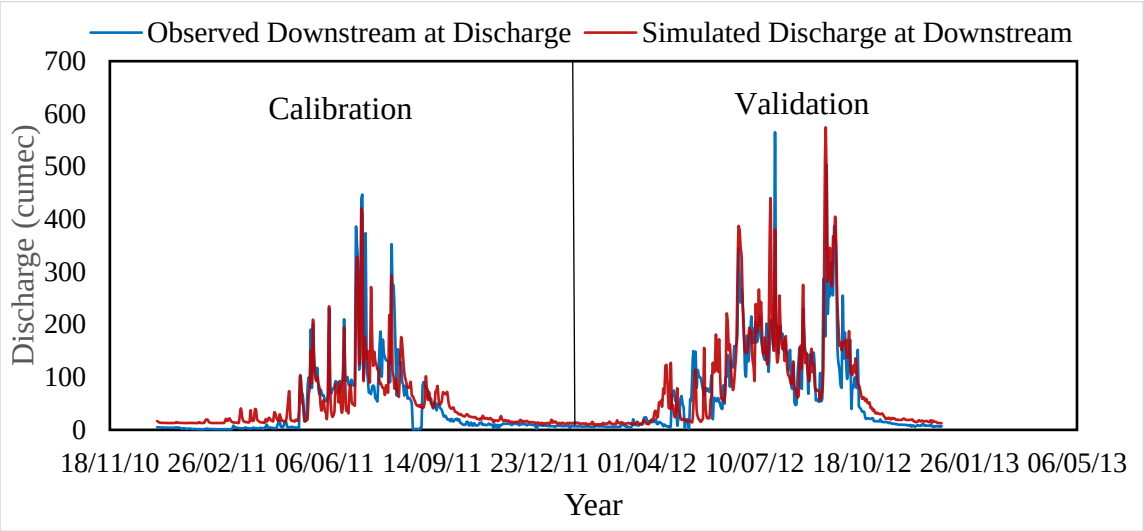

Figure 6.3: Observed and Simulated Discharge at Downstream

6.3.2 Application of the model with DAR

The model was incorporated with hourly inflow events. In RHEP, three power generation units can run continuously during the flood period for 24 hours. Figures 6.4 (a) and (b) show the inflow hydrographs, reservoir spill, and hourly power generation for Event 1 and Event 2, respectively, obtained from the reservoir operation model. In both cases, 405MW per hour of power was generated for 80 hours using the mentioned operating policy.

Two scenarios were adopted while adopting the hydrodynamic model- a) without lateral flow contribution and b) with lateral flow contribution. For the first inflow event, the maximum peak flow generated from the model was calculated as 181.2 m^3/s and 321.9 m^3/s, corresponding to Scenarios 1 and 2, respectively. For the second flood event, the simulated maximum peak flow was calculated as 300.5 m^3/s and 530.3 m^3/s for Scenario 1 and 2, respectively. The hydrographs downstream for both scenarios are shown in Figure 6.4. The flood peak increment factor was determined by Equation 6.10.

Table 6.1:Parameters Obtained from the Calibration and Validation of the Model using different algorithms

	Calibration					Validation				
Algorithm	**α_1**	**α_2**	**RMSE**	**SSE**	**NSE**	**RMSE**	**SSE**	**NSE**	**Execution Time (secs)**	**Rank**
GRG	0.24	0.26	35.01	448631.2	0.76	46.76	800277.1	0.7	0.8	1
Nonlinear Optimizion	0.45	0.45	46.46	790256.6	0.53	47.82	836951.4	0.69	1.62	2
PSO	0.94	0.28	47.13	813209	0.51	46.91	805400	0.71	117	3
GA	0.53	1	57.51	1210798	0.28	52.15	996515.3	0.62	733.7	4

(a) (b)

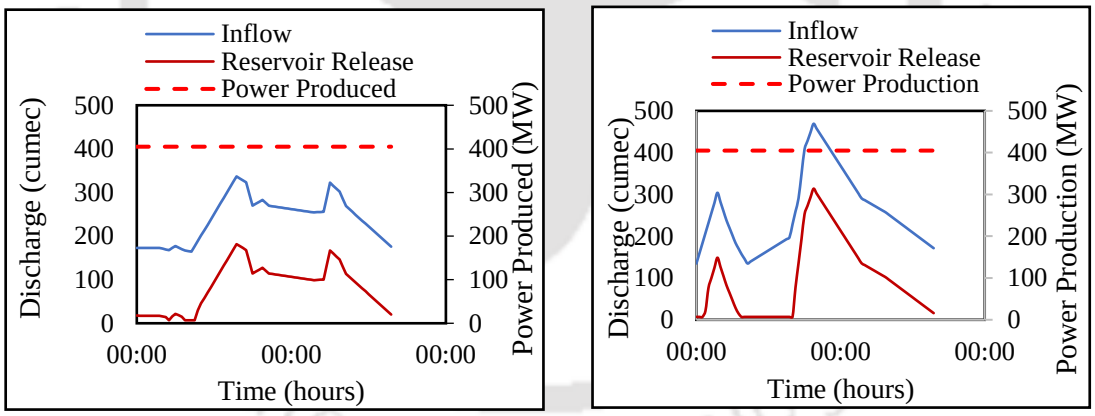

Figure 6.4:(a) Reservoir Operation for Event 1 (b) Reservoir Operation for Event 2

$$\text{Peak Increment Factor} = \frac{\text{Max Peak with lateral flow- Max Peak without lateral flow}}{\text{Max Peak without lateral flow}} \quad (6.10)$$

A magnitude of 0.78 was observed for Event 1 and 0.76 for Event 2. Analysis has revealed that with the incorporation of lateral flow, the peak flow at NT Road Crossing has increased by more than 75% and is in good agreement with the observed flow shown in Figure 6.5. Therefore, lateral flow contributions must be incorporated into the model

for precise flood prediction with reservoir operation. If the same is not included in flood modelling, the peak flow will be reduced, leading to erroneous flood warning dissemination. The maximum peak flow and water level attained from the model at NT Road Crossing, considering the lateral flow contribution of the two tributaries, were then compared with the observed flow of the same, as shown in Table 6.2.

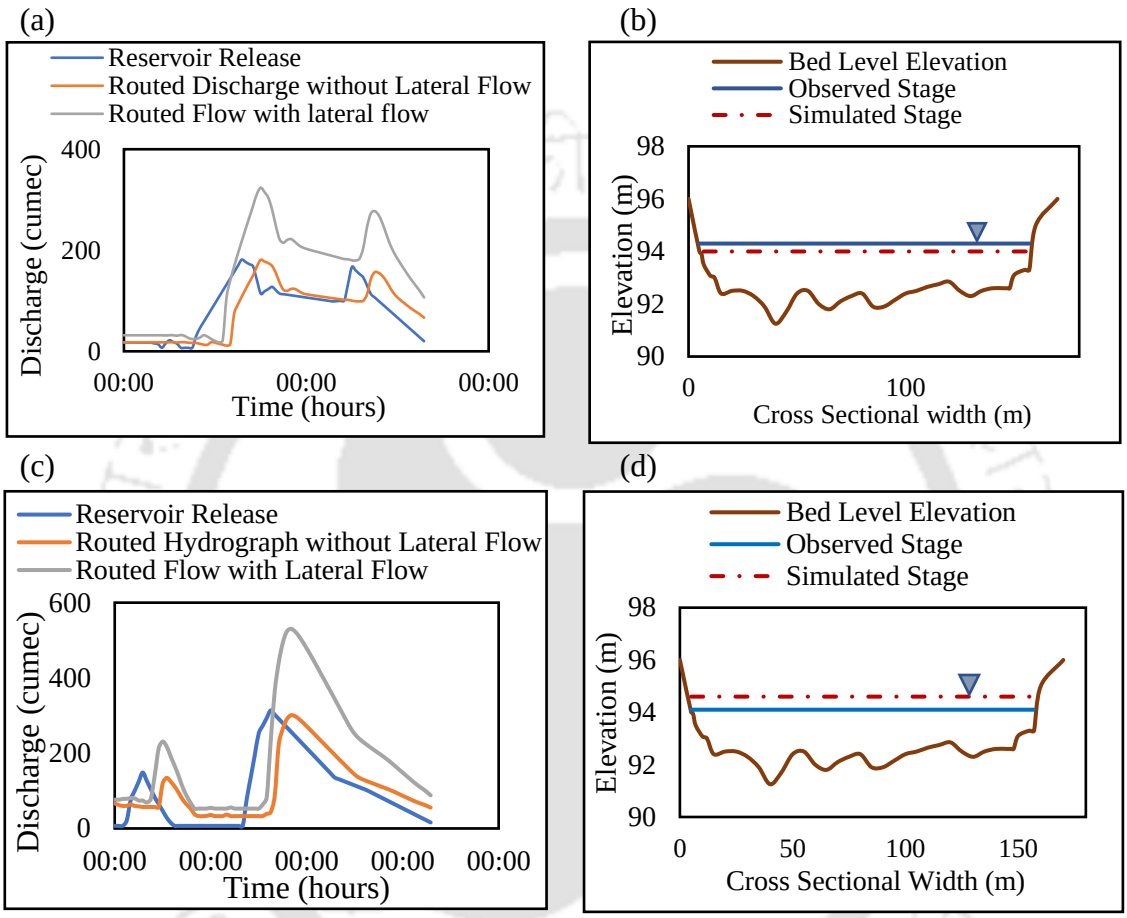

Figure 6.5:(a) Routed discharge at NT Road Crossing with and without the lateral flow of Event 1 (b) Observed and Simulated Stage at NT Road Crossing of Event 1 (c) Routed discharge at NT Road Crossing with and without the lateral flow of Event 2 (d) Observed and Simulated Stage at NT Road Crossing of Event 2

The observed and the simulated discharge impart that with the lateral flow, the magnitude of the observed and the simulated discharge was almost in the same range. The relative error of the observed and simulated discharge was calculated as 4.76 % and 5.36 % for Event 1 and Event 2, respectively, shown in Table 6.2. Similarly, the relative error of the observed and simulated stages was estimated as 0.31% and 0.63% for Event 1 and Event 2, respectively. Even though the relative errors of the stage and discharge are marginal, a

variation in the magnitude can be observed. This is because the streamflow measurement in the gauged site is generally done at a specific time based on the stage-discharge relationship. The model simulated stage and discharge may differ from the actual observation time.

Table 6.2: Observed and Simulated Discharge and Stage at NT Road Crossing

Inflow Event	**Discharge (Observed) (m^3/s)**	**Discharge (Simulated) (m^3/s)**	**Error (%)**	**Stage (Observed) (m)**	**Stage (Simulated) (m)**	**Error (%)**
Event 1	340.1	323.9	4.76	94.3	94	0.31
Event 2	503	530	5.36	94.1	94.7	0.63

6.4 Conclusions

This chapter explained the development of the methodology to incorporate the lateral flow contribution of ungauged catchments into the model, constituting the reservoir operation model and the hydrodynamic model for precise flood modelling. The DAR method was applied to the ungauged catchments of tributaries for streamflow estimation. In this study, the model parameters were estimated by minimizing the square of errors between observed and predicted streamflow using various algorithms in the calibration phase. The optimal parameters were then used in the validation phase. The ranking of the algorithms was assigned based on the Performance Metrics in the calibration and validation phase. GRG was adopted among the implemented optimization algorithms as it secured the highest rank based on the Performance Criteria. The parameter estimation of the model was done with limited data due to data unavailability. The analysis shows that even with limited data, estimating the 'α' value was possible to get the desired result. The model calibration will be better with an expanded temporal window of streamflow time series. However, the model has been established with an acceptable error margin in the data-scarce region with two years of common inflow and downstream streamflow. Therefore, this methodology has a potential application in a data-scarce region. The magnitude of the lateral flow contribution obtained was then incorporated into the 1D hydrodynamic model to compute the flood levels and discharge at NT Road Crossing, Lakhimpur. For Tributary 1, the lateral flow contribution was estimated as 44% of the

gauged streamflow, whereas for Tributary 2, the flow contribution was estimated as 36% of the gauged streamflow. Two hourly reservoir inflow events were subsumed into the reservoir operation model, and the releases from the reservoir were given input to the 1D hydrodynamic model, including the lateral flow contributions. Results showed that the peak flow had increased by more than 75% with the inclusion of flow contribution from tributaries. The model's output discharges and water levels were then compared with the observed stage and discharges. Results reveal that the magnitudes of the discharges and stage were in the same range as the observed data. The relative errors of the observed and simulated discharges of Event 1 and Event 2 were estimated as 4.76 % and 5.36 %, respectively. Similarly, for Event 1 and Event 2, the observed and simulated stage percentage errors were obtained as 0.31 and 0.63 %, respectively. The trivial variation between the observed and simulated stage and discharge can be attributed to the stage-discharge data being gauged during a specified time. Thus, the model-generated stage discharge may vary from the actual observation time.

The proposed methodology is applied successfully in a single case. Therefore, its performance must be tested on other river systems with a dam upstream to draw a generalized conclusion. As understood, the exponent "α" of the DAR method will vary from case to case and need to be optimized following the set procedure as described in this chapter. The modelling framework adopted will help improve the precision of flood warnings at downstream locations and thus help flood disaster mitigation downstream.

The analysis was then utilized in the coupled reservoir operation and hydrodynamic model to develop the significant managerial strategies of RHEP for the flood period as well as for the lean period. The detail of the model is described in Chapter 7 and Chapter 8.

7

Scope of Minimizing Downstream Flood Hydroelectric Project through Advance Release within the Forecast Horizon

7.1 Introduction

Sudden release from the hydropower dam can cause severe catastrophe downstream, leading to devastating flooding and significant damage to downstream communities. The flood triggered by such dam releases is categorized as a high hazard due to its suddenness characteristics. Under climate change scenarios, floods, and extreme precipitation are expected to increase across diverse climatic regions (Tabari 2020; Kim and Bae, 2020). Under climate change scenarios, in most global catchments, dams have the potential to mitigate the frequency of floods and reduce the extent of flooded areas (Boulange et al., 2021). The construction and management of dams can play a vital role in regulating water flow and effectively managing flood events, providing valuable flood control benefits to downstream areas. Although the frequency of flooding decreases with a dam's presence, Extreme Rainfall Events (ERE) can potentially cause significant damage downstream, leading to catastrophic flood events. The frequency of flooding will increase in the near future due to the combined effects of climate change and anthropogenic impacts. As these extreme rainfall events become more frequent and intense, they can pose more significant risks to communities, infrastructure, and the environment in downstream areas, underscoring the importance of proactive measures to address and adapt to these changing patterns. (Guhathakurta et al., 2011; Banerjee and Dimri, 2019; Myhre et al.,, 2019; Chen et al., 2020).

Reliable inflow forecasting thereby can be vital in effectively managing reservoirs with sufficient lead time. (Collischonn et al., 2007; Zhao et al., 2011; Lee et al., 2019 ; Maddu et al., 2022). Accurate and timely inflow forecasts are essential for dam managers to make informed decisions regarding water release for flood control in downstream areas. The inflow forecast horizon, which refers to the duration of predicted inflow data, plays a significant role in optimizing reservoir operations (Gragne et al., 2015; Amnatsan et al., 2018). Although it is essential for the forecast lead time to be sufficiently long to provide adequate information for decision-making purposes, the presence of forecast uncertainty and error, which typically increase as the lead time extends, can diminish the usefulness of the forecast information (Maurer & Lettenmaier, 2004; Zhao et al., 2012). In real-time management of water resources for an accurate and reliable forecast, the lead time should be at least 24 hours to 48 hours (Coulibaly et al., 2005). Over the past few decades, various techniques have been implemented to improve the accuracy of inflow forecasts. Time series models like ARIMA and SARIMA have gained popularity in this regard (Bai et al., 2014; Moeeni et al., 2017). Additionally, with the emergence of Artificial Intelligence, hydrologists worldwide have widely adopted machine learning techniques such as Artificial Neural Networks (ANN) for inflow forecasting (Ahmed and Sarma, 2007; Muluye and Coulibaly, 2007; Ray and Sarma, 2016).

In real-time reservoir operation, uncertainties are a major challenge in dealing with streamflow forecasts. The performance of a reservoir system is closely tied to the operating horizon, which is influenced by the reliability of both the inflow forecast and the reservoir operation (Simonovic and Burn, 1989). The Long Forecast horizon (LFH) represents the period within which the inflow forecast significantly impacts the release decision in the decision horizon (J. You and Cai, 2008). If the forecast extends beyond LFH, the uncertainty of the prediction becomes uncontrollable, leading to unacceptable uncertainty in the release decisions. The Effective Forecast Horizon (EFH) has been introduced to address this issue, defined based on error bounds (Zhao et al., 2012). Beyond EFH, any further extension of the forecast horizon does not result in improved accuracy; the error remains unmanageable. In summary, managing uncertainties in streamflow forecasts is crucial for efficient reservoir operation. The LFH determines the timeframe within which the forecast significantly influences decision-making, while the EFH limits forecast extensions beyond which the errors become unmanageable. Zhao et

al. (2019) extended the previous work on FH and presented a comprehensive step-by-step procedure to determine EFH and LFH along with their properties. The choice of inflow forecast horizon is thus crucial for reservoir operation planning and management. It directly affects the accuracy of inflow predictions and, therefore, plays a significant role in decision-making processes.

For reservoirs with flood control benefits, the Flood Limited Water Level (FLWL) is the maximum allowable water level during the flood season. (Li et al., 2010 ; Lu et al., 2020). This level is typically fixed, offering advantages for flood control. However, it also comes with several disadvantages. A fixed FLWL can limit the reservoir's capacity to store water during severe floods and lack the flexibility to adjust to changing weather patterns and seasonal variations. (Hua et al., 2020). In the case of the reservoir with high storage capacity with buffer storage for flood control, the integrated application of advance release with predefined FLWL can effectively manage the downstream flood. However, for a hydropower project with a small storage capacity, releasing before the occurrence of the flood is generally not done as it may adversely affect power production, which is the prime objective of such projects. Also, for a reservoir located on a steep, hilly terrain, which is the case for most of the hydel project, arbitrary pre-release can lead to advanced flooding downstream even before the arrival of the actual flood wave. Therefore, in-depth analysis is necessary to decide the optimal release in such conditions.

This chapter describes implementing the developed modelling framework to mitigate the severity of the downstream flood of a hydroelectric project. In this approach, based on the simulated flood situation downstream, a modified operating policy incorporating an advance release strategy is invoked to operate the reservoir. The process is repeated to upgrade the operating policy dynamically with an acceptable nominal power compromise if needed. For that, coupling of the reservoir operation model and hydrodynamic model is necessary. The framework consists of a coupled reservoir operation and hydrodynamic (CRH) model to moderate the flood downstream with an advance release strategy. A simulation-optimization model was developed assuming a perfectly forecasted flood event to estimate the optimal advance release within an effective forecast horizon. The advance release was decided in terms of the downstream safe discharge. The study adopted and utilized the definitions of LFH and EFH proposed by Zhao et al. 2019. The EFH was determined as the shortest forecast horizon with maximum reliability. An

uncertainty analysis was conducted using Monte Carlo Simulation for different inflow scenarios. The model analyses each inflow member individually. A flood risk assessment was performed using a FRF developed in the study. An analysis to determine the EFH based on the catchment characteristics was performed. Considering the EFH, the sensitivity of the revised operating policy incorporating optimal pre-release with peak flow and peak arrival time was conducted.

7.2 Methodology

The analysis involved the diagnosis of flood by the CRH model considering the tributary contribution described in Chapter 6. The water level estimated from the model, if it exceeds the warning level, advance release *(ar)* based on the Safe Discharge at downstream will be spilled within a forecast horizon before the arrival of the flood. The optimal ar is quantified using a simulation-optimization model Conventionally, this operating policy is termed as Adjusted Operating Policy (AOP), as the existing SOP was revised with the release of ar. AOP is conditioned upon the downstream flood level and the power production. A reliability assessment was executed using a Decision Efficiency (DE) metric to check the system's performance. The effective forecast horizon was then determined as the shortest horizon with maximum DE. The framework is represented in Figure 7.1. A risk-based analysis of downstream flood levels was conducted based on the attainment of the danger level using the Flood Risk Factor (FRF) developed in the study. An uncertainty analysis of the inflow forecast was performed with the synthetic generation of twenty inflow members using Monte Carlo Simulation considering perfect forecast event (observed inflow). The EFH was then determined using the various inflow scenarios.

The EFH determined was then fixed to assess the impact of forecast uncertainty (peak flow, arrival time) on downstream flow scenarios generated by the AOP has been analyzed. A study was also conducted to determine the EFH based on the catchment characteristics. The EFH was considered as the lag time, i.e., the time taken for peak rainfall and the peak flood. A set of rainfall-runoff events were considered to estimate the lag time. The EFH produced was then utilized as the horizon for advance release. An analysis was conducted to check the sensitivity of the revised operating policy with the forecast error corresponding to the peak flow and the time of arrival of the peak flow. A

positive forecast error refers to a peak greater than the perfect forecast, whereas a negative forecast error refers to a peak lesser than the perfect forecast. The mean flow deviation of the reservoir release using the revised operating policy and the actual operating policy was also compared. Figure 7.1. shows the flowchart of the adaptive modelling framework for flood control.

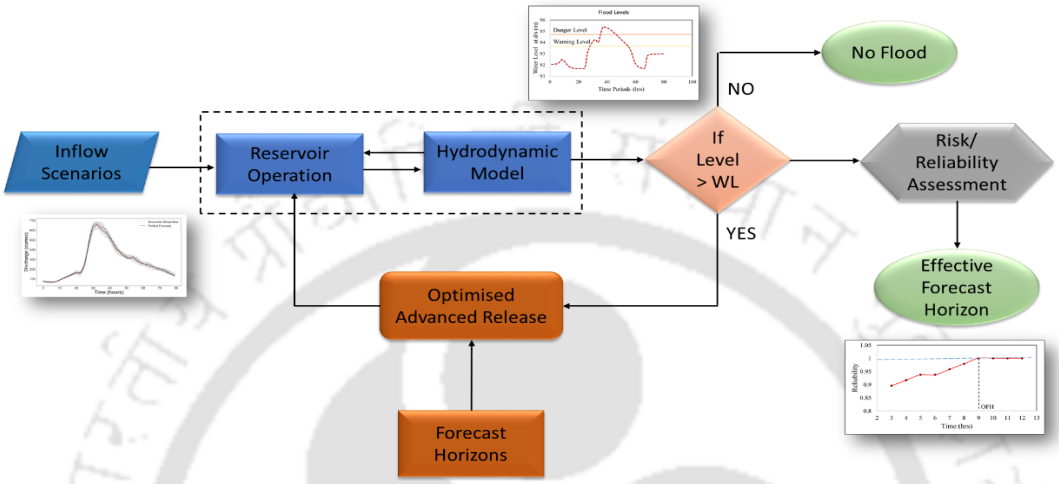

Figure 7.1:Flowchart of Adaptive Management Framework for flood control

7.2.1 Development of Coupled Modelling Framework

The model will first check the downstream flood levels using SOP. The release from the reservoir was then routed downstream by the 1-D hydrodynamic model to check the downstream flood levels. If the water level downstream exceeds the warning level, an advanced strategic release will be made before the occurrence of the flood using a simulation optimization model. The advance release *ar* will modify the existing operating policy. As per Equation 4.1 of Chapter 4, the SOP is modified by incorporating ar into the continuity equation. The incorporation of ar will revise the SOP. Thus, Equation 4.1 considering ar can be written as

$$S_{t+1} = I_t + S_t - S_{pt} - R_t - ar_t \tag{7.1}$$

The new operating policy derived with the incorporation of ar is called the Adjusted Operating Policy (AOP). The AOP is implemented as the flood moderation operating policy incorporating the optimal advance release based on the downstream flood situation. Similarly, Equations 4.5 and 4.6 can be written as

$$S_{t+1} = K \text{ ; if } (S_a + S_d - R_t - ar_t) > K \quad (7.2)$$

$$S_{t+1} = (S_a - R_t + S_d - ar_t); \text{ if } (S_a + S_d - R_t - ar_t) < K \quad (7.3)$$

where S_{t+1} is the storage at t+1, St is the storage at time t, S_{pt} is the spill at time t, R_t is the power release at time t, $ar_{,t}$ is the advance release at time t.

$$O_t = S_{pt} + ar_t \quad (7.4)$$

The total release from RHEP was again routed to the downstream section to check the flood levels. The process is repeated until the best compromise between downstream flood levels and power production is achieved through optimization. This can be attained by a simulation-optimization model described in Section 7.2.2.2 to quantify ar required to release in advance.

7.2.2 Determination of effective forecast horizon for flood moderation

In this study, the EFH was considered the FH corresponding to a maximum Decision Efficiency (DE) metric. The detail of DE is mentioned in Section 7.3.2.1. The reliability in the analysis was considered here as the number of times the flood is below the Danger Level. The EFH was determined as the shortest forecast horizon with maximum DE. The main aim of the determination of EFH was to select the most effective forecast horizon beyond which the system performance does not improve. The advance release cannot be discharged more than the EFH, as the power production will be hampered. A Long Forecast Horizon was considered as the upper bound of the FH. The procedure for the determination of EFH is shown in Figure 7.2.

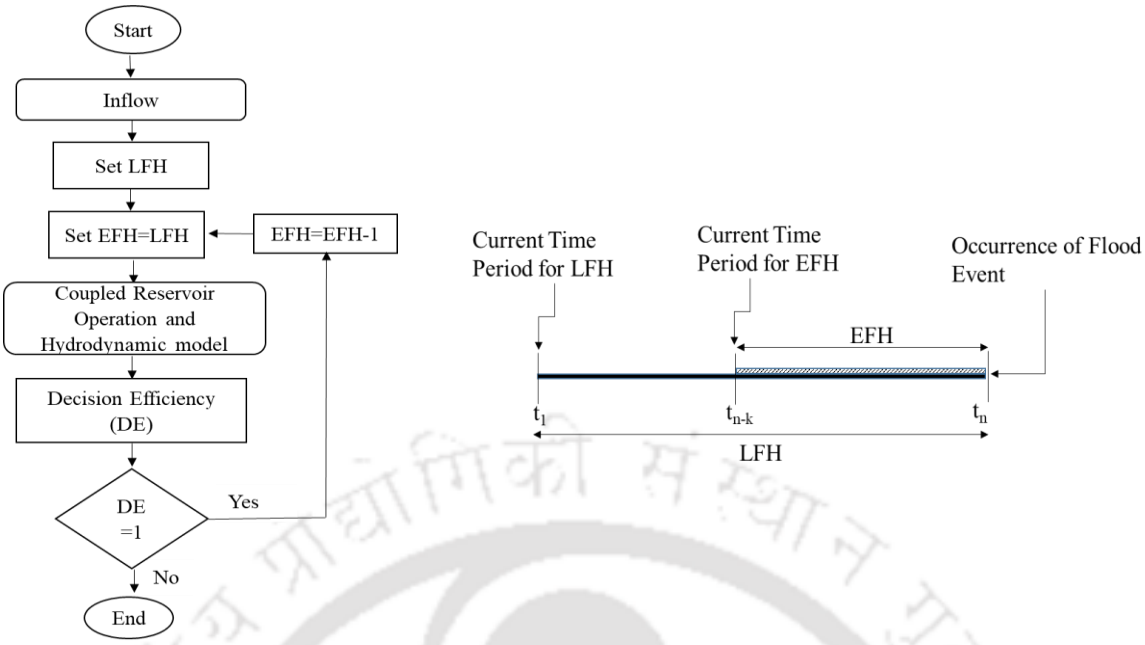

Figure 7.2: Procedure to determine EFH.

7.2.2.1 Perfect forecast flood event

The EFH was first determined considering a hypothesis of the perfect forecast, as stated below.

Hypothesis: The observed inflow event to the reservoir was considered the perfect forecast (ideal forecast: benchmark of streamflow forecast) (Zhao et al., 2011; Turner et al., 2020; Bertoni et al., 2021).

The perfect forecast event was considered by analyzing the peak and volume of the highest flood event in a year. Figure 7.3 shows the peaks and volume of the highest floods from 2013-2020. In 2017, the highest flood peak of 1511 m^3/s was observed with a volume of 170 MCM. This flood event was not considered in the analysis as it was an extreme flood event. The flood event that occurred on 28/6/2015 with a peak flood magnitude of 664.52 m^3/s with a volume of 80.34 MCM was considered as the magnitude of the peak and volume is higher than the other flood events.

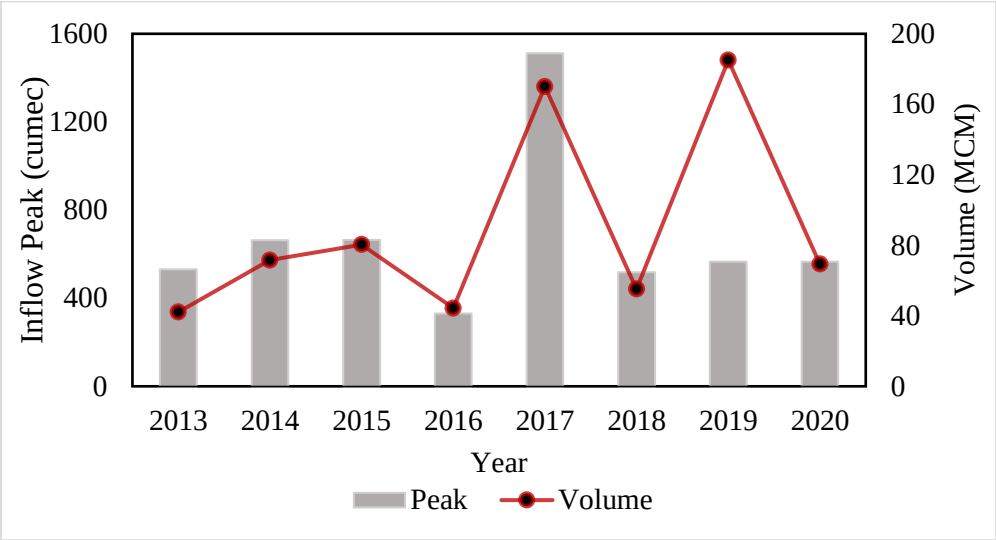

Figure 7.3:Inflow Peak and Volume over the years.

7.2.2.2 Optimization Model

The optimization model was formulated based on the objective function represented by Equation 7.5. The model's objective was to minimize:

1. The flood levels exceed the warning level: This implies that the model aimed to keep the flood levels as close as possible to the predefined warning level. By minimizing the flood levels, the system would be better equipped to handle potential flood risks and ensure that the flood levels stay within manageable limits.

2. The power deficit: The model sought to minimize the difference between power generation and power capacity. By doing so, the system would be optimized to meet the power requirements efficiently, ensuring a balance between power production and consumption.

Combining these two objectives, the optimization aimed to achieve a reliable system that can effectively manage flood control with acceptable power generation. The analysis used a classical optimization technique, combining the Golden Section Search and Parabolic Interpolation methods, to efficiently find the minimum of the objective function. This allowed for precise optimization of the model's variables to achieve desired outcomes. The algorithm searches the minimum of a function of a single variable within a fixed interval. The MATLAB function *fminbnd* was implemented in the analysis.

$$\text{Minimize } Z = \sum_{i=1}^{N}\left(\frac{FL(i)-WL}{WL}\right)+\sum_{i=1}^{T}\left(\frac{D-P(i)}{D}\right) \quad \forall N \; ; \; FL > WL$$

(7.5)

WL is the Warning Level of the downstream section in m, FL is the Flood Level of the downstream section in m, D is the power capacity in MW, P is the power generation in MW, T is the total time periods in h., and N is the total time periods in h. when FL>WL.

3. Constraints

Distribution Factor

The distribution factor, β determines the percentage of Q_s that can be spilled as the advance release. β is the distribution factor ranging from 0-1, and Q_s is the safe discharge of the considered downstream flood-prone section. The 0 value represents no release is discharged while unity represents Q_s is released within the FH. The bounds of β are shown in Equation 7.6.

$$0 \leq \beta \leq 1 \tag{7.6}$$

Reservoir Continuity Equation

$$S_{t+1} = I_t + S_t - S_{pt} - R_t - ar_t \tag{7.7}$$

The reservoir continuity equation described in Equation 7.1 is used in the simulation-optimization model to determine optimal *ar*.

Storage Constraints

The storage constraints are

$$S_a \leq S_t \leq K \tag{7.8}$$

As the operational activities of a reservoir take place in the active storage, the releases should be made so that the storage level does not go beyond the active storage zone.

Power Release Constraints

The release constraints need to be met while running the simulation optimization model.

$$R_t \leq Q_{d,t} \tag{7.9}$$

$Q_{d,t}$ is the power demand in m^3/s at time t.

The power release should be less than equal to the demand at time t. Spilling occurs if the water available at time t exceeds the reservoir capacity.

Non-Negativity Constraints

Following are the non-negativity constraints incorporated into the model

$$S_{t+1} \geq 0 \tag{7.10}$$

$$R_t \geq 0 \tag{7.11}$$

$$S_{pt} \geq 0 \tag{7.12}$$

$$S_a \geq 0 \tag{7.13}$$

7.2.3 Uncertainty Analysis using Monte Carlo Simulation

Uncertainty analysis of inflow to the reservoir and the impact on the reservoir system's performance on the risk associated with the downstream flooding is a critical issue that needs to be incorporated. Monte Carlo Simulation (MCS) is the most widely implemented numerical uncertainty analysis approach (Liu et al., 2014; Sun et al., 2018). The MCS approach is a numerical procedure for generating random numbers based on a definite Probability Distribution Function (PDF). It provides a range of potential outcomes, enabling analysts to understand the likelihood of different scenarios and make informed decisions.In this analysis, uncertainty on peak flow was conducted. Twenty inflow sequences were generated that are spread around the perfect forecast shown in Fig 7.4. In this study, the forecast error (Ɛ) values were randomly generated assuming the PDF following a Gaussian distribution with 0 mean, i.e., ≈ N (0, σ^2) (X. Li et al., 2010). A smoothening filter Savitzky-Golay (Schafer, 2011) of polynomial 2 and frame length 11 was implemented to predict the streamflow. The forecast error was given by Equation 7.14.

$$\varepsilon_t = \frac{\hat{q}_t - q_t}{q_t} \tag{7.14}$$

$$q_t = q_t\left(1+\varepsilon_t\right) \tag{7.15}$$

$Ɛ_t$ is the Forecast Error at time t, $\hat{q}_t$ is the predicted streamflow at time t in m^3/s, q_t is the observed streamflow in m^3/s at time t. Figure 7.4 shows the generated twenty inflow members spread over the perfect forecast flood event.

7.2.3.1 Performance indices

A number of performance indices were considered in the analysis of the determination of EFH. The ensemble members were individually modelled to check the system performance. The performance indices utilized in the study are discussed below.

1. Decision Efficiency (DE)

To derive the EFH analytically, the metric DE was utilized. The DE reflects the AOP's ability to reduce floods above DL. DE of the system was estimated using Equation 7.16.

$$\text{DE} = 1 - \frac{\text{Number of times the flood is above DL (AOP)}}{\text{Number of times the flood is above DL (SOP)}} \tag{7.16}$$

In this analysis, the DE depicts the improvement of the system with the implementation AOP. The magnitude of DE ranges from 0-1, where 0 represents poor system performance and 1 represents high system performance.

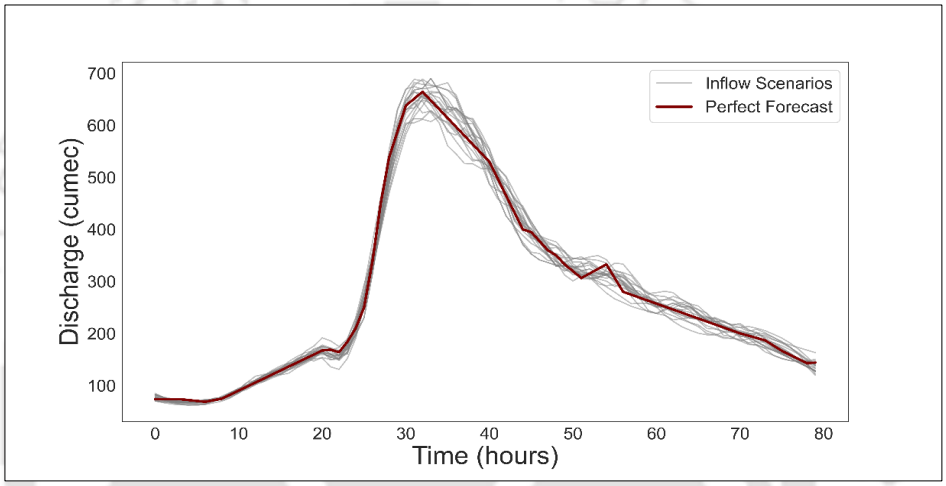

Figure 7.4:Twenty inflow members and the perfect forecast event

2. Power Production Efficiency

The power production efficiency factor, as calculated in Chapter 7 was utilized in the study

$$\eta_p = \frac{\text{Total Power Produced (MW)}}{\text{Total Power Capacity (MW)}} \tag{7.17}$$

The range of $\eta_p$varies from 0-1, where 0 indicates no power production, and 1 indicates the total power capacity is met.

3. Peak Forecast Error

The performance of the AOP was analyzed using the inflow peak forecast error, considering perfect forecast as the baseline flood event. The peak forecast error was calculated by the deviation peak flow of the inflow member from the peak flow of the

perfect forecast event as per Equation 7.18. A positive error represents a flood peak higher than the perfect forecast, and a negative error represents a peak flow lower than the perfect forecast, as shown in Figure 7.5.

$$\varepsilon_p = \frac{\hat{q}_p - q_p}{q_p} \tag{7.18}$$

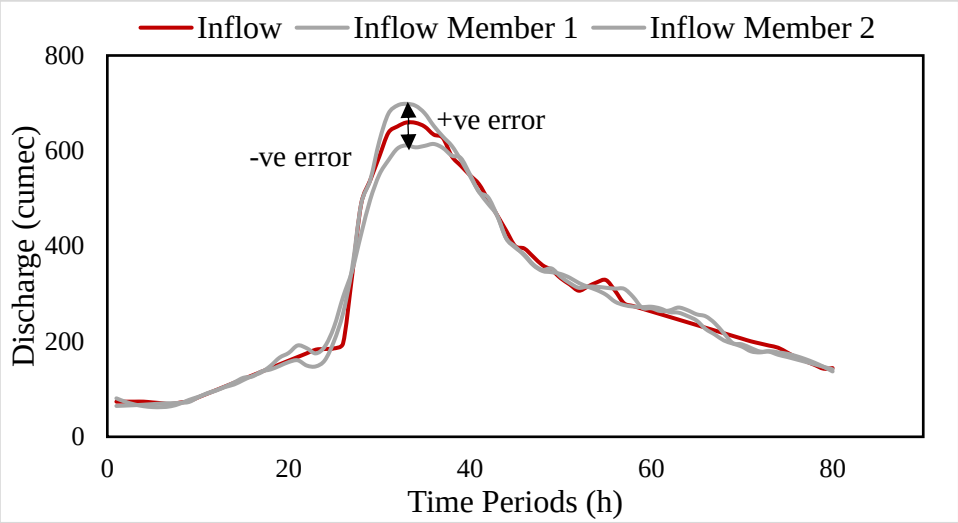

Figure 7.5:Positive and negative forecast errors employed in the analysis.

3. Flood Risk Factor

A Flood Risk Factor (FRF) was introduced in this analysis based on the flood situation in a particular location. The FRF was calculated as per Equation 7.19.

$$FRF = \frac{FL - WL}{DL - WL} \tag{7.19}$$

The values of FRF can range from 0-1. If negative values are generated, FRF will be 0 and 1 if the values are greater than 1. Figure 7.6 shows the flood levels utilized for the generation of the FRF. The range of FRF was categorized into 0-0.3, 0.3-0.6, and 0.6-1 as low, moderate, and high risk.

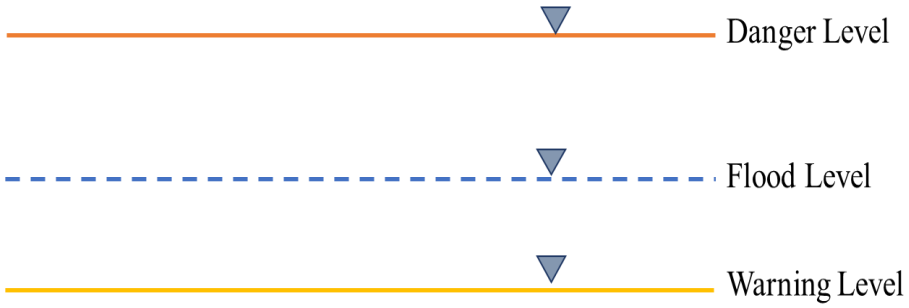

Figure 7.6: Flood Levels considered for FRF

7.2.4 Analysis of Forecast Horizon Based on Catchment Characteristics

The EFH determined per the methodology mentioned in Section 7.2.2 is based on an efficiency metric that denotes the shortest FH with maximum DE. A catchment-based analysis of FH was also conducted. The FH in this analysis is considered as the lag time of the flood event, i.e., the interval from the centroid of the hyetograph to the peak flow of the hydrograph, as shown in Figure 7.7. It measures the hydrological characteristics of a catchment, depicting the quick response of the rainfall event to produce runoff within the catchment. Lag time is a salient metric for determining the peak time and flow for planning, designing, and operating hydraulic structures. A longer lag time will give more time for planning and decision-making. The upstream catchment of the reservoir was delineated with SRTM DEM, considering the outlet as the dam site.

In this analysis, different lag times were determined from the historical data sets of the rainfall-runoff dataset. The mean value of the generated lag time was considered as the FH.

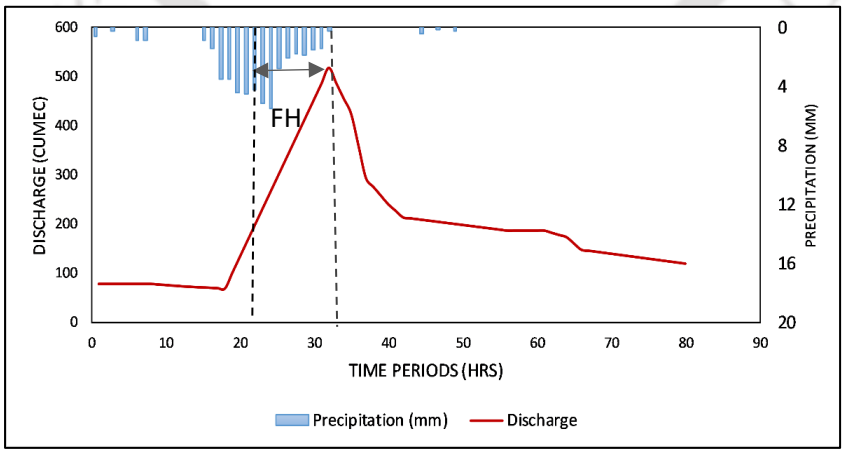

Figure 7.7:Forecast Horizon Based on Catchment Characteristics

7.2.4.1 Analysis of rainfall data used for the analysis of FH

For the determination of FH, pairs of rainfall-runoff events are necessary to determine the lag time for the event. As per the available data, monthly rainfall data of IMD is available, which cannot be integrated into the analysis. Thus, satellite-based rainfall data was used in the analysis. A comparative study of the satellite rainfall data and the available IMD was conducted to test the reliability of the rainfall product. The precipitation data of the Center for Hydrometeorology and Remote Sensing (CH) was used in the analysis. The Precipitation Estimation from Remotely Sensed Information using Artificial Neural Network (PERSIANN) was developed by CH to employ a neural network framework to estimate rainfall with a spatial scale of 0.25^0 x 0.25^0. The PERSIANN data showed a better agreement with IMD, and they can be used in climate studies and hydrological simulation in locations/river basins where the number of rain gauges is not adequate to quantify the spatial variability of precipitation (Mondal et al., 2018). The monthly rainfall data of PERSIANN from 2002-2012 was downloaded from the CH portal (https://chdata.eng.uci.edu/) to compare with the available IMD station data. The hourly PERSIANN data was then used for the determination of FH.

7.2.5 Sensitivity Analysis of the erroneous forecast

Sensitivity analysis was conducted to test the effect of inflow peak and the time of arrival of peak flow on the model results. This analysis adopted AOP by discharging advance release within the FH, considering the perfect forecast. In general, if the forecasts were accurate, AOP would be able to marginally reduce the downstream flood level above the danger level. However, uncertainties associated with forecasts might not be able to mitigate the downstream flood with the AOP adopted. The deviation from the adopted policy could augment the increase in the forecast error. Thus, a sensitivity analysis of the forecast error in terms of peak flow and time of arrival of peak flow is necessary to analyze to check the model performance.

1. Model Scenarios

Multiple inflow scenarios were generated– the first scenario is the perfect forecast event observed on 28/6/2018, and other scenarios of +10 %, +20 %, +30 % increment of the perfect forecast and -10%, -20%, -30 % of the perfect forecast was considered. Scenarios considering the inflow peak time of arrival than the expected peak time, i.e., lag time and

lead time of 2 h, 4 h,6 h, were considered in the analysis. The parameters FRF, η_p were utilized to check the performance of the model with the scenarios generated.

7.3 Results and Discussion

7.3.1 Determination of EFH for the perfect forecast

To determine EFH, a reliability assessment was performed using Equation 7.16 with the perfect forecast using a simulation optimization model. Figure. 7.8 shows the extraction of the EFH using DE of the perfect forecast flood event. With the increase of the FH, the DE increases to a specific horizon and then decreases to 0. This suggests that beyond a particular FH, the potential downstream flood moderation was not effective. The RHEP is a run-of-the-river scheme project with a low storage capacity. Even if the reservoir is emptied by releasing extra advance release, the reservoir filling up can take place within a short period. If the advance release is made for a longer FH, it will impede power production. Thus, a short FH can be utilized in the decision-making process to moderate the flood without reducing the power head. The shortest FH with maximum DE was considered the EFH. In this case, the EFH was observed as 12 h with a DE and a PE of 1. Figure 7.8 (a) shows the AOP with an optimal advance release done for 12 h before the arrival of the flood. Flow augmentation of the routed release can be observed due to major tributary contribution downstream of the dam. The optimal β value for EFH was observed as 0.61, i.e., 61% of the safe discharge was released as advance release for EFH.

With SOP, the total number of floods above DL was 6. With the implementation of AOP considering EFH as 12 h, the number of floods above DL was moderated entirely to 0 with a power production efficiency of 1.

Figure 7.8 (c) shows the downstream flood levels with the two operating policies. The maximum flood level with SOP was observed as 94.97 m. The maximum flood level has reduced to 94.81 m, with AOP considering EFH as 12 h. Thus, 0.15 m of reduction of flood level was observed. The maximum FRF with SOP was estimated as 1, which is a very high-risk flood event. With AOP, the magnitude of FRF has declined to 0.92.

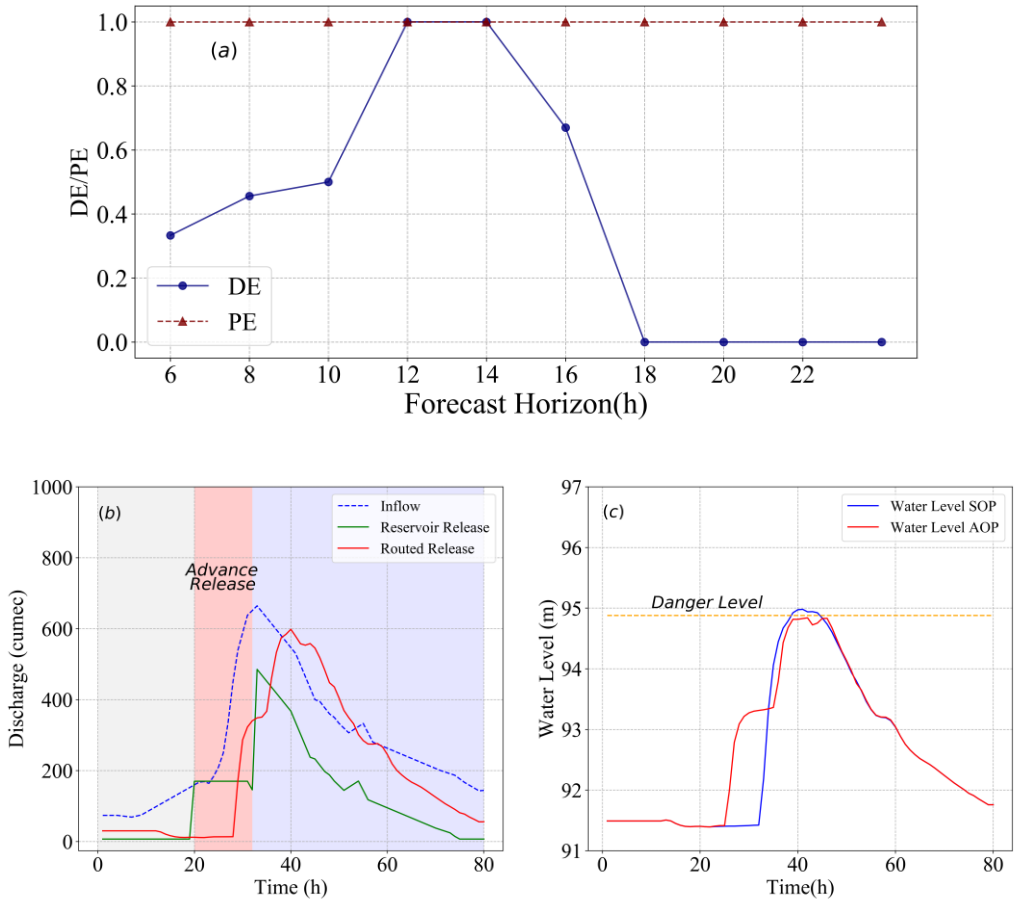

Figure 7.8: (a) Reliability Assessment with perfect forecast (b) Adopted AOP using the EFH (c) Water levels at downstream with the two operating policies.

7.3.2 Determination of EFH for the inflow scenarios generated

The analysis encompassed a set of twenty generated inflow sequences, each characterized by different peak and volume values. Individual members were modeled to estimate the EFH values. The DE and PE were calculated for each member, as depicted in Figure 7.9 Figure 7.9 (a) illustrates the DE values corresponding to all inflow members in relation to FH and the peak forecast error. As the positive peak forecast error increases, the DE decreases, indicating that the AOP was unable to moderate the flood below the DL with higher flood peaks. However, in certain FH, the magnitude of DE has increased from 0 for positive peak forecast errors, indicating a reduction in the number of floods above DL. For peak errors ranging from 0.002 to -0.054, the magnitude of DE reached 1

at some FH. This implies that the AOP successfully moderated the flood above DL for some flood events.

Additionally, it suggests that as the FH increases, the DE decreases due to the impact of the early advance release on power production. Therefore, the EFHs for the members were selected within the FH range with the DE values as unity. Consequently, no EFHs were identified for forecast errors ranging from +0.006 to +0.046 as DE values were less than unity.

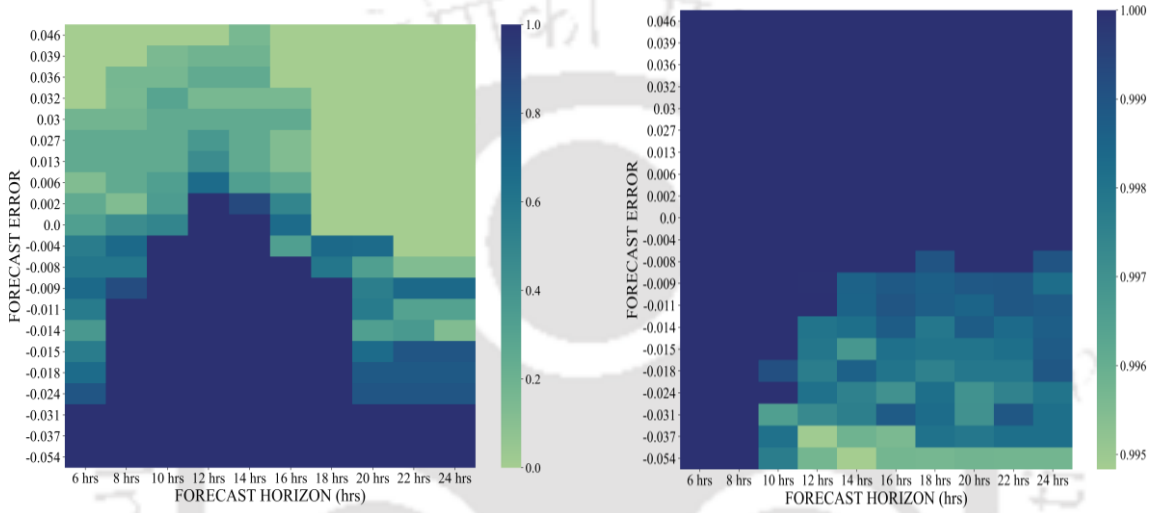

Figure 7.9:(a) DE of the twenty inflow scenarios with the FH (b) PE of the twenty inflow scenarios with the FH.

When considering power production efficiency, a decrease in η_p can be observed with negative forecast errors. This indicates that the inflow decreases as the negative forecast error increases, impacting power production. Additionally, the η_p values have also shown a decrease from an FH duration of 10 hours up to 24 hours. In Figure 7.9 (a), it is evident that for positive peak forecast errors, the magnitudes of DE were consistently found to be 0, starting from an FH of 18 hours. However, in the case of power production, the η_p remained at 1 for all FH values shown in Figure 7.9 (b). This implies that if an extended FH is utilized for advance release, the power production requirements are met, but this approach did not provide the desired benefit of flood moderation.

7.3.2.1 Risk-Based Assessment of the Generated Inflow Scenarios

A risk-based analysis was conducted for all the individual members of the inflow scenarios of the generated streamflow. The FRF mentioned in Section 7.3.2.1 was used in the analysis. The forecast error considering the perfect forecast as the baseline was assessed for all the twenty members.

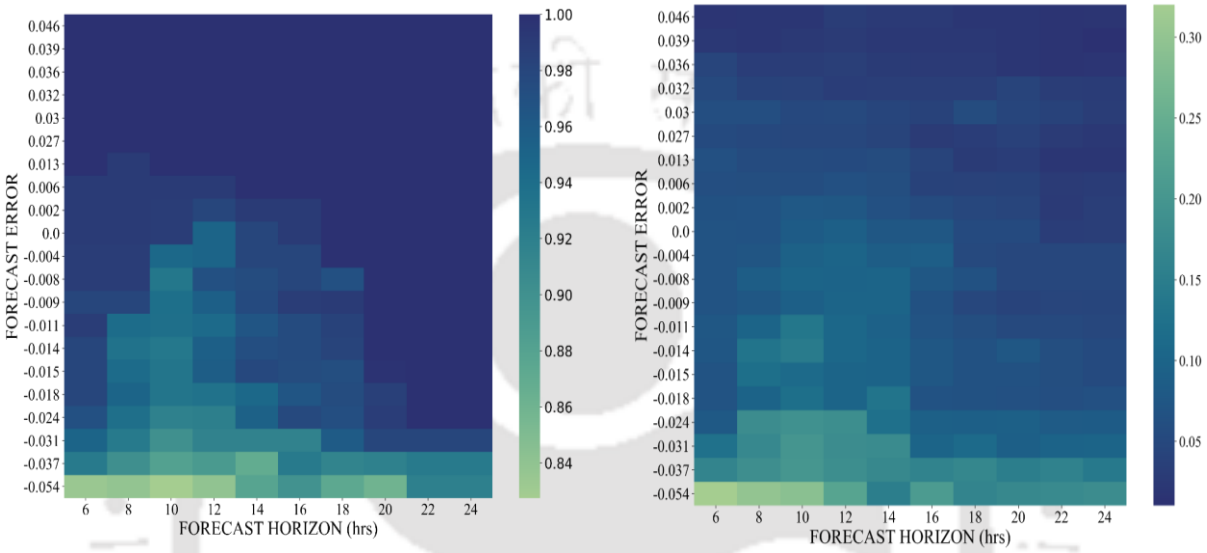

Figure 7.10:(a) FRFs with AOP over different Forecast Horizons considered (b) Flood level differences with AOP over different Forecast Horizon.

Figure 7.10 (a) shows the heatmap showing the mean FRFs with the AOP over different FH. The mean FRF increases with the increase of the peak forecast error. A similar trend can be observed in this case as well. With the increase of the FH, the FRF was reduced and then increased with the FH. Although at negative peak error, the mean FRF was reduced, which means the flood levels are below DL. This suggests that the AOP was able to moderate the flood below DL in the case of negative peak error. The lowest mean FRF was observed as 0.83 with a peak forecast error of -0.054 at 6 h FH.

Figure 7.10 (b) shows the difference in the maximum flood levels obtained from AOP and SOP. It shows that although the risk is higher, there is a significant difference in the flood levels when applying AOP. In the negative peak forecast error case, a maximum flood level difference of 0.32 m was observed with a peak error of -0.054 at 6 h FH. The minimum flood level was observed as 0.01m with a peak forecast error of +0.039 with 24 h FH. Even in the case of positive peak forecast error, the flood level is reduced. This

suggests that although the mean FRF is high, the AOP was able to reduce the count of flood levels above DL even in the case of high peak forecast error.

7.3.3 Effect of flood peak and volume on EFH

The EFHs were determined as per the methodology depicted in Section 7.2.2. This section explored the impact of EFH on flood peaks and flood volumes. Flood peak and volume are the most critical hydrologic signature of a flood event. The shape of the flood hydrograph determines the severity of the flood. The EFH is an important parameter in flood forecasts for decision-making. Figure 7.11 shows the effect of EFH on flood volume and inflow peak.

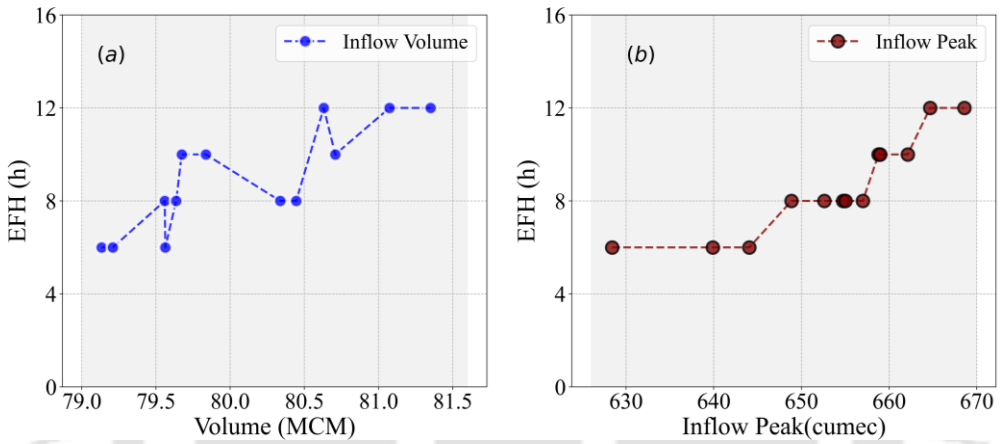

Figure 7.11: (a) Effect of Flood Volume on EFH (b) Effect of Inflow Peak on EFH.

It can be assessed that with the increase in the flood volume, there was an increment in the EFH. In the case of the peak volume, some irregular observations can be seen, as shown in Figure 7.11 (a). There was no apparent consistent trend observed between inflow volume and EFH. Considering the increase of the inflow peak, there observed a regular increasing trend of EFH. This indicates a clear sensitivity of EFH and inflow peak shown in Figure 7.11(b).

Table 7.1 presents the inflow peaks with flood moderation and power production efficiencies along with the EFH. With the increase of the inflow peak, the flood moderation efficiency has decreased. It can be assessed from Table 7.1 that with a small change in the inflow peak, the EFH was changing significantly. With an inflow peak of 662.12 m^3/s, the EFH was evaluated as 10 h, whereas with a peak of 664.52 m^3/s, the

EFH was observed as 12 h.This shows that the EFH is more sensitive to the inflow peak. Figure 7.10 (a) also reveals that floods with maximum DE values as unity can possess a maximum of 12 hours FH, making them a significant consideration of EFH. The analysis shows that the FH with the maximum DE extends up to 12 hours. Beyond this duration, the FH was found to be ineffective in satisfying both benefits simultaneously. Therefore, for the RHEP, the EFH should not exceed 12 hours.

For any decision-making process, it is crucial for the decision-maker to carefully choose the appropriate EFH to ensure optimal power production efficiency as well. The analysis clearly demonstrates that even with high inflow, the AOP has outperformed the SOP in performance.

Table 7.1:The EFH corresponding to Inflow Peak

Inflow Peak (m^3/s)	FH with max DE (h)	Flood Moderation Efficiency below DL (%)	Maximum Power Production Efficiency attained (%)	EFH (h)
628.42	6 to 24	100	100	6
639.88	6 to 24	100	100	6
644.05	6 to 24	100	100	6
648.87	8 to 18	100	100	8
652.62	8 to 18	100	100	8
654.75	8 to 18	100	100	8
655.03	8 to 18	100	100	8
657	8 to 18	100	100	8
658.80	10 to 18	100	100	10
659	10 to 16	100	100	10
662.12	10 to 14	100	100	10
664.52	12 to 14	100	100	12
665.74	12	100	100	12
668.58	12	67	100	-
673.43	12	45	100	-
682.37	12	37.5	100	-
684.41	10	30	100	-
685.67	10	25	100	-
688.29	12	25	100	-
690.56	12	18.9	100	-
695.1	14	16	100	-

7.3.4 Analysis of Forecast Horizon

Figure 7.12 shows the monthly time series plot of the rainfall data of PERSIANN and IMD. The correlation coefficient of the two datasets was computed as 0.71, which shows a strong correlation exists between the two datasets. The statistical analysis of the two datasets is shown in Table 7.2. From the analysis, the hourly rainfall events of PERSIANN were used in the analysis.

Table 7.2 shows that the cumulative annual precipitation of IMD was 6951.8 mm, and PERSIANN data was obtained as 6525.6 mm. Thus, a percentage error of the annual cumulative rainfall between the two datasets was obtained as 6.12 %. The mean of the IMD and the PERSIANN data was estimated as 62.62 mm and 58.78 mm, respectively.

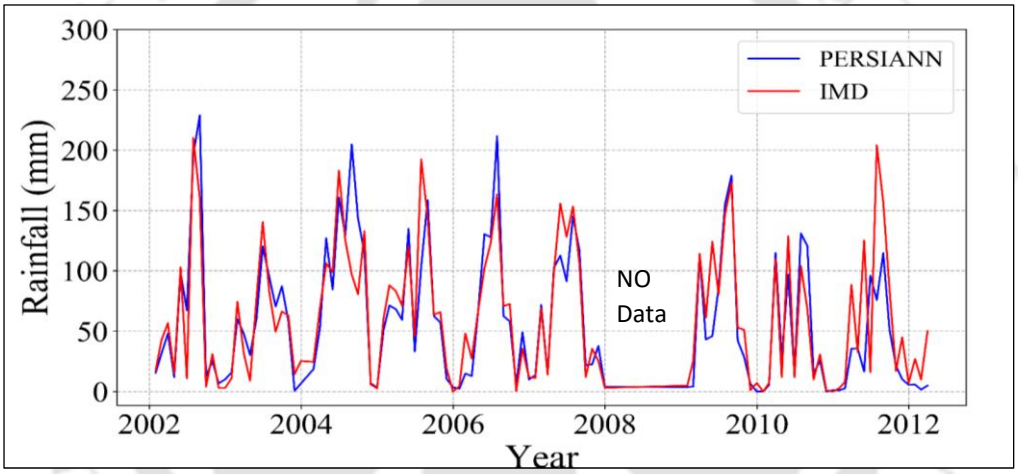

Figure 7.12:Monthly IMD and PERSIANN data

Table 7.2:Statistical Analysis of the rainfall datasets

Rainfall	Annual Cumulative (mm)	Mean (mm)	Maximum (mm)	Standard Deviation
IMD	6951.8	62.62	210.3	54.74
PERSIANN	6525.5	58.78	228.96	55.62

This analysis states that a consistent statistical agreement between the two datasets exists. The two datasets were also analyzed monthly, as shown in Figure 7.12. According to the 11 pairs of rainfall-runoff events of the upstream catchment of the reservoir, the FH can be estimated as per the method described in Section 7.2.4.

Table 7.3 shows the rainfall events and the corresponding T_L. The population was assumed to be following a normal distribution. The mean of the same was found to be 11.45 h ~ 12 h. Thus, the EFH as obtained by the efficiency metric and the graphical procedure, converged as 12 h. Therefore, the EFH was fixed as 12 h for the upstream catchment of the reservoir.

Table 7.3:Rainfall events and the Lag Time

Date	T_L (hours)
14/9/2012	12
10/6/2012	6
28/6/2013	13
8/9/2013	14
22/06/2014	12
25/08/2014	12
27/06/2015	14
15/07/2015	12
30/08/2015	14
7/4/2016	5
28/07/2020	12

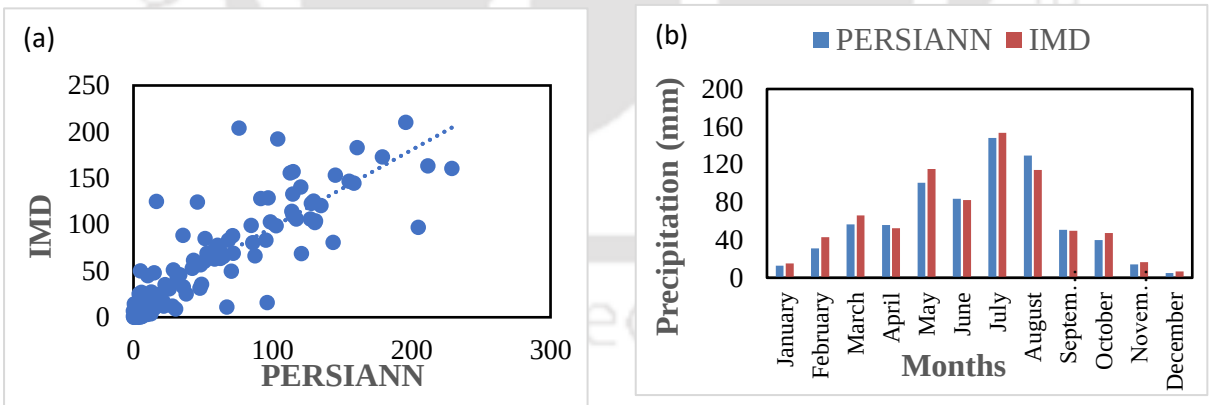

Figure 7.13:Comparative Analysis of the two datasets (a) Scatter Plot (b) Monthly precipitation analysis

7.3.4.1 Sensitivity Analysis of the erroneous forecast

According to Figure 7.14, the mean FRF increases with the increase of the inflow peak forecast error corresponding to the lead time and lag time of arrival of the peak flow than the expected time of peak arrival. The more negative forecast error represents a reduction of peak flow; hence, less magnitude of the mean FRF was observed and vice versa.

Figure 7.14 (a) shows the arrival of the flood peak lagged by 2 h to 6 h, corresponding to the inflow peak forecast error. In the negative inflow peak forecast error zone, the gradual increase of mean FRF can be seen with the increase of the lag time. In the positive forecast error zone, the mean FRF can be seen rising to 1 for all the lag time. At +0.1 peak forecast error, the magnitude of mean FRF increases from 0.95 to 0.98. If the flood arrives earlier than the actual arrival of the flood peak, the mean FRF increases with the increase of the forecast error, as observed in the previous cases. In the case of a negative forecast error, the mean FRF increases for each negative forecast error with the rise of lead time. At -0.3, the magnitude of mean FRF increased from 0 to 0.53, observed at 2 h and 6 h lead time, respectively.

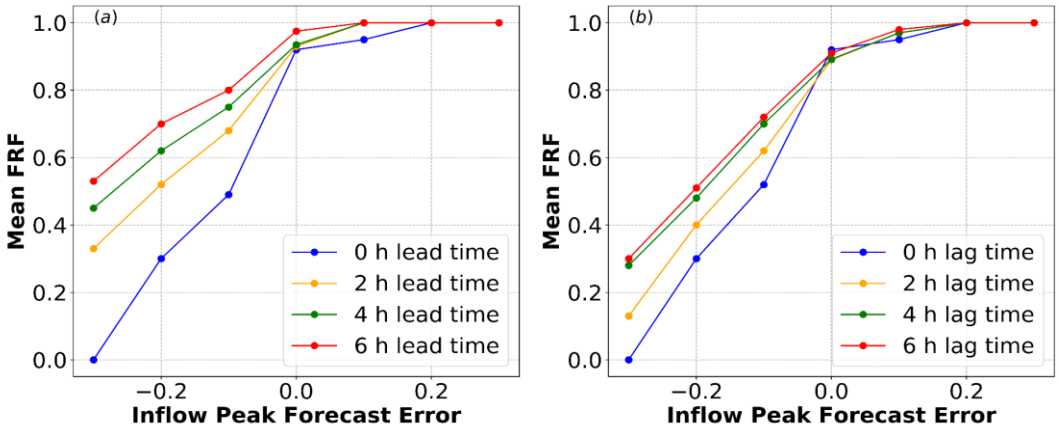

Figure 7.14: Mean FRFs of (a) flood peak lead time considered, (b) flood peak lag time considered

Similarly, at -0.1, the mean FRF increases from 0.68 to 0.8 at 2 h and 6 h, respectively. Whereas in the case of the lag time of arrival at -0.3, the mean FRF range from 0.13 to 0.3 was observed at 2 h and 6 h lag time. At -0.1, the values of mean FRF range from 0.61 to 0.7 at 2 h and 6 h lag, respectively. This shows that the risk associated with the

early arrival of the inflow flood peak is more than the flood arriving later than the expected time of arrival.

The sensitivity of the power production efficiencies with the forecast error was also analyzed for peak flow and the arrival time of peak flow. The power production efficiency for each inflow scenarios was approximated. Figure 7.15 (a) depicts the power production efficiencies of the inflow members of the peak flow. The magnitude of η_p was obtained as the high value of 1 for the considered inflow peak forecast.

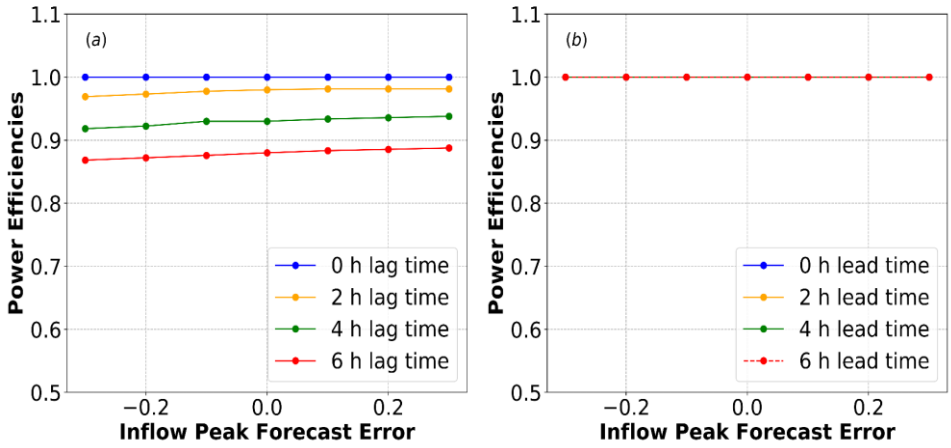

Figure 7.15: η_p for the (a) flood peak lag time considered, (b) flood peak lead time considered,

Figure 7.15 (b) shows the η_p concerning the forecast error pertaining to the flood peak lag time for 2 h. With the increase in the lag time, the η_p decreases. However, Figure 7.15 (c) describes that the η_p was 1 for all the inflow members. This shows that even if the flood peak arrives before the forecasted time, the AOP will impart 100% power production efficiency.

A study was carried out to have an idea about the range of outflow variation due to revised operation using AOP. Figure 7.16 (a) shows the mean flow deviation of the reservoir releases of the generated members from AOP with respect to the SOP. For all cases, the mean flow deviation increases with the forecast error in the negative and positive zones. This analysis reflects how much the release decision with AOP deviates from the actual SOP. Figure 7.16 shows the flow deviation of AOP from SOP corresponding to the peak

flow and the arrival time. The mean flow deviation of AOP was observed to increase with the forecast error on both positive and negative error sides.

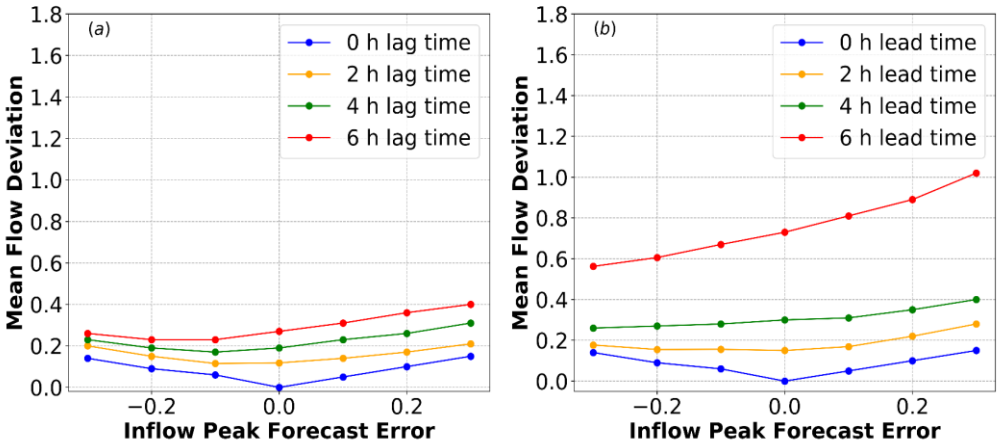

Figure 7.16: Mean Flow Deviation of the reservoir releases of AOP and SOP (a) flood peak lag time considered (b) flood peak lead time considered

Figure 7.16 (a) shows the flow deviation corresponding to the peak flow lag times. Figure 7.16 (b) depicts the flow deviation related to the peak flow lead times. In this case, the magnitude of flow deviation is substantial in the case of flood arriving earlier. This is because the AOP was releasing the advance release, and at the same time, the inflow to the reservoir was significant. The sensitivity analysis thus states that the risk associated with the flood peak arriving early is more than the flood arriving later than the expected flood. If the flood arrives later than expected, the power production efficiency decreases with the increase of lag time. Although a delay in the arrival of the flood can lead to a compromise in power generation, it still falls within an acceptable range. Even with a 6 h delay, power production efficiency does not decrease below 85%. Even the mean FRF increases with the increase of the lag time; however, with delay, the decision-maker can have more time for disaster preparedness and response plans execution.

7.4 Conclusions

The analysis revealed that the developed CRH model can be very well utilized for flood moderation downstream. A simulation-optimization technique was implemented to calculate the optimal advance release based on the downstream flood scenario. The advance release is assumed as the function of downstream safe discharge. The

distribution factor in the advance release will determine the percentage of safe discharge required to be released before the occurrence of the flood. A flood event occurred on 28/6/2015 was considered as the perfect forecast event for the analysis. The flood event was selected based on the flood peak and volume that occurred over the years. Considering the perfect forecast event, the optimal advance release was determined over different forecast horizons ranging from 6 h to 24 h. The EFH was then determined as the shortest FH with maximum DE within the LFH. With the perfect forecast flood event, the EFH was observed as 12. With SOP, the total number of floods above DL was 6. With AOP's implementation, the total number of floods above DL was reduced to 0. In terms of flood risk assessment, the average FRF was observed as 1, which is a very high-risk event. With AOP, the average FRF has reduced to 0.92, which is also categorized as a high-risk flood, but the severity of the flood has decreased significantly. This states that even in the case of a high flood event, the AOP was able to moderate the flood below DL.

An uncertainty analysis of the inflow to the reservoir was conducted by generating multiple inflow sequences spread over the perfect forecast event. A total of twenty inflow members were predicted using MCS. The inflows were individually modelled to determine the EFH for each member. The average FRFs were determined for each member. Results stated that even with a high peak, the AOP outperforms SOP. The effect of inflow peak and volume on EFH was assessed. The study imparts that the EFH is highly sensitive to inflow peaks. The analysis indicates that the FH with the maximum DE extends up to 12 h. FH beyond this duration was found to be ineffective in simultaneously satisfying both benefits. Therefore, the EFH should not exceed 12 h. in the case of RHEP. Furthermore, the generation of multiple scenarios, with different combinations of weightage to flood moderation and power generation, can facilitate the formulation of a comprehensive decision-making policy to maximize the benefits, considering other factors not explicitly considered in this study.

A catchment-based analysis was conducted to assess the EFH. The EFH in this analysis was defined as the time delay between peak rainfall and peak flood occurrence. Graphical methods was employed to determine the lag time. A series of rainfall-runoff events were examined to estimate lag time, and the resulting EFH was utilized as a reference for advance release strategies. An analysis was conducted to evaluate the sensitivity of the

revised operating policy, considering forecast errors in peak flow and the timing of peak flow arrival. Positive forecast errors indicated a peak higher than the perfect forecast, while negative forecast errors indicated a peak lower than the perfect forecast. Additionally, a comparison was made between the mean flow deviation resulting from the revised and actual operating policies. Results showed that with the increase of the lead time and the lag time of the arrival of peak flow, the mean FRF increases.

The magnitude of the mean FRF is more in the case of early peak arrival. Thus, this analysis states that the risk associated with the early flood arrival is more than the late arrival. If the advance release is discharged for 12 h EFH before the arrival of the expected time and the flood arrives early. In that case, the advance release along with the inflow peak, can generate a more hazardous situation. Again, the power production efficiencies decrease with the increase of the lag time of arrival of the flood; however, the efficiency has not reduced to 85%. Even if the FRF increases with the lag time, the disaster management authorities will get more time to disseminate warnings and devise execution plans. Accurate inflow forecasting to the reservoir is the critical input for better performance of such coupled modelling approach to have optimal output as preferred by decision-makers. Therefore, monitoring precipitation and streamflow upstream of the reservoir covering the entire basin for low-capacity reservoirs in hilly terrain should be essential to minimize flood havoc due to dam release.

During the lean period in RHEP, significant flow depletion can be observed, as described in Chapter 5, which can hinder the sustenance of aquatic species. Thus, to maintain the downstream biota, environmental flow needs to be released. The detail investigation of the lean period with the developed model is discussed in Chapter 8.

8

Impact of Inter-Basin Transfer Hydroelectric Project on Aquatic Habitat

8.1 Introduction

The health of the riverine habitat relies on the flow pattern, which is a crucial factor in the sustainable ecosystem. Reservoir operation and water diversion are the two prime sources of anthropogenic factors affecting the natural flow regime (Grantham et al., 2014; Yang et al., 2018). Although the frequency of flooding gets reduced due to the presence of a dam, the flashy characteristics of the flow increase to a greater extent during the flood period. In an inter-basin transfer of hydropower project, water is diverted to another basin for power generation. In that case, there is a variation in water availability at downstream regions due to diversion. Thus, the streamflow depletion may impede the downstream biota's sustenance (Li and Pasternack, 2021) and adversely affect agricultural land (Talukdar et al., 2021). Several methodologies were developed in the past few decades to understand the hydrologic alterations. Richter et al. (1996) developed an approach termed Indicators of Hydrologic Alteration (IHA), composed of 33 hydrologic parameters categorized into five groups that are sensitive to the anthropogenic activities of the riverine ecosystem (Marak et al., 2020; Ely et al., 2020; Gao et al., 2020; Zolfagharpour et al., 2022). Poff et al. (1997) highlighted five crucial flow regime characteristics: magnitude, frequency, duration, predictability, and rate of change. The

degree of hydrologic alterations was then evaluated using a single factor that will quantify high, moderate, and low alterations.

A hydropeaking dam upstream can affect the biodiversity of the downstream ecosystem through hydrologic alterations (Meile et al., 2011; Ray and Sarma, 2011; Moreira et al., 2019; Wang et al., 2019; Bürgler et al., 2022). Artificial flow fluctuations due to hydropeaking can hinder the sustenance rate of aquatic organisms (Greimel et al., 2018; Glowa et al., 2023; Hedger et al., 2023). Thus, to protect the ecosystem and to acquire the maximum benefit of electricity generation, there is a need for an integrated water resources management of regulated rivers (Widén et al., 2022). This implies the reoperation of the reservoir to meet the EFR for enhancing the sustainability of the downstream ecosystem. Therefore, a comprehensive understanding of low-flow hydrology is a prerequisite for water resource planning and design. A host of methodologies were implemented for the assessment of environmental flow. A total of more than 200 methodologies were applied in 44 countries. Tharme (2003) categorized those into four categories which include a) holistic (Tare et al., 2017), b) hydraulic (Książek et al., 2019; Stamou et al., 2018, Baruah and Sarma, 2021), c) habitat simulation (Leitner et al., 2017; Koutrakis et al., 2019), and d) hydrological (Richter et al., 1996; Tennant, 1976). Flow Duration Curves (FDC) are the most informative tools depicting the range of discharges from low to high flows (Smakhtin, 2001). Tennant (1976) suggested that 10% of the Mean Annual Flow (MAF) must be allocated to maintain the river flow, below which the river will be declared an unsuitable environment for thriving. It is one of the widely used methodologies for estimating environmental flow requirements because of its ease of application (Karimi et al., 2021).

The habitat suitability of target aquatic species can be expressed using Habitat Suitability Curves (HSC). The curves are developed based on flow parameters like velocity, depths, and substratum type (Rosenfeld et al., 2014; Baruah et al., 2023). The socio-economic condition of the riverine communities greatly relies on the availability of fish. As per the International Union for Conservation of Nature (IUCN), *'Tor Putitora,'* locally known as Pithia/Masheer, is listed as an endangered species on the Red List. The endemic zone of the target species is the Himalayan foothills. Due to the rapid development of hydropower projects, the habitat of the target species has fragmented, thereby affecting the spawning biology of the species. Thus, the impact of the flow alteration on fish species requires

detailed analysis, as such effects are species-dependent. The scope of minimizing the degradation of sustenance of downstream biota exists by releasing a minimum EF from the dam, which requires more scientific research. Thus, various researchers have conducted studies on the EFR along with the habitat suitability analysis of the aquatic organism. However, limited studies were carried out on environmental flow to be released from a dam to meet the downstream EFR impacting the power production efficiency.

Chapter 5 depicts the significant flow depletion in the post-dam state of the RHEP. This imparts the severity of the sustenance of the downstream biota due to the presence of the hydropower dam. Thus, a minimum environmental flow is necessary to release from the reservoir to meet the downstream flow requirement. This Chapter applies the CRH model coupled with a habitat suitability analysis to study the impact of RHEP on the downstream habitat of '*Tor Putitora.*' The study also analyses the scope of releasing different EF from the reservoir to meet the downstream EFR with an acceptable power production efficiency. The generalized methodology adopted in the analysis applies to single-purpose hydropower dams. It will help the decision-makers quantify EF to be released from the dam with a minimum compromise of power generation. The EFR at the downstream area was then evaluated using the Tennant Method and Flow Duration Curve Analysis (FDCA) technique in the pre-dam state. Tennant's method, utilized in this study, is a simplified hydrological approach that divides a natural year into the fish spawning period, which remains the primary focus of this research. Additionally, the FDCA represents a statistical characteristic curve plotted based on the duration or frequency of flow that equals or exceeds a specific value during the observation time (Ni et al., 2022). Using the simple application and direct relevance to the research objectives, both methods were effectively employed in this investigation. The monthly Non-Attainment (NA) of EFR was conducted to state how the EFR differs in the post-dam. The impact of EF released from the dam was examined on the target species downstream using the CRH, considering the tributary contribution depicted in Chapter 6. Two scenarios of 4 and 6 h peaking hours corresponding to three cases of reservoir level status a) at just above the dead storage, b) at half storage, and c) at full reservoir capacity were investigated. An analysis of the habitat suitability of the target species and power production efficiency was conducted to check the best-suited set of solutions.

8.2 Materials and Methods

8.2.1 Methodology

The minimum EFR at the downstream region was evaluated using Flow Duration Curve Analysis (FDCA) and Tennant's Method. A monthly non-attainment analysis of EFR in the pre-dam state was investigated to check whether the post-dam condition streamflow meets the target flow. A series of EFs with an upper bound based on the EFR at the downstream area and a lean period inflow event were given as input to the CRH model. Two scenarios with 4 and 6 h peaking hours and three cases at different initial storages were considered while operating the reservoir. The hydrodynamic part of the model estimates the downstream flow, depths, and velocities by routing the reservoir releases along with the EF released from the dam. The habitat suitability of the fish species *Tor Putitora* was analyzed based on the estimated downstream flow depths and velocities. Figure 8.1 shows the overall methodology.

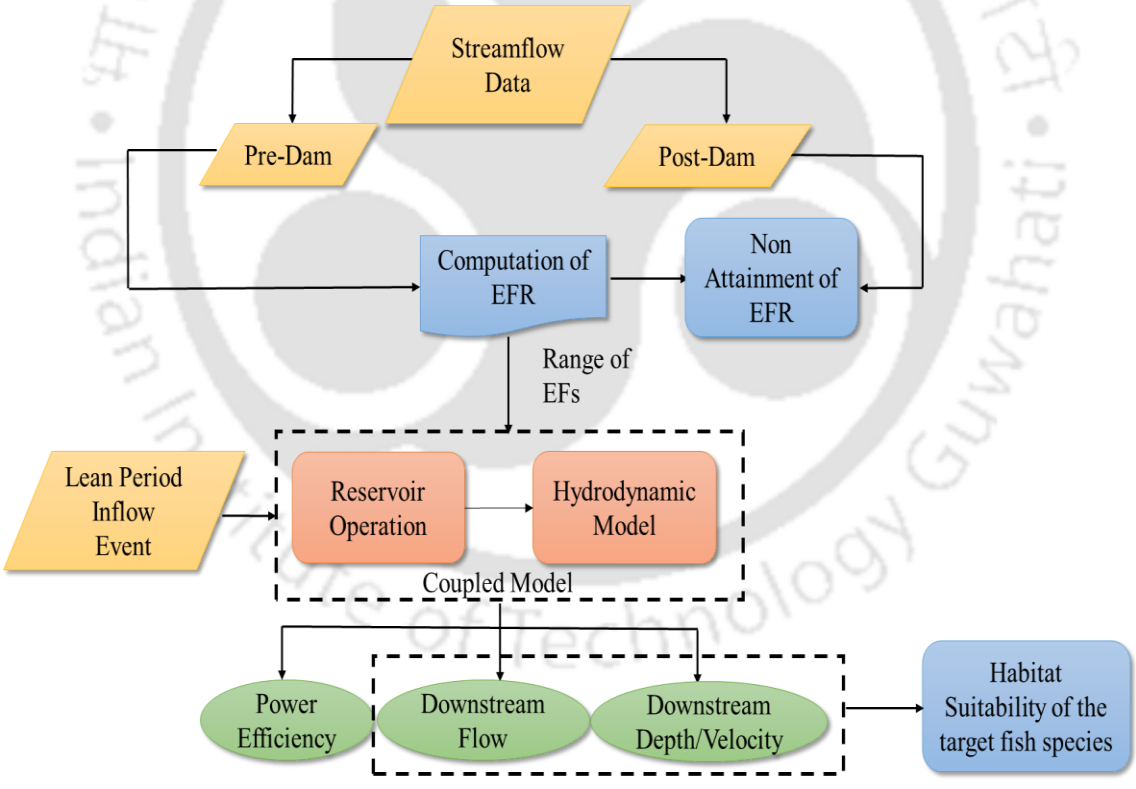

Figure 8.1:Methodology Adopted in the Analysis

8.2.2 Assessment of Minimum EFR at Downstream

8.2.2.1 Flow Duration Curve Analysis (FDCA)

The Flow Duration Curve is the graphical representation of the observed historical variation of the streamflow. It represents the percentage of time the flow occurred or exceeded. Low Flow indices can be estimated using the FDCA. The flow within the range Q70-Q99 is the most widely accepted low-flow index (Smakhtin, 2001). In this analysis, the Q90 flow was considered the low flow indicator. A comparative study of the low flows was conducted for the pre-dam and post-dam conditions.

8.2.2.2 Tennant (Montana) Method

Donald Tennant, in the year 1976, introduced a method of instream flow requirements of fish habitat quality (Tennant, 1976). This method is based on the percentage of Mean Annual Flow (MAF) for two different six-month periods- one for a low flow period (October-March) and the other for a high flow period (April-September). Tennant concluded that 10% of MAF is the minimum instantaneous flow requirement for the short-term survival of most aquatic life forms. Flows lower than 10% of MAF represent severe degradation of the ecosystem. The recommended flow regime is shown in Table 6.3.

Table 8.1:Flow recommendation by Tennant (Montana) Method

Description of Flows	Recommended base flow regime (% MAF)	
	October-March	April-September
Flushing or Maximum	200	200
Optimum Range	60-100	60-100
Outstanding	40	60
Excellent	30	50
Good	20	40
Fair or Degrading	10	30
Poor or Minimum	10	10
Severe degradation	<10	<10

8.2.2.3 Non-attainment of EFR in the post-dam

Assuming Tennant's Method of minimum streamflow, the monthly non-attainment analysis of EFR was conducted. The study was done to check whether the flow pertaining to the post-dam could meet the target EFR. The calculated EFR in the pre-dam condition was then utilized to analyze the monthly non-attainment analysis in the post-dam state. A factor Non-Attainment (NA) was incorporated to analyze the non-attainment of EFR values as per Equation 8.1. It is the ratio of the NA of EFR in months to the total number of months.

$$\text{NA}=\frac{\text{No. of Non-Attainment of EFR in Months}}{\text{Total No. of Months in post-dam}} \tag{8.1}$$

This factor is essential to understand how the downstream streamflow deviates from its natural flow regime.

8.2.3 Impact of EF released from the dam on Power Generation and Downstream Flow

The coupled model was applied to simulate the downstream flow, depths, and velocities. Due to flow diversion for power generation during the lean period, streamflow alteration is a common phenomenon that can hinder the aquatic species' spawning biology. Thus, a minimum environmental flow is necessary downstream. If a minimum environmental flow is released from the reservoir, Equation 4.1 of Chapter 4 can be written as

$$S_{t+1} = I_t + S_t - EF - S_{pt} - R_t \tag{8.2}$$

EF is the minimum environmental flow released from the reservoir to meet the downstream flow requirement. EF is assumed to be released from the reservoir when no spilling occurs. If there is a spill, the EF is assigned as zero. Thus, Equations 4.5 and 4.6 can be rewritten as

$$S_{t+1} = K; \text{ if } (S_a - R_t - EF + S_d) > K \tag{8.3}$$

$$S_{t+1} = (S_a - R_t - EF + S_d); \text{ if } (S_a - R_t - EF + S_d) < K \tag{8.4}$$

$$O_t = EF \tag{8.5}$$

The reservoir release during the lean period will be the environmental flow. The release will be routed down to check the downstream flow depth and velocity. A series of EF ranging from 2 m^3/s to 34 m^3/s was used in the simulation model to check the downstream flow requirement. Two scenarios of 4 hours and 6 hours of peaking power were considered. Each Scenario consists of three cases of initial storage: a) at 3.30 MCM (just above the dead storage), b) at 5.49 MCM (at half storage), and d) at 7.71 MCM (at gross storage).

The power production efficiency factor is calculated based on Equation 8.6.

$$\eta_p = \frac{\text{Total Power Produced (MW)}}{\text{Total Power Demand (MW)}} \tag{8.6}$$

The range of η_p varies from 0-1, where 0 indicates no power production, and 1 indicates the total power demand is met.

8.2.4 Instream Habitat Analysis of Tor Putitora

The instream habitat analysis of species *Tor Putitora* was conducted. It is locally known as *Pithia/Masheer*, a common fish species distributed within mid hills and foothills of the Himalayan region. In India, this fish species is a native of Assam, Arunachal Pradesh, Himachal Pradesh, Bihar, Uttarakhand, Kashmir, Manipur, Meghalaya, Nagaland, Sikkim, West Bengal (Jha et al., 2018) (Figure 8.2). According to the International Union of Conservation of Nature (IUCN), this species is labeled as *Endangered*. Sixty-seven fish species, including *Tor Putitora*, were reported in the Ranganadi River (Sinha, 2019).

The life span of '*Tor Putitora*' includes Fingerling, Juvenile, and Adult Stages. The fingerlings can mostly be seen at (0.1-0.6) m and velocity (0-1.2) m/s; juveniles can be seen at (0.1-1.8) m and velocity (0.3-1.2) m/s. Adults are mostly seen at depths greater than 2m (Johnson et al., 2021).

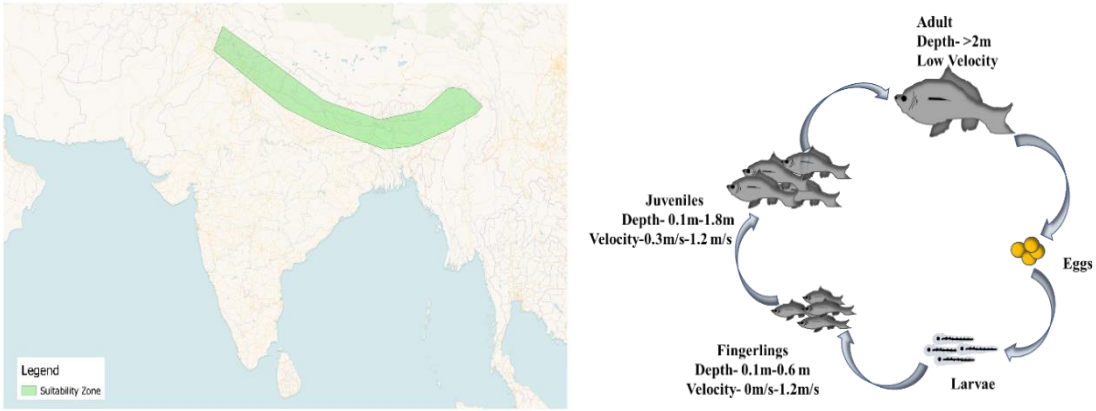

Figure 8.2:(a) Suitability Zone of Tor Putitora (b) Life Span of Tor Putitora

The habitat suitability criteria suggest how much the habitat is suitable for the sustenance of a target species. The flow parameters like streamflow, flow depth, and velocity are the pivotal factors that can determine the suitability of the target species. The suitability can be represented in the form of the Habitat Suitability Curve (HSC). The habitat suitability analysis of Juveniles of Tor Putitora was conducted in this analysis. For the development of HSC, various flow depths and velocities were divided into class intervals based on the range of suitable hydrologic variables of the target species available (Johnson et al., 2021). The values range from 0 to 1, where 0 represents an unsuitable environment, and 1 illustrates a suitable environment. The Habitat Suitability Index (HSI) of the flow depths and velocities for the corresponding EF were extracted from the HSC. The composite suitability indices (CSI) were computed from the suitable indices as per Equation 8.7 (Jowett and Davey, 2007).

$$CSI=WI*VI \tag{8.7}$$

where WI is the HSI corresponding to flow depth, and VI is the HSI corresponding to flow velocities.

A total length of 46 km from the dam site to the downstream area was considered in the analysis. Ten cross-sections were used in the investigation from upstream to downstream with a reach length of 4600 m. The usable area by the target species over the river reaches was estimated by incorporating the CSI values.

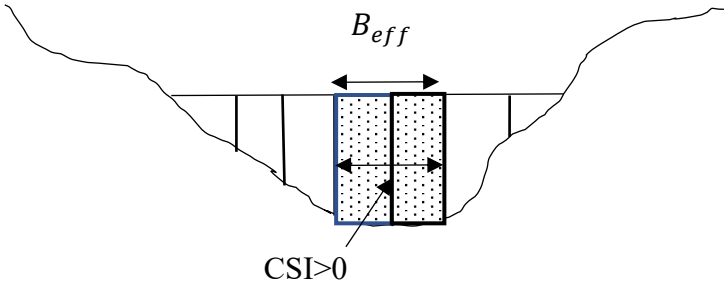

Figure 8.3: Effective Usable Section Width of a cross-section utilized by the target species.

The generated CSIs corresponding to depths and velocities of the cross sections were multiplied by the average effective usable section width (B_{eff}) shown in Figure 8.3 to compute the usable area over the river reach as per Equation 8.8.

$$\text{Usable Area}=\sum_{i=1}^{n}(CSI_i * B_{eff,i}) * L_{reach} \tag{8.8}$$

The total usable area (TUA) by the target species over the entire river reach was then estimated by summing up the usable areas over the reaches. The percentage of the TUA over the actual area was checked using a factor Area Utilization Rate (AUR) computed as per Equation 8.9.

$$\text{Area Utilization Rate (AUR)}=\frac{\text{Total Usable Area}}{\text{Actual Area}} \tag{8.9}$$

8.3 Results and Discussion

8.3.1 Assessment of Environmental Flow Requirement

The MAF from the available data series for the pre-dam condition was calculated as 113 m^3/s. As per the Tennant Method, the minimum flow to sustain short-term aquatic habitat was 10% of MAF, i.e., 11.3 m^3/s. In the post-dam condition of the river, the MAF was estimated as 48.19 m^3/s and 10% of the MAF was calculated as 4.8 m^3/s. Thus, the percentage reduction of 10% MAF was calculated as $\frac{11.3-4.8}{11.3}=0.57$, i.e., 57% of the total decrease in the minimum flow as per Tennant's Method can be observed in the post-dam condition.

From the FDCA, the Q90 in the pre-dam condition was observed as 34.3 m^3/s, whereas in the post-dam, the value of Q90 is 3.9 m^3/s. The percentage reduction of 90% of the dependable flow was estimated as $\frac{34.3-3.9}{34.3} = 0.886$, i.e., 88% of the 90% dependable flow reduction was observed in the post-dam condition.

8.3.2 Non-attainment of Environmental Flow Analysis

It can be observed that the magnitude of NA values during dry periods is significant, as shown in Figure 8.4. A high magnitude of 0.8 was observed from December to March, followed by 0.5 and 0.4 in April and November. From the month of May to October, the value of NA was observed as 0. This suggests the frequency of non-attainment was more in the dry than in the wet period.

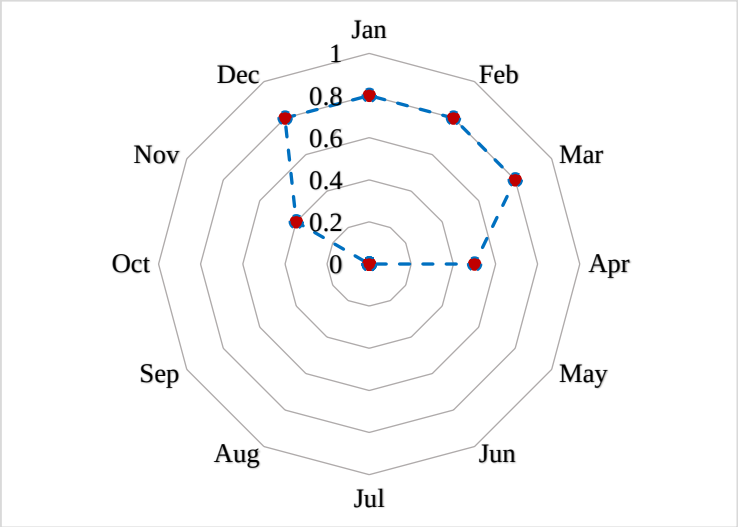

Figure 8.4:The monthly non-attainment factors of EFR.

8.3.3 Impact of EF on Power Generation and Downstream Flow

From the analysis, it can be ascertained that the streamflow alteration has dramatically impacted the downstream areas. The effect is maximum during the months of the lean period. During the lean period, the average inflow to the reservoir is around 15 m^3/s (calculated from the available inflow data). In most lean period months, the downstream flow was lower than the required EFR. To maintain the EFR at downstream, an analysis was conducted to release EF from the reservoir for two scenarios of 4 and 6 hours of peaking power generation. A series of EF ranging from 2-34 m^3/s was used in the simulation to check the downstream flow requirement. As per the FDCA, the Q90 in

the pre-dam condition was observed as 34.3 m^3/s. Hence, the upper bound of EF was considered as 34 m^3/s.

An inflow event of 80 h during the lean period (1/1/2010-4/1/2010) was considered in the analysis. The demand for power production is 405 MW per hour. The lean period inflow event is given as input to the coupled model. The power produced, average flow, average depths, and velocities were estimated for each EF considered. The power production efficiencies for all the scenarios were calculated per Equation 8.6.

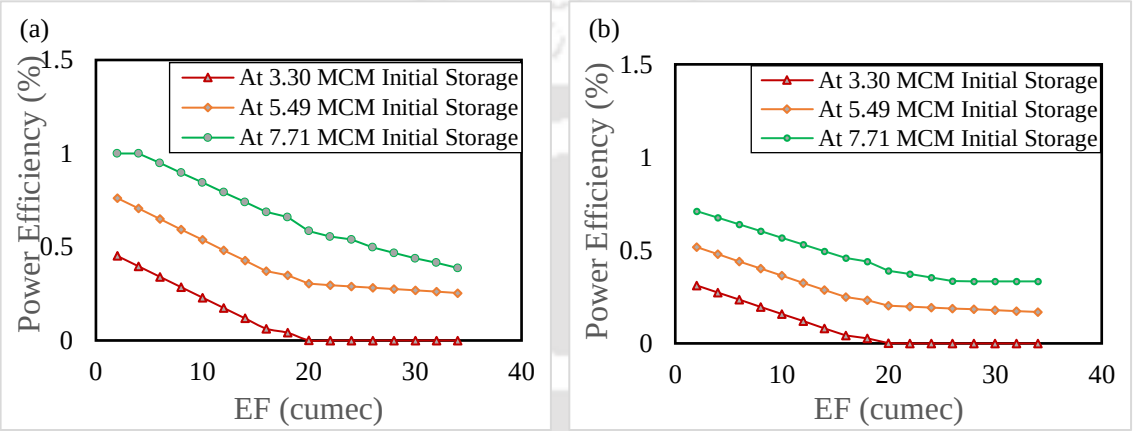

Figure 8.5: Power Efficiency at different EF (a) Scenario 1 (4 h peaking hours) (b) Scenario 2 (6 h peaking hours).

The analysis shows that with the increase of EF, the power efficiency decreases for both scenarios (Figure 8.5). The reduction of η_p can be attributed to the fact that as RHEP is an inter-basin transfer hydropower project, water is diverted to the Dikrong watershed for power production. Thus, if more water is discharged as the EF, power production would be lowered. Scenario 1 depicts at 7.71 MCM at 2 m^3/s and 4 m^3/s EF, 100 % power efficiency was observed, which gradually decreases to a value of 0.38 at the upper bound of EF. In the case of 3.30 MCM and 5.49 MCM, a similar trend can be observed with the highest power efficiency of 0.45 and 0.76 at 2 m^3/s EF. In the case of Scenario 2, an analogous trend of gradual decrease of η_p can be observed with the increase in EF. The maximum value of 0.71 η_p was observed at 7.71 MCM. The results indicate that power production efficiency rises as the initial reservoir storage increases. This implicates the significant role of initial storage in power production.

8.3.4 Instream Habitat Analysis of Tor Putitora

The HSCs of flow depth and velocities for Juveniles of the target species are shown in Figure 8.6. The estimation of CSIs was done as per Equation 8.7 from the HSC and the outputs from the hydrodynamic model. The total usable area was estimated for the entire river reaches considering the Scenarios.

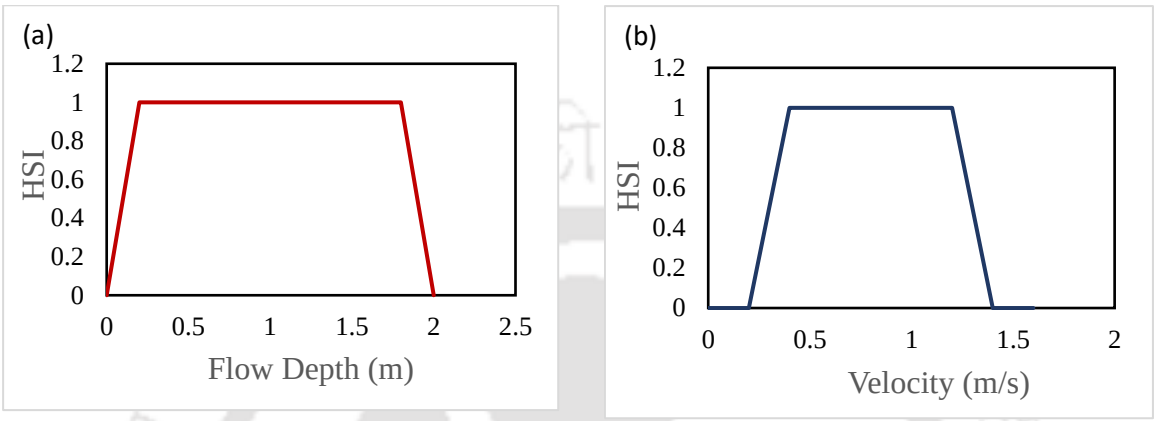

Figure 8.6: Habitat Suitability Curves of Juveniles considering (a) Flow Depth, (b) Velocity.

The estimated TUA for both Scenarios is shown in Figure 8.7. The magnitude of TUA was the same for the 4 h peaking hours and 6 h peaking hours at 3.30 MCM and 5.49 MCM (Figure 8.7). This is due to the fact that at the mentioned initial storages, there was no spill, so an equal amount of EF was released. However, when the reservoir storage is at gross capacity, the reservoir spills along with EF, contributing to the flow of the river, thereby increasing the TUA. A comparative analysis of both Scenarios depicts that a meagre change of TUA was observed in the case of initial storage at gross capacity.

The AUR for the considered Scenarios was estimated using Equation 8.9. ANNEXURE III shows the various scenario-based EF, the AUR, and the downstream flow at the gauging site in the lean period. For Scenario 1, at 3.30 MCM, the maximum power efficiency was observed at 2 m^3/s EF, whereas the maximum AUR was observed at 14 m^3/s EF. At 5.49 MCM, the maximum power efficiency was observed at 2 m^3/s EF. The maximum AUR was also observed at 14 m^3/s. At gross storage, full power production efficiency was observed at 2m^3/s and 4 m^3/s. The maximum AUR was observed at 16 m^3/s.

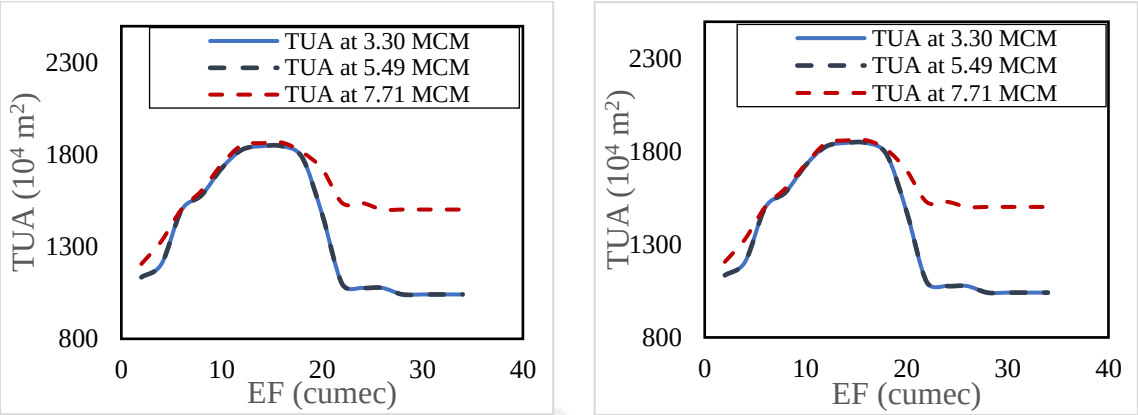

Figure 8.7:Total Usable Area of Tor Putitora corresponding to EFs (a) 4 h peaking hour (b) 6 h peaking hours

For Scenario 2, the magnitude AUR at 3.30 MCM and 5.49 MCM was the same as that of Scenario 1. However, there is a significant change can be observed in the case of power efficiencies. At 3.30 MCM and 5.49 MCM, the maximum power efficiency was observed at 2 m^3/s, which was lower than the observation in Scenario 1. At 7.71 MCM, the maximum AUR was observed at 14 m^3/s EF.

The average flow at the gauged site (NT Road Crossing, Lakhimpur) at 3.30 MCM and 5.49 MCM for 2m^3/s, 4m^3/s, and 6 m^3/s were lower than the required EFR, i.e., 11.3 m^3/s. At gross capacity for both Scenarios, the EFR was able to meet from 6 m^3/s EF. The analysis shows that the best solution can be achieved if the initial storage is at full reservoir capacity. However, maintaining the reservoir storage at gross capacity is not possible during the lean period, as the inflow to the reservoir is very low. The issue can be resolved if an additional seasonal storage reservoir is constructed upstream of RHEP. The storage reservoir will be utilized in the lean period to maintain the water level of RHEP at FRL. With this structural measure upstream, the flow downstream can be improved along with the power production.

8.4 Conclusions

Chapter 5 depicts the severity of streamflow alterations, which implies the necessity of EF from the dam to sustain the aquatic biodiversity. This study analyzed the scope of EF released from the dam to meet the downstream EFR. The total area utilization of an endangered species Tor. Putitora was also explored. The minimum environmental flow at downstream was calculated using Tennant's method and FDCA. The minimum flow

per Tennant's method has reduced to 57% in the post-dam state. The Q90 in the pre-dam state has reduced to 88%, as observed in the post-dam. The impact of EF released from the dam was conducted considering the mentioned scenarios and the three cases. A lean period inflow hydrograph, along with the series of EF released from the dam, was incorporated into the CRH model coupled with a habitat-suitable model. The analysis showed that with the increase of EF, the power production efficiency decreases for both scenarios. The CSIs were estimated based on the HSC and the flow variables from the hydrodynamic part of the model. The TUA and the AUR were evaluated for the scenarios considered. The analysis states that the best solution was obtained when the initial storage was at gross storage. However, maintaining the reservoir level at the FRL is difficult during the lean period. So, to maintain the reservoir level at FRL, a structural measure can be implemented by constructing a seasonal storage reservoir upstream of the dam. The storage reservoir will store water that can be utilized in the lean period to maintain the reservoir level of the RHEP at FRL. This measure can help to retain the downstream flow requirement to sustain aquatic species. A conflicting water allocation requirement exists while considering EF and power production. Hence, a scenario-based robust decision must be made with proper weightage on the required benefit while releasing EF with minimum compromised power production. The power efficiencies and AUR for the scenarios and different EFs were developed in a tabular format that can be used as a decision-support tool during the lean period. The decision-making and planning committee can adopt this generalized methodology to decide the feasible EF from the dam to maintain the downstream habitat in a healthy state with minimal power compromisation.

9

Conclusions and Recommendations

9.1 A brief review of the work done

This study presented a modelling framework for analyzing the impact of hydropower dams on downstream flow. The framework primarily consists of a reservoir operation model and a hydrodynamic model. A comprehensive study was carried out to examine the impact of hydropower dams over the entire water year. Further, a detailed analysis of the characterization of outflow hydrographs from IBWT and NIBWT hydropower dams was conducted. A streamflow generation module was developed for ungauged tributaries located downstream of the dam using the DAR method incorporated into the coupled model. The impact of the dams during the flood period was investigated. A methodology for flood peak moderation was developed subject to the availability of a reservoir inflow forecast model. A simulation-optimization approach was employed using the CRH model. The analysis quantifies the advance release to be made within the EFH before the arrival of the flood. Monte Carlo Simulation was used to generate multiple inflow scenarios into the coupled model to carry out the uncertainty analysis. EFH was found to be more sensitive to the inflow peak as compared to the inflow volume. The effect of the magnitude of peak and its time of arrival on FRF was evaluated using the AOP, and system performance was checked for various inflow scenarios. The analysis inferred that with AOP, the inflow forecast must be conservative towards the amount of peak flow as well as early arrival time than the expected time of arrival. For the lean period, the effect of IBWT hydropower dams on the downstream habitat of an IUCN red-listed endangered species, *Tor Putitora*, was also investigated. The analysis utilized the CRH model coupled with a habitat suitability analysis to determine the scope of releasing different

EF from the reservoir to meet the downstream EFR with an acceptable power production efficiency. A decision support tool was developed to provide information on power efficiency and area utilization rate of the fish species across various scenarios and EF. This tool can assist the planning and decision-making committee in identifying viable EF release strategies while minimizing any adverse impacts on power generation.

9.1.1 Characterization of Downstream Flow of a hydropower dam

A comparative analysis of downstream flood scenarios was presented first for a proposed NIBWT hydroelectric project (LSHP) with and without a dam. The study showed that the presence of a dam reduces the frequency of flooding but maintains a similar peak magnitude compared to regional floods. However, the outflow hydrograph becomes more abrupt. The F.I. value increases from 0.26 to 0.52 when the dam is filled to its full reservoir level. At downstream, the F.I. values decrease, but the magnitude increases with higher initial reservoir storages. The analysis also reveals a significant decrease in peak time from 7 hours to 2 hours, reducing the disaster response time by 5 hours. This states that with the dam's presence, the flashy characteristic of the release hydrograph increases, which can lead to flash floods. The F.I. developed in the study is a more case-specific metric and is very sensitive to the initial flow. If the initial flow is substantially lower than the peak flow, the numerical value of the index can be very high. The numerical value, though, indicates the severity of flashiness characteristics, which can lead to inconvenience in providing a standard range value for a more generalized index. Thus, the index is more suitable for comparing flashiness characteristics of the same river in different periods. Hence, a more generalized index SDFI was developed to determine the flashiness of different flood events. The SDFI has been implemented in both the NIBWT and IBWT hydropower dams. Results showed that the magnitude of SDFI increases in the with-dam condition as compared to the without-dam condition in the case of both NIBWT and IBWT hydropower dams. This implies that dam-induced flood is a combination of both regional floods and flash floods. An analysis was conducted to rank dam-induced floods among the global hazard lists by considering the factors suggested by Bryant. The study ranks dam-induced floods as the second-highest among the global hazards. This ranking suggests revising flood disaster management policies downstream of hydropower dams. Additionally, a streamflow analysis of RHEP which is in operation, confirms a drastic decrease in flow during the dry period with the dam's presence, from 28 m^3/s to 0.84 m^3/s. The R-B Index also increases, indicating a

flashier flow during the wet period. These alterations highlight the importance of environmental flow release from the dam to preserve aquatic biodiversity.

9.1.2 Flow Assessment of a downstream of a hydropower dam

This study aimed to develop a methodology for accurate flood modeling by incorporating lateral flow from ungauged catchments into a reservoir operation and a hydrodynamic model. The DAR method is used for streamflow estimation in ungauged catchments. Model parameters were calibrated using various algorithms, with GRG performing the best. The model successfully estimated the 'α' value despite limited data availability. Therefore, this methodology has a potential application in a data-scarce region. The exponent α will vary from case to case and must be optimized following the procedure described in Chapter 6.

The magnitude of the lateral flow contribution obtained was incorporated into the 1D hydrodynamic model to compute the flood levels and discharge at N.T. Road Crossing, Lakhimpur. The lateral flow contribution of Tributary 1 was estimated as 44% of the gauged streamflow, whereas Tributary 2's was estimated as 36% of the gauged streamflow. Therefore, this analysis concluded that there is a substantial contribution from the tributaries that cannot be neglected. Two hourly reservoir inflow events were then subsumed into the reservoir operation model, and the releases from the reservoir were given input to the 1D hydrodynamic model, including the lateral flow contributions. Results showed that the peak flow had increased by more than 75% with flow contribution from tributaries. Thus, in the case of the Ranganadi River System, the flow contribution from the tributaries located downstream of the hydel project contributes substantially to the total downstream flow. The model's output discharges and water levels were then compared with the observed stage and discharges. Results revealed that the magnitudes of the discharges and stage were in the same range as the observed data. The relative errors of the observed and simulated discharges of Event 1 and Event 2 were estimated as 4.76 % and 5.36 %, respectively. Similarly, for Event 1 and Event 2, the observed and simulated stage percentage errors are obtained as 0.31 and 0.63 %, respectively. Minor differences can be attributed to the variations in the actual observation time of streamflow. This approach was then implemented in the coupled modelling framework developed and utilized for flood and lean periods. This methodology was employed to formulate the management strategies of RHEP during the

flood and lean periods. In the lean period, the inflow to the reservoir is low, as a result, the lateral flow contribution is also less.

9.1.3 Optimal Advance Release Scheme Based on Effective Forecast Horizon to minimize flood

Chapter 9 described a model that utilizes the CRH model to manage downstream flooding effectively. A simulation-optimization technique was utilized to determine the optimal release strategy based on the anticipated flood conditions downstream. The advance release was determined by considering the safe downstream discharge and employing a distribution factor to determine the percentage of safe downstream discharge that should be released before the onset of flooding. For the analysis, a flood event of 28/6/2015 was selected as a perfect forecast event based on historical flood peaks and volumes. The optimal advance release was evaluated for various forecast horizons, ranging from 6 to 24 h. The study inferred that in the case of the perfect forecast, the EFH was determined as 12 h. By implementing the SOP, six flood events exceeded the DL. However, with the introduction of the AOP, the number of floods above the DL decreased to zero. This proves that AOP was successful in moderating the peak flow. An uncertainty analysis was carried out to assess the variability in inflow to the reservoir by generating multiple inflow sequences for the perfect forecast event. Using MCS, a total of twenty inflow sequences were generated. Each sequence was individually modeled to determine the EFH and the corresponding mean FRF. The findings indicated that the AOP demonstrated better flood moderation capabilities in all twenty inflow scenarios compared to the SOP. Additionally, the study emphasized that the EFH is more sensitive to the magnitude of the inflow peak than the inflow volume. The analysis also revealed that the forecast horizon with the maximum flood moderation can be extended up to 12 h. Beyond this timeframe, it was ineffective in simultaneously achieving both benefits of power production and flood peak moderation. Therefore, it is recommended that the EFH should not exceed 12 h for RHEP. Furthermore, the generation of multiple scenarios, with different combinations of weightage to flood moderation and power generation, can facilitate the formulation of a comprehensive decision-making policy to maximize the benefits, considering other factors not explicitly considered in this study.

The previous study described a decision efficiency-based assessment of determining EFH. A catchment-based analysis was also conducted to determine the EFH, representing the time delay between peak rainfall and peak flood occurrence. A sensitivity analysis was conducted with EFH as 12 h and different inflow members generated by forecast error in peak flow and arrival time. Positive forecast errors indicated higher peaks than the perfect forecast, while negative ones indicated lower ones. A comparison was made between the mean flow deviation from the AOP with the different inflow sequences and the actual SOP. The results demonstrated that increased lead time and lag time of peak flow arrival corresponded to higher mean FRF. If the flood arrives later than the forecasted time, the power production efficiency decreases with the lag time of arrival of the flood. However, the AOP imparts 100 % power production efficiency if the flood peak arrives earlier than that of the forecasted one.

With the implementation of AOP, the reservoir outflow varies from that of the operation made using SOP. A study was carried out to have an idea about the range of outflow variation due to revised operation using AOP. The results showed that the mean flow deviation is greater when the peak flood arrives earlier than the expected time compared to when the peak flow arrives later. The sensitivity analysis showed that the risk associated with the flood peak arriving earlier than the expected time of arrival is more than the flood peak arriving later. While there is a compromise in power generation when the flood arrives later than expected, it remains within an acceptable range, with power production efficiency not dropping below 85%, even with a 6 h delay. Although the mean FRF was observed as 1 in the case of flood peak arriving later than the estimated flood peak, decision makers can have more time for disaster preparedness. If the flood arrives earlier than anticipated, there may be less time to disseminate warnings, leading to reduced awareness among the affected communities. Thus, the inflow forecast must be conservative towards the magnitude of peak flow as well as the arrival time (i.e., early arrival).

9.1.4 Impact of Inter-Basin Water Transfer hydroelectric project on aquatic habitat

Chapter 9 applies the CRH model coupled with a habitat suitability analysis to analyze the impact of RHEP on the downstream habitat of an endangered aquatic species ‘Tor Putitora’.

Chapter 5 highlighted the severity of streamflow alterations and the need for EF from the dam to sustain aquatic biodiversity. The minimum EFR was calculated using Tennant's method and FDCA, resulting in a reduction of 57% compared to the pre-dam state. The impact of EF release was evaluated through the CRH model, considering different scenarios. The Q90 in the pre-dam state has reduced to 88%, as observed in the post-dam. This analysis depicts the severity of streamflow alteration of low flow in the post-dam condition. An analysis of the non-attainment of the downstream environmental flow requirement was conducted. Results showed that non-attainment frequency was observed more in the dry period than in the wet period. This states the necessity to release a minimum EF from the dam to meet the downstream EFR. The impact of EF released from the dam was assessed considering different initial storages and peak hours. A lean period inflow hydrograph and the series of EF released from the dam were incorporated into the CRH and the habitat suitability model. The analysis showed that with the increase of EF, the power production efficiency decreases for both scenarios. The decrease in η_p can be explained by the fact that the RHEP project involves transferring water to the Dikrong basin for hydropower generation. Consequently, when more water is discharged as EF, it results in a reduction in power production. The CSIs were then estimated based on the available HSC and the flow variables from the hydrodynamic part of the model. The TUA and the AUR were estimated for the scenarios considered. The analysis revealed that the best solution was achieved when the initial storage was at gross storage, although maintaining the reservoir level at the FRL during the lean period was challenging. To address this, a structural measure involving the construction of a seasonal storage reservoir upstream of the dam is proposed. This reservoir would store water to be used during the lean period, maintaining the reservoir level at FRL and ensuring downstream flow to sustain aquatic species. The study emphasizes the need for a robust decision-making process that considers both EF and power production requirements. A decision support tool was developed, presenting power efficiencies and AUR for different scenarios and EF levels, aiding the planning and decision-making committee in determining feasible EF releases while minimizing power compromises. This generalized methodology can guide the maintenance of a healthy downstream habitat with minimal impact on power generation.

9.2 Key Contributions of the Thesis

- A coupled model consisting of a reservoir operation and hydrodynamic model is developed. This model will help in comprehensive understanding and effective management of the reservoir system considering the downstream scenario.
- The total downstream flow at far distance is basically combination of reservoir release and lateral flow contribution from major tributaries. Therefore, flood modelling must also constitute the tributary contributions as well. Thus, a streamflow generation module for ungauged tributaries is developed using the DAR method.
- Another contribution is the development of an adaptive management framework for controlling downstream floods, subject to availability of a reservoir inflow forecast system. The study quantifies the advance release over diverse inflow forecast horizons before the actual arrival of the flood. Impact of forecast uncertainty on downstream flow scenarios generated by the AOP has also been analysed.
- During the lean period, the scope of releasing different amount of environmental flow from the dam to meet the downstream environmental flow requirement is investigated by considering a habitat suitability index of an endangered species. The total usable area over the river reach of the mentioned fish species was evaluated from the flow parameters simulated by the hydrodynamic component of the model. The power production efficiencies and area utilization rate by the target species were assessed in all the cases to prepare an easy-to-use decision support tool in a tabular form depicting the possible states of environmental flow.

9.3 Recommendations for future work

This study utilizes a coupled model to reduce the severity of the downstream impact of a hydropower dam in lean and flood periods. The scope of extension of the current research includes the following points.

1. The hydrodynamic simulation in the analysis was performed using a 1-D hydrodynamic model. The methodology can be improved by coupling a 2-D hydrodynamic model for the spread of flood inundation and its impact on river training works.

2. During the monsoon period, it has been assumed that the turbines run continuously for 24 hours a day. As a result, water is diverted to the Dikrong River continuously for power

generation. This may create adverse flooding situation at Dikrong. A comprehensive analysis of the impact of flooding at Dikrong is necessary.

3. The coupled modelling approach can be enhanced by incorporating the damage potential of the downstream areas for an efficient decision-making process of the dam authority and disaster management authority.

4. The habitat suitability analysis can be carried out for other species as well applying the similar methodology. Researchers working in the core field of fish habitat may look into the suitable fish density in their habitat area so that a direct fish count can also be made.

References

Abdo, T. F., Marcon, L., & Bazzoli, N. (2018). Downstream effects of a large reservoir on the reproductive activity of Prochilodus hartii (Pisces: Prochilodontidae). *Animal Reproduction Science*, *190*(February), 102–107. https://doi.org/10.1016/j.anireprosci.2018.01.013

Agostinho, A. A., Pelicice, F. M., & Gomes, L. C. (2008). Dams and the fish fauna of the Neotropical region: Impacts and management related to diversity and fisheries. *Brazilian Journal of Biology*, *68*(4 SUPPL.), 1119–1132. https://doi.org/10.1590/S1519-69842008000500019

Ahmed, J. A., & Sarma, A. K. (2005). Genetic algorithm for optimal operating policy of a multipurpose reservoir. *Water Resources Management*, *19*(2), 145–161. https://doi.org/10.1007/s11269-005-2704-7

Ahmed, J. A., & Sarma, A. K. (2007). Artificial neural network model for synthetic streamflow generation. *Water Resources Management*, *21*(6), 1015–1029. https://doi.org/10.1007/s11269-006-9070-y

Ali, K., Bajracharyar, R. M., & Raut, N. (2017). Advances and Challenges in Flash Flood Risk Assessment: A Review. *Journal of Geography & Natural Disasters*, *07*(02). https://doi.org/10.4172/2167-0587.1000195

Althoff, D., Rodrigues, L. N., & Silva, D. D. da. (2022). Predicting runoff series in ungauged basins of the Brazilian Cerrado biome. *Environmental Modelling and Software*, *149*(December 2021), 105315. https://doi.org/10.1016/j.envsoft.2022.105315

Amnatsan, S., Yoshikawa, S., & Kanae, S. (2018). Improved forecasting of extreme monthly reservoir inflow using an analogue-based forecasting method: A case study of the Sirikit Dam in Thailand. *Water (Switzerland)*, *10*(11). https://doi.org/10.3390/w10111614

Anderson, E. P., Freeman, M. C., & Pringle, C. M. (2006). Ecological consequences of hydropower development in Central America: Impacts of small dams and water diversion on neotropical stream fish assemblages. *River Research and Applications*, *22*(4), 397–411. https://doi.org/10.1002/rra.899

Andrei, A., Robert, B., & Erika, B. (2017). Numerical Limitations of 1D Hydraulic Models Using MIKE11 or HEC-RAS software - Case study of Baraolt River, Romania. *IOP Conference Series: Materials Science and Engineering*, *245*(7), 11–14. https://doi.org/10.1088/1757-899X/245/7/072010

Annys, S., Ghebreyohannes, T., & Nyssen, J. (2020). Impact of hydropower dam operation and management on downstream hydrogeomorphology in semi-arid environments (Tekeze, Northern Ethiopia). *Water (Switzerland)*, *12*(8). https://doi.org/10.3390/w12082237

Ashrafi, S. M., & Dariane, A. B. (2017). Coupled Operating Rules for Optimal Operation of Multi-Reservoir Systems. *Water Resources Management*, *31*(14), 4505–4520. https://doi.org/10.1007/s11269-017-1762-y

Azad, A. S., Md, M. S., Watada, J., Vasant, P., & Vintaned, J. A. G. (2020). Optimization of the hydropower energy generation using Meta-Heuristic approaches: A review. *Energy Reports*, *6*, 2230–2248. https://doi.org/10.1016/j.egyr.2020.08.009

Azmeri, Hadihardaja, I. K., and Vadiya, R. 2016. Identification of flash flood hazard zones in mountainous small watershed of Aceh Besar Regency, Aceh Province, Indonesia. *Egyptian Journal of Remote Sensing and Space Science*, 19(1), 143–160. https://doi.org/10.1016/j.ejrs.2015.11.001

Bai, Y., Wang, P., Xie, J., Li, J., & Li, C. (2014). Additive Model for Monthly Reservoir Inflow Forecast. *Journal of Hydrologic Engineering*, *20*(7), 04014079. https://doi.org/10.1061/(asce)he.1943-5584.0001101

Baird, I. G., Manorom, K., Phenow, A., & Gaja-Svasti, S. (2020). Opening the gates of the Pak Mun Dam: Fish migrations, domestic water supply, irrigation projects and politics. *Water Alternatives*, *13*(1), 141–159.

Baker, D. B., Richards, R. P., Loftus, T. T., & Kramer, J. W. (2004). A new flashiness index: Characteristics and applications to Midwestern rivers and streams. *Journal of the American Water Resources Association*, *40*(2), 503–522. https://doi.org/10.1111/j.1752-1688.2004.tb01046.x

Banerjee, A., & Dimri, A. P. (2019). Comparative analysis of two rainfall retrieval algorithms during extreme rainfall event: a case study on cloudburst, 2010 over Ladakh (Leh), Jammu

and Kashmir. *Natural Hazards*, *97*(3), 1357–1374. https://doi.org/10.1007/s11069-019-03714-0

Barati, R. 2013. Application of excel solver for parameter estimation of the nonlinear Muskingum models. *KSCE Journal of Civil Engineering*, 17, 1139-1148.

Baruah, A., Barman, D., Arjun, B. M., Chyne, B. L., Kurbah, S., & Aggarwal, S. P. (2023). Habitat response of adult fish species under the influence of ecological flow and hydrodynamic regime in perennial river system. *Ecohydrology*, *16*(1). https://doi.org/10.1002/eco.2481

Baruah, A., & Sarma, A. K. (2021a). A fully coupled two-dimensional flow—vegetation routing model in open channel flow. *Environmental Fluid Mechanics*, *21*(5), 1091–1117. https://doi.org/10.1007/s10652-021-09810-9

Baruah, A., & Sarma, A. K. (2021b). Ecological flow assessment using hydrological and hydrodynamic routing model in Bhogdoi river, India. *Modeling Earth Systems and Environment*, *7*(4), 2453–2462. https://doi.org/10.1007/s40808-020-00982-9

Berga, L. (2016). The Role of Hydropower in Climate Change Mitigation and Adaptation: A Review. *Engineering*, *2*(3), 313–318. https://doi.org/10.1016/J.ENG.2016.03.004

Bertoni, F., Giuliani, M., Castelletti, A., & Reed, P. M. (2021). Designing With Information Feedbacks: Forecast Informed Reservoir Sizing and Operation. Water Resources Research, 57(3), 1–19. https://doi.org/10.1029/2020WR028112

Bhattacharjya, R. K. (2011). Solving Groundwater Flow Inverse Problem Using Spreadsheet Solver. *Journal of Hydrologic Engineering*, *16*(5), 472–477. https://doi.org/10.1061/(asce)he.1943-5584.0000329

Borgohain, P. L. (2019). Downstream impacts of the Ranganadi hydel project in Brahmaputra Basin, India: Implications for design of future projects. *Environmental Development*, *30*(April), 114–128. https://doi.org/10.1016/j.envdev.2019.04.005

Boulange, J., Hanasaki, N., Yamazaki, D., & Pokhrel, Y. (2021). Role of dams in reducing global flood exposure under climate change. *Nature Communications*, *12*(1), 1–7. https://doi.org/10.1038/s41467-020-20704-0

Branquinho, A. A., & Brito, D. (2016). Impactos de grandes barragens na biodiversidade: Uma

análise cienciométrica. *Neotropical Biology and Conservation*, *11*(2), 101–109. https://doi.org/10.4013/nbc.2016.112.07

Bryant, E. (2005). Natural hazards. Cambridge University Press.

Bürgler, M., Vetsch, D. F., Boes, R. M., & Vanzo, D. (2022). Systematic comparison of 1D and 2D hydrodynamic models for the assessment of hydropeaking alterations. *River Research and Applications*, *June 2022*, 460–477. https://doi.org/10.1002/rra.4051

Caporali, E. (2001). A Distributed Hydrological Model of Flash-Floods. *Coping With Flash Floods*, 203–218. https://doi.org/10.1007/978-94-010-0918-8_20

Chaudhari, S., & Pokhrel, Y. (2022). Alteration of River Flow and Flood Dynamics by Existing and Planned Hydropower Dams in the Amazon River Basin. *Water Resources Research*, *58*(5). https://doi.org/10.1029/2021WR030555

Chen, J. C., Huang, W. S., & Tsai, Y. F. (2020). Variability in the characteristics of extreme rainfall events triggering debris flows: a case study in the Chenyulan watershed, Taiwan. *Natural Hazards*, *102*(3), 887–908. https://doi.org/10.1007/s11069-020-03938-5

Chen, Q., Zhang, X., Chen, Y., Li, Q., Qiu, L., & Liu, M. (2015). Downstream effects of a hydropeaking dam on ecohydrological conditions at subdaily to monthly time scales. *Ecological Engineering*, *77*, 40–50. https://doi.org/10.1016/j.ecoleng.2014.12.017

Chernet, H. H., Alfredsen, K., & Midttømme, G. H. (2014). Safety of Hydropower Dams in a Changing Climate. *Journal of Hydrologic Engineering*, *19*(3), 569–582. https://doi.org/10.1061/(asce)he.1943-5584.0000836

Chuan, W., Lei, Y., & Jianguo, Z. (2014). Study on optimization of radiological worker allocation problem based on nonlinear programming function-fmincon. *2014 IEEE International Conference on Mechatronics and Automation, IEEE ICMA 2014*, 1073–1078. https://doi.org/10.1109/ICMA.2014.6885847

Collischonn, W., Morelli Tucci, C. E., Clarke, R. T., Chou, S. C., Guilhon, L. G., Cataldi, M., & Allasia, D. (2007). Medium-range reservoir inflow predictions based on quantitative precipitation forecasts. *Journal of Hydrology*, *344*(1–2), 112–122. https://doi.org/10.1016/j.jhydrol.2007.06.025

Coulibaly, P., Haché, M., Fortin, V., & Bobée, B. (2005). Improving daily reservoir inflow forecasts with model combination. *Journal of Hydrologic Engineering*, *10*(2), 91–99.

https://doi.org/10.1016/(ASCE)1084-0699(2005)10:2(91)

Cui, T., Tian, F., Yang, T., Wen, J., & Khan, M. Y. A. (2020). Development of a comprehensive framework for assessing the impacts of climate change and dam construction on flow regimes. *Journal of Hydrology*, *590*(May), 125358. https://doi.org/10.1016/j.jhydrol.2020.125358

de Carvalho Barreto, I. D., Stosic, T., Filho, M. C., Delrieux, C., Singh, V. P., & Stosic, B. (2020). Complexity Analyses of Sao Francisco River Streamflow: Influence of Dams and Reservoirs. *Journal of Hydrologic Engineering*, *25*(10), 1–8. https://doi.org/10.1061/(asce)he.1943-5584.0001996

Denaro, S., Anghileri, D., Giuliani, M., & Castelletti, A. (2017). Informing the operations of water reservoirs over multiple temporal scales by direct use of hydro-meteorological data. *Advances in Water Resources*, *103*, 51–63. https://doi.org/10.1016/j.advwatres.2017.02.012

DHI Report. (2019). Detailed Project Report (DPR) for Development of Subansiri River , National Waterway-95, *Inland Waterways Authority of India*. *March*.

Ding, W., Zhang, C., Peng, Y., Zeng, R., Zhou, H., & Cai, X. (2015). An analytical framework for flood water conservation considering forecast uncertainty and acceptable risk. Water Resources Research, 51(6), 4702-4726.

Dugan, P. J., Barlow, C., Agostinho, A. A., Baran, E., Cada, G. F., Chen, D., Cowx, I. G., Ferguson, J. W., Jutagate, T., Mallen-Cooper, M., Marmulla, G., Nestler, J., Petrere, M., Welcomme, R. L., & Winemiller, K. O. (2010). Fish migration, dams, and loss of ecosystem services in the mekong basin. *Ambio*, *39*(4), 344–348. https://doi.org/10.1007/s13280-010-0036-1

Ely, P., Fantin-Cruz, I., Tritico, H. M., Girard, P., & Kaplan, D. (2020). Dam-Induced Hydrologic Alterations in the Rivers Feeding the Pantanal. *Frontiers in Environmental Science*, *8*(December), 1–17. https://doi.org/10.3389/fenvs.2020.579031

Fang, H. Bin, Hu, T. S., Zeng, X., & Wu, F. Y. (2014a). Simulation-optimization model of reservoir operation based on target storage curves. *Water Science and Engineering*, *7*(4), 433–445. https://doi.org/10.3882/j.issn.1674-2370.2014.04.008

Fang, H. Bin, Hu, T. S., Zeng, X., & Wu, F. Y. (2014b). Simulation-optimization model of

reservoir operation based on target storage curves. *Water Science and Engineering*, *7*(4), 433–445. https://doi.org/10.3882/j.issn.1674-2370.2014.04.008

Feng, Z. kai, Niu, W. jing, Zhang, R., Wang, S., & Cheng, C. tian. (2019). Operation rule derivation of hydropower reservoir by k-means clustering method and extreme learning machine based on particle swarm optimization. *Journal of Hydrology*, *576*(June), 229–238. https://doi.org/10.1016/j.jhydrol.2019.06.045

Fráguas, P. S., & Pompeu, P. S. (2021). Hydropower affects fish trophic structure both downstream of the dam and upstream of the reservoir. *Neotropical Ichthyology*, *19*(1), 1–15. https://doi.org/10.1590/1982-0224-2020-0071

Gao, Y., Xie, Y. hong, & Zou, D. sheng. (2020). Hydrological regime change and its ecological responses in East Dongting Lake, China. *Ecohydrology and Hydrobiology*, *20*(1), 142–150. https://doi.org/10.1016/j.ecohyd.2019.07.003

Garcia, M., Juan, A., & Bedient, P. (2020). Integrating reservoir operations and flood modeling with HEC-RAS 2D. *Water (Switzerland)*, *12*(8). https://doi.org/10.3390/w12082259

Georgakakos, K. P., & Hudlow, M. D. (1984). Quantitative precipitation forecast techniques for use in hydrologic forecasting. *Bulletin - American Meteorological Society*, *65*(11), 1186–1200. https://doi.org/10.1175/1520-0477(1984)065<1186:QPFTFU>2.0.CO;2

Ghimire, B. N. S., & Reddy, M. J. (2013). Optimal reservoir operation for hydropower production using particle swarm optimization and sustainability analysis of hydropower. *ISH Journal of Hydraulic Engineering*, *19*(3), 196–210. https://doi.org/10.1080/09715010.2013.796691

Ghosh, S., & Guchhait, S. K. (2016). Dam-induced changes in flood hydrology and flood frequency of tropical river: a study in Damodar River of West Bengal, India. *Arabian Journal of Geosciences*, *9*(2), 1–26. https://doi.org/10.1007/s12517-015-2046-6

Gianfagna, C. C., Johnson, C. E., Chandler, D. G., & Hofmann, C. (2015). Watershed area ratio accurately predicts daily streamflow in nested catchments in the Catskills, New York. *Journal of Hydrology: Regional Studies*, *4*, 583–594. https://doi.org/10.1016/j.ejrh.2015.09.002

Gibbs, M. S., Maier, H. R., & Dandy, G. C. (2012). A generic framework for regression regionalization in ungauged catchments. *Environmental Modelling and Software*, *27–28*,

1–14. https://doi.org/10.1016/j.envsoft.2011.10.006

Glowa, S. E., Kneale, A. J., Watkinson, D. A., Ghamry, H. K., Enders, E. C., & Jardine, T. D. (2023). Applying a two-dimensional hydrodynamic model to estimate fish stranding risk downstream from a hydropeaking hydroelectric station. Ecohydrology, 16(4), e2530. https://doi.org/10.1002/eco.2530

Gogoi, C., & Goswami, D. C. (2014). A study on channel migration of the Subansiri river in Assam using remote sensing and GIS technology. Current Science, 1113-1120.

Gragne, A. S., Sharma, A., Mehrotra, R., & Alfredsen, K. (2015). Improving real-time inflow forecasting into hydropower reservoirs through a complementary modelling framework. *Hydrology and Earth System Sciences*, *19*(8), 3695–3714. https://doi.org/10.5194/hess-19-3695-2015

Grantham, T. E., Viers, J. H., & Moyle, P. B. (2014). Systematic screening of dams for environmental flow assessment and implementation. *BioScience*, *64*(11), 1006–1018. https://doi.org/10.1093/biosci/biu159

Greimel, F., Schülting, L., Graf, W., Bondar-Kunze, E., Auer, S., Zeiringer, B., & Hauer, C. (2018). Hydropeaking Impacts and Mitigation. *Riverine Ecosystem Management*, 91–110. https://doi.org/10.1007/978-3-319-73250-3_5

Guhathakurta, P., Sreejith, O. P., & Menon, P. A. (2011). Impact of climate change on extreme rainfall events and flood risk in India. *Journal of Earth System Science*, *120*(3), 359–373. https://doi.org/10.1007/s12040-011-0082-5

Guo, H. (2010). Understanding global natural disasters and the role of earth observation. *International Journal of Digital Earth*, *3*(3), 221–230. https://doi.org/10.1080/17538947.2010.499662

Hashimoto, T., Stedinger, J. R., & Loucks, D. P. (1982). Reliability, Resiliency, and Vulnerability Criteria. *Water Resources Research*, *18*(1), 14–20.

Hassan, R., Cohanim, B., De Weck, O., and Venter, G. 2005. A comparison of particle swarm optimization and the genetic algorithm. I*n 46th AIAA/ASME/ASCE/AHS/ASC structures, structural dynamics and materials conference* (p. 1897).

He, B., Huang, X., Ma, M., Chang, Q., Tu, Y., Li, Q., Zhang, K., & Hong, Y. (2018). Analysis

of flash flood disaster characteristics in China from 2011 to 2015. *Natural Hazards*, *90*(1), 407–420. https://doi.org/10.1007/s11069-017-3052-7

Hedger, R. D., Sundt-Hansen, L. E., Juárez-Gómez, A., Alfredsen, K., & Foldvik, A. (2023). Exploring sensitivities to hydropeaking in Atlantic salmon parr using individual-based modelling. *Ecohydrology*, *March*, 1–18. https://doi.org/10.1002/eco.2553

Hogeboom, R. J., Knook, L., & Hoekstra, A. Y. (2018). The blue water footprint of the world's artificial reservoirs for hydroelectricity, irrigation, residential and industrial water supply, flood protection, fishing and recreation. *Advances in Water Resources*, *113*, 285–294. https://doi.org/10.1016/j.advwatres.2018.01.028

Holland, J. H. 1992. Adaptation in natural and artificial systems: an introductory analysis with applications to biology, control, and artificial intelligence. *MIT press*.

IHA. (2020). Hydropower Status Report 2020. *International Hydropower Association*, 1–44. https://www.hydropower.org/sites/default/files/publications-docs/2019_hydropower_status_report_0.pdf

Jamshidi, J., & Shourian, M. (2019). Hedging Rules-Based Optimal Reservoir Operation Using Bat Algorithm. *Water Resources Management*, *33*(13), 4525–4538. https://doi.org/10.1007/s11269-019-02402-9

Jha, B. R., Rayamajhi, A., Dahanukar, N., Harrison, A., & Pinder, A. C. (2018). Tor putitora. *The IUCN Red List of Threatened Species*, *8235*(2018–2).

Ji, W., & Shao, T. (2021). Finite Element Model Updating for Improved Box Girder Bridges with Corrugated Steel Webs Using the Response Surface Method and Fmincon Algorithm. *KSCE Journal of Civil Engineering*, *25*(2), 586–602. https://doi.org/10.1007/s12205-020-0591-3

Johnson, J. A., Dhawan, B., & Kuppusamy, S. (2021). Study on ecology and migratory patterns of golden mahseer (Tor putitora) in River Ganga using radio telemetry techniques project reportjJuly 2021. January2022. https://doi.org/10.13140/RG.2.2.30906.06084

Jowett, I. G., & Davey, A. J. H. (2007). A Comparison of Composite Habitat Suitability Indices and Generalized Additive Models of Invertebrate Abundance and Fish Presence–Habitat Availability. *Transactions of the American Fisheries Society*, *136*(2), 428–444.

https://doi.org/10.1577/t06-104.1

Kalita, H. M. (2020). A Numerical Model for 1D Bed Morphology Calculations. *Water Resources Management*, *34*(15), 4975–4989. https://doi.org/10.1007/s11269-020-02707-0

Kalita, H. M. (2022). An Efficient 1D Hybrid Numerical Model for Bed Morphology Calculations in Alluvial Channels. *Iranian Journal of Science and Technology, Transactions of Civil Engineering*, *47*(2), 1189–1196. https://doi.org/10.1007/s40996-022-00977-9

Kansal, M. L., & Singh, S. (2022). Flood Management Issues in Hilly Regions of Uttarakhand (India) under Changing Climatic Conditions. *Water (Switzerland)*, *14*(12). https://doi.org/10.3390/w14121879

Karahan, H., Gurarslan, G., & Geem, Z. W. (2015). A new nonlinear Muskingum flood routing model incorporating lateral flow. *Engineering Optimization*, *47*(6), 737–749. https://doi.org/10.1080/0305215X.2014.918115

Karimi, S., Salarijazi, M., Ghorbani, K., & Heydari, M. (2021). Comparative assessment of environmental flow using hydrological methods of low flow indexes, Smakhtin, Tennant and flow duration curve. *Acta Geophysica*, *69*(1), 285–293. https://doi.org/10.1007/s11600-021-00539-z

Kates, R. W. (1971). Natural Hazard in Human Ecological Perspective: Hypotheses and Models. *Economic Geography*, *47*(3), 438. https://doi.org/10.2307/142820

Katoch, S., Chauhan, S. S., & Kumar, V. (2021). *Katoch2021_Article_AReviewOnGeneticAlgorithmPastP.pdf*. Multimedia Tools and Applications.

Kaygusuz, K. (2004). Hydropower and the World's Energy Future. *Energy Sources*, *26*(3), 215–224. https://doi.org/10.1080/00908310490256572

Kern, J. D., Characklis, G. W., Doyle, M. W., Blumsack, S., & Whisnant, R. B. (2012). Influence of Deregulated Electricity Markets on Hydropower Generation and Downstream Flow Regime. *Journal of Water Resources Planning and Management*, *138*(4), 342–355. https://doi.org/10.1061/(asce)wr.1943-5452.0000183

Kim, J. B., & Bae, D. H. (2020). Intensification characteristics of hydroclimatic extremes in

the Asian monsoon region under 1.5 and 2.0°C of global warming. *Hydrology and Earth System Sciences*, *24*(12), 5799–5820. https://doi.org/10.5194/hess-24-5799-2020

Kim, N. W., Lee, J. E., & Kim, J. T. (2012). Assessment of Flow Regulation Effects by Dams in the Han River, Korea, on the Downstream Flow Regimes Using SWAT. *Journal of Water Resources Planning and Management*, *138*(1), 24–35. https://doi.org/10.1061/(asce)wr.1943-5452.0000148

Koutrakis, E. T., Triantafillidis, S., Sapounidis, A. S., Vezza, P., Kamidis, N., Sylaios, G., & Comoglio, C. (2019). Evaluation of ecological flows in highly regulated rivers using the mesohabitat approach: A case study on the Nestos River, N. Greece. *Ecohydrology and Hydrobiology*, *19*(4), 598–609. https://doi.org/10.1016/j.ecohyd.2018.01.002

Książek, L., Woś, A., Florek, J., Wyrębek, M., Młyński, D., & Wałęga, A. (2019). Combined use of the hydraulic and hydrological methods to calculate the environmental flow: Wisloka river, Poland: case study. *Environmental Monitoring and Assessment*, *191*(4). https://doi.org/10.1007/s10661-019-7402-7

Labadie, J. W. (2004). Optimal Operation of Multireservoir Systems: State-of-the-Art Review. *Journal of Water Resources Planning and Management*, *130*(2), 93–111. https://doi.org/10.1061/(asce)0733-9496(2004)130:2(93)

Lai, V., Huang, Y. F., Koo, C. H., Ahmed, A. N., & El-Shafie, A. (2022). A Review of Reservoir Operation Optimisations: from Traditional Models to Metaheuristic Algorithms. *Archives of Computational Methods in Engineering*, *29*(5), 3435–3457. https://doi.org/10.1007/s11831-021-09701-8

Lee, K. T., Ho, J. Y., Kao, H. M., Lin, G. F., & Yang, T. H. (2019). Using ensemble precipitation forecasts and a rainfall-runoff model for hourly reservoir inflow forecasting during typhoon periods. *Journal of Hydro-Environment Research*. https://doi.org/10.1016/j.jher.2018.05.002

Leitner, P., Hauer, C., & Graf, W. (2017). Habitat use and tolerance levels of macroinvertebrates concerning hydraulic stress in hydropeaking rivers – A case study at the Ziller River in Austria. *Science of the Total Environment*, *575*, 112–118. https://doi.org/10.1016/j.scitotenv.2016.10.011

Li, W., Lin, K., Zhao, T., Lan, T., Chen, X., Du, H., & Chen, H. (2019). Risk assessment and

sensitivity analysis of flash floods in ungauged basins using coupled hydrologic and hydrodynamic models. *Journal of Hydrology*, *572*(February), 108–120. https://doi.org/10.1016/j.jhydrol.2019.03.002

Li, X., Guo, S., Liu, P., & Chen, G. (2010). Dynamic control of flood limited water level for reservoir operation by considering inflow uncertainty. *Journal of Hydrology*, *391*(1–2), 124–132. https://doi.org/10.1016/j.jhydrol.2010.07.011

Li, T., & Pasternack, G. B. (2021). Revealing the diversity of hydropeaking flow regimes. Journal of Hydrology, 598, 126392. https://doi.org/10.1016/j.jhydrol.2021.126392

Liu, P., Li, L., Chen, G., & Rheinheimer, D. E. (2014). Parameter uncertainty analysis of reservoir operating rules based on implicit stochastic optimization. *Journal of Hydrology*, *514*, 102–113. https://doi.org/10.1016/j.jhydrol.2014.04.012

Lobera, G., Muñoz, I., López-Tarazón, J. A., Vericat, D., & Batalla, R. J. (2017). Effects of flow regulation on river bed dynamics and invertebrate communities in a Mediterranean river. *Hydrobiologia*, *784*(1), 283–304. https://doi.org/10.1007/s10750-016-2884-6

López-Moreno, J. I., Beguería, S., & García-Ruiz, J. M. (2002). Influence of the Yesa reservoir on floods of the Aragón River, central Spanish Pyrenees. *Hydrology and Earth System Sciences*, *6*(4), 753–762. https://doi.org/10.5194/hess-6-753-2002

Lu, Q., Zhong, P. an, Xu, B., Zhu, F., Wang, H., & Ma, Y. (2020). Risk analysis of reservoir floodwater utilization coupling meteorological and hydrological uncertainties. *Stochastic Environmental Research and Risk Assessment*, *34*(10), 1507–1521. https://doi.org/10.1007/s00477-020-01834-9

Maddu, R., Pradhan, I., Ahmadisharaf, E., Singh, S. K., & Shaik, R. (2022). Short-range reservoir inflow forecasting using hydrological and large-scale atmospheric circulation information. *Journal of Hydrology*, *612*(PB), 128153. https://doi.org/10.1016/j.jhydrol.2022.128153

Maier, H. R., Kapelan, Z., Kasprzyk, J., Kollat, J., Matott, L. S., Cunha, M. C., Dandy, G. C., Gibbs, M. S., Keedwell, E., Marchi, A., Ostfeld, A., Savic, D., Solomatine, D. P., Vrugt, J. A., Zecchin, A. C., Minsker, B. S., Barbour, E. J., Kuczera, G., Pasha, F., … Reed, P. M. (2014). Evolutionary algorithms and other metaheuristics in water resources: Current status, research challenges and future directions. *Environmental Modelling and Software*,

62, 271–299. https://doi.org/10.1016/j.envsoft.2014.09.013

Marak, J. D. K., Sarma, A. K., & Bhattacharjya, R. K. (2020). Assessing the Impacts of Interbasin Water Transfer Reservoir on Streamflow. *Journal of Hydrologic Engineering*, *25*(10), 1–13. https://doi.org/10.1061/(asce)he.1943-5584.0001984

Mason, V., Andrews, H., & Upton, D. (2010). The psychological impact of exposure to floods. *Psychology, Health and Medicine*, *15*(1), 61–73. https://doi.org/10.1080/13548500903483478

Mateo, C. M., Hanasaki, N., Komori, D., Tanaka, K., Kiguchi, M., Champathong, A., ... & Oki, T. (2014). Assessing the impacts of reservoir operation to floodplain inundation by combining hydrological, reservoir management, and hydrodynamic models. Water Resources Research, 50(9), 7245-7266.

Maurer, E. P., & Lettenmaier, D. P. (2004). Potential effects of long-lead hydrologic predictability on Missouri River main-stem reservoirs. *Journal of Climate*, *17*(1), 174–186. https://doi.org/10.1175/1520-0442(2004)017<0174:PEOLHP>2.0.CO;2

Meile, T., Boillat, J. L., & Schleiss, A. J. (2011). Hydropeaking indicators for characterization of the Upper-Rhone River in Switzerland. *Aquatic Sciences*, *73*(1), 171–182. https://doi.org/10.1007/s00027-010-0154-7

Mishra, A. K., & Nagaraju, V. (2021). Remote sensing of extreme flash floods over two southern states of India during North-East monsoon season of 2020. *Natural Hazards*, *107*(2), 2015–2020. https://doi.org/10.1007/s11069-021-04631-x

Moeeni, H., Bonakdari, H., & Ebtehaj, I. (2017). Monthly reservoir inflow forecasting using a new hybrid SARIMA genetic programming approach. *Journal of Earth System Science*, *126*(2). https://doi.org/10.1007/s12040-017-0798-y

Mondal, A., Lakshmi, V., & Hashemi, H. (2018). Intercomparison of trend analysis of Multisatellite Monthly Precipitation Products and Gauge Measurements for River Basins of India. *Journal of Hydrology*, *565*(August), 779–790. https://doi.org/10.1016/j.jhydrol.2018.08.083

Moran, E. F., Lopez, M. C., Moore, N., Müller, N., & Hyndman, D. W. (2018). Sustainable hydropower in the 21st century. *Proceedings of the National Academy of Sciences of the United States of America*, *115*(47), 11891–11898.

https://doi.org/10.1073/pnas.1809426115

Moreira, M., Hayes, D. S., Boavida, I., Schletterer, M., Schmutz, S., & Pinheiro, A. (2019). Ecologically-based criteria for hydropeaking mitigation: A review. *Science of the Total Environment*, *657*, 1508–1522. https://doi.org/10.1016/j.scitotenv.2018.12.107

Morsy, M. M., Goodall, J. L., O'Neil, G. L., Sadler, J. M., Voce, D., Hassan, G., & Huxley, C. (2018). A cloud-based flood warning system for forecasting impacts to transportation infrastructure systems. *Environmental Modelling and Software*, *107*(May), 231–244. https://doi.org/10.1016/j.envsoft.2018.05.007

Muller, M. (2009). *Nature Comment 19 Feb 2019 Dams have the power to slow climate change*. 6–8.

Muluye, G. Y., & Coulibaly, P. (2007). Seasonal reservoir inflow forecasting with low-frequency climatic indices: A comparison of data-driven methods. *Hydrological Sciences Journal*, *52*(3), 508–522. https://doi.org/10.1623/hysj.52.3.508

Myhre, G., Alterskjær, K., Stjern, C. W., Hodnebrog, Marelle, L., Samset, B. H., Sillmann, J., Schaller, N., Fischer, E., Schulz, M., & Stohl, A. (2019). Frequency of extreme precipitation increases extensively with event rareness under global warming. *Scientific Reports*, *9*(1), 1–10. https://doi.org/10.1038/s41598-019-52277-4

Nagesh Kumar, D., Baliarsingh, F., & Srinivasa Raju, K. (2010). Optimal reservoir operation for flood control using folded dynamic programming. *Water Resources Management*, *24*(6), 1045–1064. https://doi.org/10.1007/s11269-009-9485-3

Neelakantan, T. R., & Sasireka, K. (2013). Hydropower reservoir operation using standard operating and standard hedging policies. *International Journal of Engineering and Technology*, *5*(2), 1191–1196.

Neelakantan, T. R., & Sasireka, K. (2015). Review of hedging rules applied to reservoir operation. *International Journal of Engineering and Technology*, *7*(5), 1571–1580.

Nguyen, T. H., & Gourbesville, P. (2022). Optimal operation of multi-reservoir system for flood control and hydroelectric generation. *E3S Web of Conferences*, *346*, 1–14. https://doi.org/10.1051/e3sconf/202234603006

Nruthya, K., & Srinivas, V. V. (2015). Evaluating Methods to Predict Streamflow at Ungauged Sites Using Regional Flow Duration Curves: A Case Study. *Aquatic Procedia*,

4(Icwrcoe), 641–648. https://doi.org/10.1016/j.aqpro.2015.02.083

O'donnell, T. (1985). A direct three-parameter muskingum procedure incorporating lateral inflow. *Hydrological Sciences Journal*, *30*(4), 479–496. https://doi.org/10.1080/02626668509491013

OECD, IEA. (2016). Energy and air pollution: world energy outlook special report 2016.

Oliveira, R., & Loucks, D. P. (1997). Operating rules for multireservoir systems. *Water Resources Research*, *33*(4), 839–852. https://doi.org/10.1029/96WR03745

Patowary, S., & Sarma, A. K. (2017). A modified hydrodynamic model for routing unsteady flow in a river having piedmont zone. *Journal of Hydrology and Hydromechanics*, *65*(1), 60–67. https://doi.org/10.1515/johh-2016-0052

Petts, G. E., & Gurnell, A. M. (2021). Hydrogeomorphic effects of reservoirs, dams, and diversions. In Reference Module in Earth Systems and Environmental Sciences.

Poff, N. L. R., Allan, J. D., Bain, M. B., Karr, J. R., Prestegaard, K. L., Richter, B. D., Sparks, R. E., & Stromberg, J. C. (1997). The natural flow regime: A paradigm for river conservation and restoration. *BioScience*, *47*(11), 769–784. https://doi.org/10.2307/1313099

Pokhrel, Y., Shin, S., Lin, Z., Yamazaki, D., & Qi, J. (2018). Potential disruption of flood dynamics in the lower Mekong River basin due to upstream flow regulation. Scientific reports, 8(1), 17767.

Pramanik, N., Panda, R. K., & Sen, D. (2010). One dimensional hydrodynamic modeling of river flow using DEM extracted river cross-sections. *Water Resources Management*, *24*(5), 835–852. https://doi.org/10.1007/s11269-009-9474-6

Qiu, R., Wang, D., Singh, V. P., Zhang, H., Tao, Y., Wu, J., & Wang, Y. (2023). Ecological responses of spawning habitat suitability to changes in flow and thermal regimes influenced by hydropower operation. Ecohydrology, 16(2), e2507.

Ray, M. R., & Sarma, A. K. (2011). Minimizing diurnal variation of downstream flow in hydroelectric projects to reduce environmental impact. *Journal of Hydro-Environment Research*, *5*(3), 177–185. https://doi.org/10.1016/j.jher.2010.12.001

Ray, M. R., & Sarma, A. K. (2016). Influence of Time Discretization and Input Parameter on

the ANN Based Synthetic Streamflow Generation. *Water Resources Management*, *30*(13), 4695–4711. https://doi.org/10.1007/s11269-016-1448-x

Richter, B. D., Baumgartner, J. V, Powell, J., Braun, D. P., Richter, B. D., Baumgartner, J. V, Powell, J., & Braunt, D. P. (1996). A Method for Assessing Hydrologic Alteration within Ecosystems Published by : Wiley for Society for Conservation Biology All use subject to http://about.jstor.org/terms A Method for Assessing Hydrologic Alteration within E. *Conservation Biology*, *10*(4), 1163–1174.

Rosenfeld, J. S., Bouwes, N., Wall, C. E., & Naman, S. M. (2014). Successes, failures, and opportunities in the practical application of drift-foraging models. *Environmental Biology of Fishes*, *97*(5), 551–574. https://doi.org/10.1007/s10641-013-0195-6

Schafer, R. W. (2011). What is a savitzky-golay filter? *IEEE Signal Processing Magazine*, *28*(4), 111–117. https://doi.org/10.1109/MSP.2011.941097

Silvestro, F., Rebora, N., Giannoni, F., Cavallo, A., & Ferraris, L. (2016). The flash flood of the Bisagno Creek on 9th October 2014: An "unfortunate" combination of spatial and temporal scales. *Journal of Hydrology*, *541*(October 2014), 50–62. https://doi.org/10.1016/j.jhydrol.2015.08.004

Simonovic, S. P., & Burn, D. H. (1989). An improved methodology for short-term operation of a single multipurpose reservoir. *Water Resources Research*, *25*(1), 1–8. https://doi.org/10.1029/WR025i001p00001

Sinha, B. (2019). *Ichthyofauna of Lower Subansiri district , Arunachal Pradesh w . s . r . to Ranga River*. *119*(2), 128–164. https://doi.org/10.26515/rzsi/v119/i2/2019/142748

Smakhtin, V. (2001). Smakhtin 2010- Low flow hydrology.pdf. *Journal of HydrologyJournal of Hydrology*, *240*, 147–186.

Song, Y., Park, Y., Lee, J., Park, M., & Song, Y. (2019). Flood forecasting and warning system structures: Procedure and application to a small urban stream in South Korea. *Water (Switzerland)*, *11*(8). https://doi.org/10.3390/w11081571

Spada, E., Sinagra, M., Tucciarelli, T., Barbetta, S., Moramarco, T., & Corato, G. (2017). Assessment of river flow with significant lateral inflow through reverse routing modeling. *Hydrological Processes*, *31*(7), 1539–1557. https://doi.org/10.1002/hyp.11125

Spiliotis, M., Sordo-Ward, A., & Garrote, L. (2021). Estimation of fuzzy parameters in the

linear muskingum model with the aid of particle swarm optimization. *Sustainability (Switzerland)*, *13*(13), 1–26. https://doi.org/10.3390/su13137152

Spreafico, M. (2006). Flash floods in mountain areas. *IAHS-AISH Publication*, *308*, 232–238.

Stamou, A., Polydera, A., Papadonikolaki, G., Martínez-Capel, F., Muñoz-Mas, R., Papadaki, C., Zogaris, S., Bui, M. D., Rutschmann, P., & Dimitriou, E. (2018). Determination of environmental flows in rivers using an integrated hydrological-hydrodynamic-habitat modelling approach. *Journal of Environmental Management*, *209*, 273–285. https://doi.org/10.1016/j.jenvman.2017.12.038

Stefanescu, V. (2013). Decision support system based on the history of flood and flash flood events in Romania. *Natural Hazards*, *65*(3), 2331–2352. https://doi.org/10.1007/s11069-012-0479-8

Sudheer, K. P., Murty Bhallamudi, S., Narasimhan, B., Thomas, J., Bindhu, V. M., Vema, V., & Kurian, C. (2019). Role of dams on the floods of August 2018 in Periyar River Basin, Kerala. *Current Science*, *116*(5), 780–794. https://doi.org/10.18520/cs/v116/i5/780-794

Sun, Y., Zhu, F., Chen, J., & Li, J. (2018). Risk analysis for reservoir real-time optimal operation using the scenario tree-based stochastic optimization method. *Water (Switzerland)*, *10*(5). https://doi.org/10.3390/w10050606

Tabari, H. (2020). Climate change impact on flood and extreme precipitation increases with water availability. *Scientific Reports*, *10*(1), 1–10. https://doi.org/10.1038/s41598-020-70816-2

Talukdar, G., Sarma, A. K., & Bhattacharjya, R. K. (2021). Sediment analysis and modelling based approach for optimal allocation of riverine sandbar for socio economic benefits. *Ecological Engineering*, *173*(August), 106415. https://doi.org/10.1016/j.ecoleng.2021.106415

Talukdar, G., Sarma, A. K., & Bhattacharjya, R. K. (2022). Assessment of land use change in riverine ecosystem and utilizing it for socioeconomic benefit. *Environmental Monitoring and Assessment*, *194*(11). https://doi.org/10.1007/s10661-022-10495-w

Tare, V., Gurjar, S. K., Mohanta, H., Kapoor, V., Modi, A., Mathur, R. P., & Sinha, R. (2017). Eco-geomorphological approach for environmental flows assessment in monsoon-driven highland rivers: A case study of Upper Ganga, India. *Journal of Hydrology: Regional*

Studies, *13*(July), 110–121. https://doi.org/10.1016/j.ejrh.2017.07.005

Tennant, D. L. (1976). Instream flow regimens for fish, wildlife, recreation and related environmental resources. Fisheries, 1(4), 6–10.

Tharme, R. E. (2003). A global perspective on environmental flow assessment: Emerging trends in the development and application of environmental flow methodologies for rivers. *River Research and Applications*, *19*(5–6), 397–441. https://doi.org/10.1002/rra.736

Tomczyk, P., Willems, P., & Wiatkowski, M. (2021). Comparative analysis of changes in hydromorphological conditions upstream and downstream hydropower plants on selected rivers in Poland and Belgium. *Journal of Cleaner Production*, *328*(October). https://doi.org/10.1016/j.jclepro.2021.129524

Trung, T., Thuan, N., Nguyen, T., & Dinh, T. (2022). Finding optimal solutions for reaching maximum power energy of hydroelectric plants in cascaded systems. *Journal of Ambient Intelligence and Humanized Computing*, *13*(9), 4369–4384. https://doi.org/10.1007/s12652-021-03361-z

Tsegaw, A. T., Alfredsen, K., Skaugen, T., & Muthanna, T. M. (2019). Predicting hourly flows at ungauged small rural catchments using a parsimonious hydrological model. *Journal of Hydrology*, *573*(October 2018), 855–871. https://doi.org/10.1016/j.jhydrol.2019.03.090

Turner, S. W. D., Xu, W., & Voisin, N. (2020). Inferred inflow forecast horizons guiding reservoir release decisions across the United States. Hydrology and Earth System Sciences, 24(3), 1275–1291. https://doi.org/10.5194/hess-24-1275-2020

Vedula, S., & Mujumdar, P. P. (1992). Optimal reservoir operation for irrigation of multiple crops. Water Resources Research, 28(1), 1-9.

Viero, D. Pietro, D'Alpaos, A., Carniello, L., & Defina, A. (2013). Mathematical modeling of flooding due to river bank failure. *Advances in Water Resources*, *59*, 82–94. https://doi.org/10.1016/j.advwatres.2013.05.011

Wang, J., Zhao, T., Zhao, J., Wang, H., & Lei, X. (2021). Improving real-time reservoir operation during flood season by making the most of streamflow forecasts. *Journal of Hydrology*, *595*(November 2020), 126017. https://doi.org/10.1016/j.jhydrol.2021.126017

Wang, K., Shi, H., Chen, J., & Li, T. (2019). An improved operation-based reservoir scheme

integrated with Variable Infiltration Capacity model for multiyear and multipurpose reservoirs. *Journal of Hydrology*. https://doi.org/10.1016/j.jhydrol.2019.02.006

Widén, Å., Malm Renöfält, B., Degerman, E., Wisaeus, D., & Jansson, R. (2022). Environmental Flow Scenarios for a Regulated River System: Projecting Catchment-Wide Ecosystem Benefits and Consequences for Hydroelectric Production. *Water Resources Research*, *58*(1), 1–22. https://doi.org/10.1029/2021WR030297

William W-G. Yeh. (1985). Reservoir Management and Operations Models '. *Water Resources Research*, *21*(12), 1797–1818.

Williams, G. P., & Wolman, M. G. (1984). Downstream effects of dams on alluvial rivers (Vol. 1286). US Government Printing Office.

World Commission on Dams. (2000). Dams and development: A new framework for decision-making: The report of the world commission on dams. Earthscan.

Xiong, L., Jiang, C., Guo, S., Li, S., Li, R., & Li, W. (2022). Multivariate Dam-Site Flood Frequency Analysis of the Three Gorges Reservoir Considering Future Reservoir Regulation and Precipitation. *Water (Switzerland)*, *14*(2). https://doi.org/10.3390/w14020138

Xu, W., Meng, F., Guo, W., Li, X., & Fu, G. (2021). Deep Reinforcement Learning for Optimal Hydropower Reservoir Operation. *Journal of Water Resources Planning and Management*, *147*(8), 04021045. https://doi.org/10.1061/(asce)wr.1943-5452.0001409

Yang, Y., Yang, Z., Yin, X. an, & Liu, Q. (2018). A framework for assessing flow regime alterations resulting from the effects of climate change and human disturbance. In *Hydrological Sciences Journal* (Vol. 63, Issue 3, pp. 441–456). https://doi.org/10.1080/02626667.2018.1430897

Yeniay, Ö. (2005). Penalty function methods for constrained optimization with genetic algorithms. *Mathematical and Computational Applications*, *10*(1), 45–56. https://doi.org/10.3390/mca10010045

Yildiz, V., & Vrugt, J. A. (2019). A toolbox for the optimal design of run-of-river hydropower plants. *Environmental Modelling and Software*, *111*(August 2017), 134–152. https://doi.org/10.1016/j.envsoft.2018.08.018

You, G. J. Y., & Yu, C. W. (2013). Theoretical error convergence of limited forecast horizon

in optimal reservoir operating decisions. *Water Resources Research*, *49*(3), 1728–1734. https://doi.org/10.1002/wrcr.20114

You, J., & Cai, X. (2008). *Determining forecast and decision horizons for reservoir operations under hedging policies*. *44*(August), 1–14. https://doi.org/10.1029/2008WR006978

You, J. Y., & Cai, X. (2008). Hedging rule for reservoir operations: 1. A theoretical analysis. *Water Resources Research*, *44*(1), 1–9. https://doi.org/10.1029/2006WR005481

Yun, R., & Singh, V. P. (2008). Multiple duration limited water level and dynamic limited water level for flood control, with implications on water supply. *Journal of Hydrology*, *354*(1–4), 160–170. https://doi.org/10.1016/j.jhydrol.2008.03.003

Zakwan, M. (2018). Spreadsheet-based modelling of hysteresis-affected curves. *Applied Water Science*, *8*(4), 1–5. https://doi.org/10.1007/s13201-018-0745-3

Zakwan, M., Muzzammil, M., & Alam, J. (2017). Developing Stage-Discharge Relations using Optimization Techniques. *Aquademia: Water, Environment and Technology*, *1*(2), 1–8. https://doi.org/10.20897/awet/81286

Zarfl, C., Berlekamp, J., He, F., Jähnig, S. C., Darwall, W., & Tockner, K. (2019). Future large hydropower dams impact global freshwater megafauna. *Scientific Reports*, *9*(1), 1–10. https://doi.org/10.1038/s41598-019-54980-8

Zarfl, C., Lumsdon, A. E., Berlekamp, J., Tydecks, L., & Tockner, K. (2015). A global boom in hydropower dam construction. *Aquatic Sciences*, *77*(1), 161–170. https://doi.org/10.1007/s00027-014-0377-0

Zeng, S., Liu, X., Xia, J., Du, H., Chen, M., & Huang, R. (2023). Evaluating the hydrological effects of the Three Gorges Reservoir based on a large-scale coupled hydrological-hydrodynamic-dam operation model. *Journal of Geographical Sciences*, *33*(5), 999–1022. https://doi.org/10.1007/s11442-023-2117-7

Zhai, X., Zhang, Y., Zhang, Y., Guo, L., & Liu, R. (2021). Simulating flash flood hydrographs and behavior metrics across China: Implications for flash flood management. *Science of the Total Environment*, *763*, 142977. https://doi.org/10.1016/j.scitotenv.2020.142977

Zhang, F., & Zhang, Y. (2021). A multi-objective optimization prediction approach for water resources based on swarm intelligence. *Earth Science Informatics*, *14*(1), 457–468.

https://doi.org/10.1007/s12145-020-00521-1

Zhao, Q., Cai, X., & Li, Y. (2019). Determining Inflow Forecast Horizon for Reservoir Operation. *Water Resources Research*, *55*(5), 4066–4081. https://doi.org/10.1029/2019WR025226

Zhao, T., Cai, X., & Yang, D. (2011). Effect of streamflow forecast uncertainty on real-time reservoir operation. *Advances in Water Resources*, *34*(4), 495–504. https://doi.org/10.1016/j.advwatres.2011.01.004

Zhao, T., Yang, D., Cai, X., Zhao, J., & Wang, H. (2012). Identifying effective forecast horizon for real-time reservoir operation under a limited inflow forecast. *Water Resources Research*, *48*(1), 1–15. https://doi.org/10.1029/2011WR010623

Zhu, S., Ouyang, S., Zhou, J., Qiu, H., Qin, H., Huang, J., & Niu, X. (2022). Water Balance Calculation Based on Hydrodynamics in Reservoir Operation. *Water (Switzerland)*, *14*(13), 1–17. https://doi.org/10.3390/w14132001

Zolfagharpour, F., Saghafian, B., & Delavar, M. (2022). Hydrological alteration and biodiversity change along the river network caused by anthropogenic activities and climate variability. *Ecological Processes*, *11*(1). https://doi.org/10.1186/s13717-022-00362-4

List of publications

Journals

1. **Dipsikha Devi,** Anupal Baruah, and Arup Kumar Sarma (2022). Characterization of dam-impacted flood hydrograph and its degree of severity as a potential hazard. *Natural Hazards*, Springer, *112*(3), 1989-2011. https://doi.org/10.1007/s11069-022-05253-7

2. **Dipsikha Devi**, and Arup Kumar Sarma. Impact of Inter-Basin Transfer Hydroelectric Project on Aquatic Habitat. *Ecohydrology*, Wiley. https://doi.org/10.1002/eco.2584

3. Dipsikha Devi, and Arup Kumar Sarma. Flow Assessment at Downstream of a Hydroelectric Project in Ungauged Reach. *Journal of Hydrologic Engineering*, ASCE. https://doi.org/10.1061/JHYEFF.HEENG-6050

4. **Dipsikha Devi**, and Arup Kumar Sarma. Optimal Advanced Release Scheme Based on Effective Forecast Horizon to Minimize Flood at Downstream of a Hydroelectric Project. *Journal of Hydrology*, Elsevier (*Under Review*).

5. Dipsikha Devi, and Arup Kumar Sarma. Minimizing Downstream Flood Risk from a Hydropower Dam under Inflow Uncertainty Within a Forecast Horizon. *Journal of Hydrology*, Elsevier (*Submitted*).

Under Preparation

1. A New Event Based Flashiness Index to Characterize Dam Induced Flood.

Conferences

1. **Dipsikha Devi**, Khyati Chaudhury, and Arup Kumar Sarma (2019, August). Application of BRAHMA hydrodynamic model for flood forecasting. In *Journal of Physics: Conference Series* (Vol. 1276, No. 1, p. 012015). IOP Publishing.

2. **Dipsikha Devi**, Anupal Baruah, and Arup Kumar Sarma (2021). Characterizing Dam Induced Flood at Downstream of a Hydel Project. In *EGU General Assembly Conference Abstracts* (pp. EGU21-8757).

3. **Dipsikha Devi**, and Arup Kumar Sarma (2022). Impact of Downstream Flow Contribution on the Flood Prone Areas of a Hydropower Project. In *AGU Fall Meeting Abstracts* (Vol. 2022, pp. H55M-0743).

4. **Dipsikha Devi**, Gaurav Talukdar, Amit Kalita and Arup Kumar Sarma (2022) . Introducing a Flood Risk Factor (FRF) for Effective Flood Warning at Downstream of a Hydel Project using BRAHMA 1-D Model. STREAM 2022.

ANNEXURE I

Ranking of Global hazards Characteristics (Bryant, 2005)

	Event	Degree of severity	Length of event	Total Areal Extent	Total loss of life	Total Economic Loss	Social Effect	Long term Impact	Suddenness	Number of associated Hazards	Additive Likert Scale Score
1	Drought	1	1	1	1	1	1	1	4	3	14
2	Tropical Cyclone	1	2	2	2	2	2	1	5	1	18
3	Regional flood	2	2	2	1	1	1	2	4	3	18
4	Earthquake	1	5	1	2	1	1	2	3	3	19
5	Volcano	1	4	4	2	2	2	1	3	1	20
6	Extra tropical storm	1	3	2	2	2	2	5	3	2	22
7	Tsunami	2	4	1	2	2	2	3	4	5	25
8	Bushfire	3	3	3	3	3	3	3	2	5	28
9	Expansive soils	5	1	1	5	4	5	3	1	5	30
10	Sea-level rise	5	1	1	5	3	5	1	5	4	30
11	Icebergs	4	1	1	4	4	5	5	2	5	31
12	Dust storm	3	3	2	5	4	5	4	1	5	32
13	Landslides	4	2	2	4	4	4	5	2	5	32
14	Beach erosion	5	2	2	5	4	4	4	2	5	33
15	Debris avalanches	2	5	5	3	4	3	5	1	5	33
16	Creep and solifluction	5	1	2	5	4	5	4	2	5	33
17	Tornado	2	5	3	4	4	4	5	2	5	34
18	Snowstorm	4	3	3	5	4	4	5	2	4	34
19	Ice at shore	5	4	1	5	4	5	4	1	5	34

Event	Degree of severity	Length of event	Total Areal Extent	Total loss of life	Total Economic Loss	Social Effect	Long term Impact	Suddenness	Number of associated Hazards	Additive Likert Scale Score	
20	Flash flood	3	5	4	4	4	4	5	1	5	35
21	Thunderstorm	4	5	2	4	4	5	5	2	4	35
22	Lightning strike	4	5	2	4	4	5	5	1	5	35
23	Blizzard	4	3	4	4	4	5	5	1	5	35
24	Ocean waves	4	4	2	4	4	5	5	3	5	36
25	Hail storm	4	5	4	5	3	5	5	1	5	37
26	Freezing rain	4	4	5	5	4	4	5	1	5	37
27	Localized strong wind	5	4	3	5	5	5	5	1	5	38
28	Subsidence	4	3	5	5	4	4	5	3	5	38
29	Mud and debris flows	4	4	5	4	4	5	5	4	5	40
30	Air supported flows	4	5	5	4	5	5	5	2	5	40
31	Rockfalls	5	5	5	5	5	5	5	1	5	41

ANNEXURE II

Percentage attenuation of the second flood peak considering with dam and without dam scenarios

Initial Storages (Mm^3)	**Flood Peak of the Inflow hydrograph (m^3/s)**	**Flood Peak of the reservoir outflow hydrographs (m^3/s)**	**Flood Peak at downstream (m^3/s)**	**Flood Peak attenuation compared to inflow hydrograph, Q_a (m^3/s)**	**Percentage Peak Attenuation (%)**
With Dam Scenario					
1305		3864.59	3364.34	1735.66	34
1315		4677.56	3850.40	1249.60	24.50
1320		4864.69	4091.63	1008.37	19.70
1365	5100	5074.70	4695.14	404.86	7.90
Without Dam Scenario					
Natural Flow Condition	5100	--	4829.41	270.59	5.30

ANNEXURE III

η_p and AUR corresponding to EF of the three cases of 4 hours peaking power production

Scenario 1: 4 h Peaking Hours

Initial Storage (MCM)		EF (cumec) 2	4	6	8	10	12	14	16	18	20	22	24	26	28	30	32	34
3.30 (Low)	η_p	0.452	0.397	0.341	0.285	0.230	0.174	0.118	0.063	0.041	0.001	0.000	0.000	0.000	0.000	0.000	0.000	0.000
	AUR	0.223	0.237	0.295	0.311	0.340	0.359	0.363	0.363	0.351	0.291	0.216	0.212	0.212	0.205	0.205	0.205	0.205
5.49 (Medium)	η_p	0.762	0.706	0.650	0.594	0.538	0.483	0.427	0.372	0.348	0.303	0.296	0.289	0.282	0.275	0.268	0.261	0.254
	AUR	0.223	0.237	0.295	0.311	0.340	0.359	0.363	0.363	0.351	0.291	0.216	0.212	0.212	0.205	0.205	0.205	0.205
7.71 (High)	η_p	1.000	1.000	0.949	0.897	0.845	0.793	0.741	0.687	0.660	0.585	0.555	0.540	0.498	0.468	0.439	0.416	0.388
	AUR	0.237	0.262	0.296	0.316	0.344	0.364	0.366	0.367	0.357	0.339	0.302	0.302	0.295	0.295	0.295	0.295	0.295

Scenario 2: 6 h Peaking Hours

3.30 (Low)	η_p	0.312	0.273	0.235	0.196	0.158	0.120	0.081	0.043	0.028	0.001	0.000	0.000	0.000	0.000	0.000	0.000	0.000
	AUR	0.223	0.237	0.295	0.311	0.340	0.359	0.363	0.363	0.351	0.291	0.216	0.212	0.212	0.205	0.205	0.205	0.205
5.49 (Medium)	η_p	0.518	0.479	0.441	0.402	0.364	0.325	0.287	0.249	0.232	0.202	0.197	0.193	0.188	0.183	0.179	0.174	0.169
	AUR	0.223	0.237	0.295	0.311	0.340	0.359	0.363	0.363	0.351	0.291	0.216	0.212	0.212	0.205	0.205	0.205	0.205
7.71 (High)	η_p	0.711	0.675	0.639	0.603	0.568	0.532	0.496	0.459	0.440	0.391	0.372	0.354	0.335	0.333	0.333	0.333	0.333
	AUR	0.237	0.261	0.293	0.312	0.336	0.359	0.364	0.364	0.356	0.356	0.300	0.301	0.290	0.295	0.295	0.295	0.295